Reimagining Wearable Sensing: Smart Jewelry for Unobtrusive Health Monitoring

Qiuyue (Shirley) Xue

A dissertation
submitted in partial fulfillment of the
requirements for the degree of

Doctor of Philosophy

University of Washington

2025

Reading Committee:

Shwetak Patel, Co-Chair

Vikram Iyer, Co-Chair

James Fogarty

Program Authorized to Offer Degree:
Computer Science & Engineering

University of Washington

Abstract

Reimagining Wearable Sensing: Smart Jewelry for Unobtrusive Health Monitoring

Qiuyue (Shirley) Xue

Co-Chairs of the Supervisory Committee:
Shwetak Patel
Computer Science & Engineering

Vikram Iyer
Computer Science & Engineering

Health and wellness are fundamental to everyone's life, yet effective monitoring outside clinical settings remains a challenge. Wearable devices have emerged as a promising solution due to their direct contact with the human body, enabling continuous physiological sensing. However, current wearables often fail to meet the demands of practical health monitoring due to limitations in accuracy, functionality, and user comfort. For example, smartwatches struggle with accurate heart rate and temperature measurements because their wrist placement is susceptible to motion artifacts and is far away from the core body. Moreover, existing wearables are unable to continuously monitor many critical physiological signals, such as electrocardiography (ECG), blood pressure, and more.

This dissertation advances unobtrusive health monitoring in people's daily lives by creating the next generation of wearable devices without adding any burden to users. Imagine everyday accessories transformed into intelligent systems that are small and lightweight enough not to let users notice. These devices are passively part of the user with ultra-long battery lives. Most importantly, the unique placement of these innovative wearables allows for capturing advanced physiological signals, enabling new health capabilities.

In this dissertation, I will introduce three novel wearables that ensure long-term comfort by preserving their original form factors and achieving month-long battery life: Thermal Earring, PPG Earring, and ECG Necklace. These novel wearable devices demonstrate

three core contributions: (1) **Improved sensing accuracy** by leveraging new body locations that offer stronger and more stable physiological signals, unlocking new applications for daily wellness. (2) **Enhanced continuity** through low-power system design that supports continuous, uninterrupted monitoring. (3) **Expanded sensing capabilities** that traditional wearables cannot achieve by rethinking the form factors. In conclusion, this dissertation demonstrates that creating the next generation of wearable devices can unlock new health insights and applications by enabling truly unobtrusive monitoring in everyday life.

TABLE OF CONTENTS

Page

List of Figures . . . iii

Chapter 1: Introduction . . . 1
- 1.1 Contribution: Wearable Space Advancement . . . 2
- 1.2 Thesis Statement . . . 4
- 1.3 Research Challenges . . . 4
- 1.4 Research Approach . . . 6
- 1.5 Dissertation Structure . . . 9

Chapter 2: Related Work . . . 14
- 2.1 Smart Jewelry and Fashion-related Wearable Devices . . . 14
- 2.2 Body Temperature Monitoring . . . 15
- 2.3 PPG Sensing . . . 16
- 2.4 ECG Sensing . . . 16

Chapter 3: Thermal Earring . . . 19
- 3.1 Introduction . . . 19
- 3.2 Thermal Earring System Design . . . 23
- 3.3 Lab-controlled Experiments . . . 32
- 3.4 In-the-Wild Results . . . 40
- 3.5 Discussion . . . 48
- 3.6 Summary . . . 52

Chapter 4: PPG Earring . . . 53
- 4.1 Introduction . . . 53
- 4.2 PPG Earring System Design . . . 56
- 4.3 Signal Processing . . . 64
- 4.4 Lab controlled studies . . . 66
- 4.5 In-the-wild Study . . . 75

4.6 Discussion . . . 81
4.7 Summary . . . 84

Chapter 5: ECG Necklace . . . 86
5.1 Introduction . . . 86
5.2 Background on ECG . . . 89
5.3 System Design . . . 92
5.4 Signal Processing Pipeline . . . 99
5.5 Electrode Evaluation . . . 101
5.6 Necklace vs. Ground Truth Evaluation . . . 106
5.7 In-the-wild study . . . 111
5.8 Discussion . . . 115
5.9 Summary . . . 117

Chapter 6: Lessons Learned & General Design Principles . . . 118
6.1 Wearable Form Factor Design . . . 118
6.2 Size Minimization . . . 120
6.3 Power Optimization . . . 122

Chapter 7: Conclusion and Future Directions . . . 125
7.1 Conclusion . . . 125
7.2 Future Directions . . . 126

Bibliography . . . 129

LIST OF FIGURES

Figure Number Page

1.1 New wearables unlock new opportunities by advancing the wearable space in three dimensions: (1) Accuracy, which means providing fundamentally better sensing data by moving closer to the source of the signals. (2) Continuity, which means sense longer by improving wearable comfort for more people, and is less interrupted by daily motions and noises. (3) Capability, which means new kinds of physiological data that existing wearables cannot sense continuously. 2

1.2 This dissertation aims to achieve both high sensing accuracy and high wearability, demonstrating a balance between effectiveness and practicality 4

1.3 This thesis aims to create novel wearable devices to enable superior, unobtrusive health intelligence in people's daily lives. The approach consists of (1) embedded system building, (2) novel longitudinal data investigation, and (3) real-world health insights analysis. 6

1.4 Thermal Earring: A wireless smart earring that demonstrates how leveraging a new sensing site significantly improves physiological monitoring accuracy, unlocking new applications for daily health and wellness. 10

1.5 PPG Earring is a wireless stud-hoop earring designed for continuous photoplethysmography (PPG) monitoring. By optimizing the system's size, weight, and mechanical attachment, it achieves more stable and continuous PPG signals than commercial smartwatches like Fitbit (as shown in the left spectrogram). The reliable PPG enables not only uninterrupted heart rate monitoring, but also extends opportunistic measurements, such as heart rate variability (HRV), breathing rate, and arrhythmia detection, beyond sleep and into everyday activities. 11

1.6 By exploring a novel wearable form factor, ECG Necklace can not only measure what existing smartwatches can do, but also enables continuous ECG monitoring, which existing wearables cannot achieve. This adds a new dimension to wearable sensing, supporting early detection of heart disease and capturing transient conditions as they evolve over time. 12

3.1 Thermal Earring is a first-of-its-kind smart wireless earring that enables a reliable wearable solution for continuous temperature monitoring. By leveraging the earring's unique position near the head, it significantly improves temperature sensing accuracy, enabling new health applications such as continuous fever monitoring, eating and exercise detection, acute stress detection, and women's cycle tracking. . . . 19

3.2 The Thermal Earring system with one dime coin as reference. (a) The back side of the Thermal Earring. (b) the front side of the Thermal Earring. (c) The zoomed-in view of the Thermal Earring components. 23

3.3 (a) The table of average current and battery life with different Bluetooth transmitting periods. (b) The plot of battery voltage drop during transmission with four different capacitors connected in parallel. 28

3.4 (a) The Received Signal Strength Indicator (RSSI) of the Thermal Earring Bluetooth packets. (b) The Thermal Earring's Bluetooth packet loss rate using Bluetooth receiver. (c) The floor plan of the space where we conducted the experiment. 30

3.5 (a) The Received Signal Strength Indicator (RSSI) of the Thermal Earring Bluetooth packets. (b) The Thermal Earring's Bluetooth packet loss rate using Bluetooth receiver. 31

3.6 (a) The Thermal Earring's earlobe temperature data on healthy and febrile people. (b) Day 1 when the participant was having a fever with an oral temperature of 39C (102.2F) at 19:10. (c) Day 2 after the fever was gone. The participant's oral temperature was 37.2C (98.96F) at 22:30. 33

3.7 The Thermal Earring temperature results for six participants during the eating study. 35

3.8 The Thermal Earring temperature results for six participants during the exercise study. 36

3.9 The Thermal Earring temperature results when room temperature changes. 38

3.10 The Thermal Earring temperature results across activities. 39

3.11 An example of the Thermal Earring's data on a participant for a day: (a) from Thermal Earring, (b) from Empatica Watch. 41

3.12 (a) A heuristic ambient temperature change detection model using a threshold. The empirical threshold is applied on the earlobe temperature minus dangling temperature. (b) A heuristics event detection model using the user-specific model. The plot shows the earlobe temperature delta over time computed using the average in a 30-minute sliding window minus the average in the window 30 minutes prior. The threshold is then applied to the computed results to detect various events. 42

3.13 (a) Heuristic algorithm results on detecting ambient temperature change. (b) Heuristic algorithm result of detecting temperature-increasing events (eating and stress), and temperature-decreasing events (exercising). 44

3.14 Thermal Earring temperature data vs. Empatica Watch temperature data during resting time. 45

3.15 The Thermal Earring temperature results from stressful events. 47

3.16 An example of Thermal Earring with fashion design. 49

4.1 (a) (b) The front and side view of PPG Earring with fashion design. (c) The smartphone app that connects to PPG Earring through Bluetooth and displays a real-time PPG signal. 53

4.2 Demonstration of how PPG light reflects under different conditions: (a) when the emitted PPG light is not on the blood pulse (low blood volume, absorbing less light), (b) when the emitted PPG light is on the blood pulse (high blood volume, absorbing more light), and (c) when motion artifacts cause a portion of the PPG light to be directly reflected by the skin. 57

4.3 The PPG Earring system PCB with a US penny coin as reference, and the battery for PPG Earring. 59

4.4 Demonstration of how to wear the PPG Earring (without the decorative components). 63

4.5 An example of a valid PPG signal window and its FFT results, an invalid PPG signal window and its FFT results, and their corresponding representations in the spectrogram. 64

4.6 (a) The PPG Ring is made from the same system as PPG Earring. (b) The PPG Watch is made from the same system as PPG Earring. (c) The demonstration of how users wear the PPG Ring and PPG Watch during the study. Both the PPG Ring and PPG Watch are attached to the user using an elastic band with velcro to adjust tightness. 67

4.7 The SNR of PPG signal from earring vs. ring vs. watch, (a) using green light, (b) using IR light, and (c) using red light. 68

4.8 (a) Example of the synchronized PPG Earring signal and the BioRadio signal. (b) The average absolute heart rate error of PPG Earring and Ring compared to the BioRadio ground truth signal. 70

4.9 (a) The average valid PPG percentage from the earring, ring, and watch while playing on the phone. (b) The average valid PPG percentage from the earring, ring, and watch while using the laptop. 71

4.10 (a) The spectrogram of PPG data from the earring during exercise. (b) The spectrogram of PPG data from the Fitbit during exercise. 73

4.11 (a) The valid percentage of PPG signal from PPG Earring and Fitbit for each participant during exercise. (b) The average valid percentage of PPG signal for each exercise. 74

4.12 The spectrogram of P6's eight hours of PPG data from PPG Earring compared to the Fitbit, along with a zoomed-in spectrogram of one hour of activity. 75

4.13 (a) The percentage of valid PPG signal during the whole day in the wild study from PPG Earring vs. from Fitbit. (b) The average SNR of PPG during the whole day in the wild study from PPG Earring vs. from Fitbit. 77

4.14 The comfort level comparison of PPG Earring vs. normal earring, and PPG Earring vs. Fitbit smartwatch. 78

4.15 The comfort rating scale results of PPG Earring and Fitbit on six comfort aspects of wearables. 80

5.1 (a) The ECG Necklace with fashion design. (b) An exploded view of the ECG Necklace, showing the PCB beneath the central pendant and the novel skin moisture-enhanced electrodes. c) The smartphone app visualizing ECG data wirelessly transmitted from the necklace. 86
5.2 (a) Example of an ECG waveform from a heart in normal sinus rhythm. (b) The electrode placement in clinical standard 12-Lead ECG and the necklace's electrode placement. 90
5.3 Demonstration of skin contact with (a) a simple dry electrode, (b) a gel electrode, (c) a dry electrode when pressed to the skin 91
5.4 The front and back sides of the ECG necklace system, with a US coin as reference for size. 92
5.5 (a) The demonstration of the necklace electrode that leverages natural human skin moisture as the ECG "gel". (b) The components of the necklace electrode. 93
5.6 ECG signals from different electrodes placement: (a) standard clinical lead I placement, (b) front center and back center, (c) front left and front right under the collarbones, (d) back left and back right. 95
5.7 Demonstration of wearing the ECG Necklace (without any fashion decorations). . . 98
5.8 The processing pipeline for ECG data. 99
5.9 Tested necklace electrodes with diameters ranging from 25 mm to 5 mm. 101
5.10 (a) The impedance of our electrodes (without moisture) and the standard adhesive electrode at different frequencies. (b) The impedance of our electrode at 10 Hz with different amounts of moisture level. 102
5.11 Example of an ECG signal obtained from the necklace electrode over a 20-minute period, with the zoomed-in plots on the signal at the start and at the end. 104
5.12 (a) The average ECG SNR obtained from electrodes with different diameters. (b) The average ECG signal quality converging time. 105
5.13 (a) The percentage of available valid ECG signal from the necklace during different activities. (b) The average SNR of the P, R, and T peaks in the ECG signals captured by the necklace. 107
5.14 An example of synchronized ECG signals obtained from the ECG necklace and the ground truth device, with the P, R, and T waves identified by the NeuroKit2 Python tool. 109
5.15 The average timing error of P, R, T peaks identified from the necklace ECG versus from the ground truth. 110
5.16 (a) The percentage of valid ECG signals by necklace versus by chest strap for each participant. (b) The average SNR results by necklace versus by chest strap for each participant. 112
5.17 (a) The overall comfort level of ECG Necklace and the Polar chest strap. (b) The comfort rating scale results of ECG Necklace and Polar chest strap. 114

ACKNOWLEDGMENTS

This dissertation marks one of the most significant milestones in my academic journey, and I am deeply grateful to everyone who has supported me along the way.

First, I would like to thank my advisors, Shwetak Patel and Vikram Iyer, for their support, guidance, and encouragement throughout my PhD. I feel incredibly fortunate to have had both of you as advisors. Thank you for creating a supportive and collaborative research environment. I am especially grateful for the freedom you gave me to pursue the ideas I was passionate about. Your trust enabled me to follow my heart and develop this dissertation. I also want to thank my committee members, James Fogarty, GSR Nadya Peek, and Martin Nisser, for helping shape and refine this dissertation. Your feedback has been invaluable in strengthening this dissertation and preparing me for the next stage of my career.

To my labmates and friends at UW: thank you for the countless hours we spent together, whether discussing research or simply chatting and laughing. Thank you to Richard Li, Joe Breda, Anandghan Waghmare, Ishan Chatterjee, Jason Hoffman, and Alvin Cao. It is incredible that we all joined the lab at the same time. We worked together, spent time together, and grew together. Thank you to Girish Narayanswamy, Jerry Cao, Zhihan Zhang, Zachary Englhardt, Vidya Srinivas, Alex Ching, Lisa Elkin, Poojita Garg, and Jiexin Ding for bringing fun and inspiring discussions to the lab. Thank you to Xin Liu, Matt Whitehill, Farshid Salemi Parizi, and Manuja Sharma for generously sharing your research experience and guiding us from when we first joined. And thank you to Kyle Johnson and Vicente Arroyos for sharing insightful thoughts and inspiring discussion.

I would like to thank my mentors from before my PhD: Gregory Abowd, Thad Starner, Cheng Zhang, and Chenren Xu. The research experiences I gained under your guidance inspired my passion for ubiquitous computing and set me on the path to pursue this field

further.

I also want to thank my industry mentors during my PhD. I was fortunate to intern at Google Health, Apple AI/ML, and Microsoft Research, and I am grateful for the guidance. Thank you to D. Shin, Saman Naderiparizi, Vaishnavi Ranganathan, and Bodhi Priyantha for your mentorship and support. Your perspectives and encouragement greatly enriched my research.

During my PhD, I was fortunate to mentor and work with many talented students. I want to thank Yujia (Nancy) Liu, Jiaqing Liu, Dilini Nissanka, Eric Martin, Tammy Yan, Jiayi Shao, and Ruiqing Wang. This dissertation would not have been possible without your contributions and hard work.

Finally, I am forever grateful to my parents, Yuling Zeng and Kaizhu Xue. Your constant love and support have helped me pursue my dreams and shaped the person I am today. I also want to thank my partner, Jason Wu, for always being there and for supporting me unconditionally through everything.

Chapter 1

INTRODUCTION

Computing has continuously evolved from desktops to smartphones to wearable devices, with each step bringing technology closer to our daily lives. Wearables represent a significant shift, redefining our relationship with computing. Unlike previous devices, wearables are worn directly on the body and are capable not only of computing but also of sensing and understanding human activities, context, health, and intentions. Among them, health and wellness are one of the most common use cases for wearables and are the focus of this dissertation.

Despite their promise, current wearables are limited in **form factor options, sensing accuracy, and capabilities**. The main devices on the market today are smartwatches, with a growing presence of rings and glasses. However, these devices may not suit all users, as some may find them bulky or intrusive. Moreover, current wearables' limited placement and form factors cause fundamental limitations that restrict their accuracy, continuity, and range of capabilities. For example, smartwatches are worn on the wrist, which is a bad location for sensing physiological signals because it is far from the heart, head, and other critical regions, and is highly susceptible to motion artifacts. These limitations make it difficult to reliably monitor signals such as heart rate, temperature, and stress. Additionally, current wearables cannot continuously capture many important physiological signals, such as electrocardiography (ECG) and blood pressure, presenting a large gap between wearable capability and clinical measurements.

This dissertation introduces the next generation of wearables by transforming everyday accessories into intelligent systems that subtly integrate into users' lives while unlocking new insights and applications. Specifically, this dissertation introduces practical smart jewelry, including Thermal Earring, PPG Earring, and ECG Necklace. These devices are designed to be small and lightweight enough to go unnoticed, passively worn with ultra-long battery

life. Most importantly, their unique placements on the body allow capturing advanced physiological signals, enabling new health capabilities that were previously difficult or impossible to achieve. Example applications include continuous heart disease monitoring, stress tracking, menstrual cycle awareness, and more. While this dissertation focuses specifically on smart jewelry, the underlying technology can be extended to other everyday accessories.

1.1 Contribution: Wearable Space Advancement

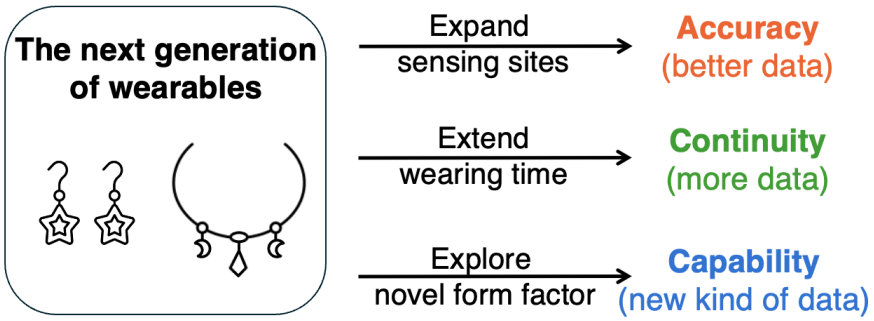

Figure 1.1: New wearables unlock new opportunities by advancing the wearable space in three dimensions: (1) Accuracy, which means providing fundamentally better sensing data by moving closer to the source of the signals. (2) Continuity, which means sense longer by improving wearable comfort for more people, and is less interrupted by daily motions and noises. (3) Capability, which means new kinds of physiological data that existing wearables cannot sense continuously.

This dissertation explores how common accessories can be transformed into smart wearables while preserving their original form factor. Developing such next-generation wearables can unlock new opportunities and expand the boundaries of the wearable design space. Figure 1.1 summarizes the three key dimensions (accuracy, continuity, and capability) advanced by this work, each of which is discussed in detail below.

1.1.1 Accuracy – better data

Wearable placement matters a lot. Different parts of the body are designed to do different things. With jewelry and new wearables in unique locations, we can expand wearable sensing beyond just the wrist to unlock new applications with high accuracy. Compared to

a smartwatch, which might be great for sensing hand movements but much less ideal for measuring physiological signals, smart earrings positioned close to the head might be able to sense the human in a totally different way. The earring's close proximity to the head and the core body can significantly boost the sensing accuracy for important vital signs like temperature and heart rate. And capturing signals with higher fidelity enables more accurate health monitoring and opens up new applications.

1.1.2 Continuity – more data

Some form factors, such as earrings and necklaces, are inherently more comfortable and appealing for some users because of their size, weight, and placement. If we can develop smart wearables in their original design and make them as comfortable as everyday accessories, people are more likely to wear them for longer periods without needing to take them off frequently. This allows for more continuous monitoring and improves the chances of capturing transient or rare health events that would likely be missed with only short-term use. In addition, exploring wearables in new form factors provides users with more options, improving adoption in daily life.

This increased temporal and population coverage is especially valuable for detecting sudden, life-threatening conditions such as heart attacks and strokes. Currently, physiological signals related to these events are often recorded only after the person has arrived at the hospital. With continuous and unobtrusive monitoring, these new wearables could capture the onset of critical conditions, contributing to a richer dataset of high-quality physiological signals that are currently lacking. This can support earlier detection, more accurate diagnosis, and even the prediction of serious health conditions before they occur.

1.1.3 Capability – new kind of data

While wearables show great potential for monitoring human health, such as heart rate and activity level, there are still many measurements that are limited in the clinical setup that current wearables cannot achieve yet. By reimagining novel form factors of our daily accessories, like rethinking their shape and design, we can unlock new clinical capabilities

to sense different kinds of physiological signals that existing wearables cannot monitor. For example, the necklace can provide continuous ECG monitoring leveraging its unique shape around the chest, while wrist-worn devices cannot.

1.2 Thesis Statement

The thesis statement is:

New wearable form factors can unlock new opportunities, advancing the wearable space in sensing accuracy, continuity, and capability. This dissertation demonstrates this by transforming conventional jewelry into smart wearable devices without changing their typical form factors, enabling novel health monitoring applications that are traditionally challenging or impossible to achieve.

1.3 Research Challenges

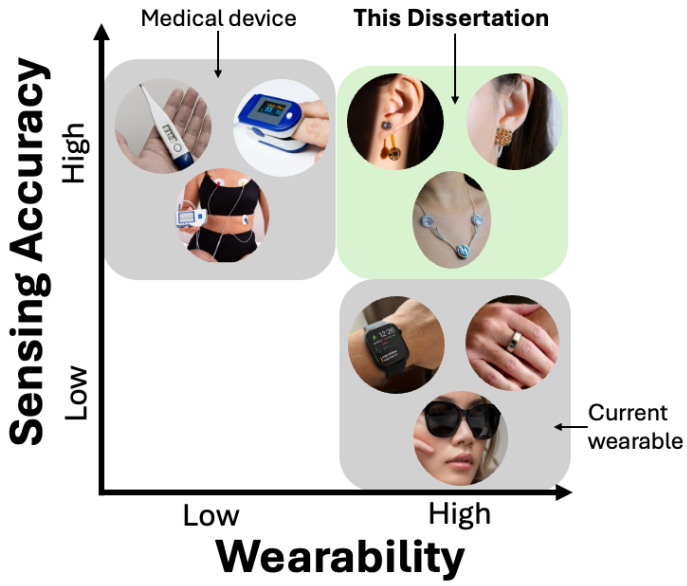

Figure 1.2: This dissertation aims to achieve both high sensing accuracy and high wearability, demonstrating a balance between effectiveness and practicality

Integrating technology into everyday accessories, such as jewelry, presents several significant challenges. To create wearable systems that are both functional and practical for daily

use, we must overcome constraints across size, weight, wireless communication, power consumption, and overall system integration. This section outlines the key technical challenges that must be addressed to make smart jewelry truly effective and wearable.

1.3.1 Size and weight

For wearable accessories to be adopted by users, they must maintain the original form factor of familiar items, which introduces strict limitations on both size and weight. To ensure practicality and comfort for continuous use, smart jewelry must be both compact and aesthetically appealing. Achieving a form factor that fits comfortably on the body is essential, particularly for accessories like earrings, which typically weigh less than 3 grams, while most smartwatches exceed 30 grams. Prior research has explored the use of earrings [111, 102] and necklaces [156, 157, 67, 33] for interaction and health sensing; however, these systems are usually much larger than ideal, which limits their suitability for long-term wear.

1.3.2 Wireless

For practical, everyday use, wearable systems must operate wirelessly to allow users to move freely without being constrained by cables. All sensed data must be processed and transmitted to a larger computing device, such as a smartphone, where users can access and interact with their health information in real time. Wireless transmission is often the most energy-intensive component of a wearable system, typically drawing high current (in mA) during short transmission periods (lasting milliseconds). The high power consumption of wireless operation makes developing the smart wireless wearable more challenging.

1.3.3 Power

Another critical constraint is power. Wearable devices must support continuous monitoring with a reasonable battery life, without requiring frequent recharging. Frequent charging introduces additional burdens on users and reduces the device's practicality in real-world scenarios. However, small form factors inherently limit the available space for batteries, constraining the overall energy capacity.

1.3.4 Interconnected constraints

These constraints of size, weight, wireless communication, and power are actually interconnected. The battery is typically the largest component in a wearable device, so any reduction in size or weight directly reduces battery capacity and battery life. At the same time, wireless communication consumes substantial power, particularly in small form factors operating at 2.4 GHz. So developing a functional and practical smart wearable is not just about optimizing these constraints individually. We must carefully balance all these constraints to make it functional and truly practical for everyday use.

This dissertation will demonstrate how to push the limits of size, weight, and power in wearable systems. It presents a set of smart jewelry devices that are not only technically capable but also comfortable, aesthetically appealing, and practical for long-term, real-world deployment.

1.4 Research Approach

Figure 1.3: This thesis aims to create novel wearable devices to enable superior, unobtrusive health intelligence in people's daily lives. The approach consists of (1) embedded system building, (2) novel longitudinal data investigation, and (3) real-world health insights analysis.

To achieve the next generation of wearable devices for health applications, all the re-

search projects in this dissertation take a bottom-up, end-to-end systems approach, as illustrated in Figure 1.3. This methodology spans the full design pipeline, from hardware integration and embedded software development, to smartphone Apps and signal processing, to in-the-wild user studies and end-user applications.

1.4.1 Compact low-power system design

The first component of this approach involves the design and implementation of ultra-compact, low-power, wireless wearable systems that are comfortable for continuous wear and capable of operating for up to one month. This design goal can minimize user burden and enable long-term physiological monitoring in real-world settings.

To achieve this, the development of functional and wearable smart jewelry centers around three core aspects: (1) system and hardware integration, (2) embedded computing for power-aware operation, and (3) energy-efficient wireless communication. Each of these components is carefully optimized to meet the stringent constraints of size, weight, and energy consumption imposed by the jewelry form factor.

In the hardware design phase, although we do not develop custom chips, we integrate state-of-the-art miniature components into a fully functional system. These components are usually exceptionally small and require precision assembly under a microscope, along with carefully designed multilayer printed circuit boards (PCBs) to minimize footprint while maintaining full functionality.

Power efficiency is optimized through embedded software design. We need to develop efficient embedded code into the tiny 3mm x 3mm microcontroller to coordinate sensing, local signal processing, and wireless communication. A key strategy for minimizing power consumption is using deep sleep modes whenever we identify the inactive time, which can reduce power consumption by an order of hundreds of times, depending on wake-up frequency.

Wireless communication, as a major contributor to energy consumption in wearable systems, is carefully optimized to reduce power draw. The research in this dissertation leverages optimized Bluetooth Low Energy (BLE) protocols. These strategies allow the

system to adaptively structure data transmissions based on the type and urgency of the sensed data. The device only exhibits microsecond-scale power spikes during transmission events and maintains near-zero power draw during deep sleep periods, thereby extending overall battery life.

1.4.2 Real-world in-the-wild study

The second component of the research method involves deploying the developed wearable devices in real-world, everyday environments. These deployments aim to ensure that the devices are not only functional but also comfortable, practical, and effective for long-term use.

While much of the prior research in wearable computing has focused primarily on demonstrating device functionality, this work prioritizes both functionality and wearability. Earlier studies often assume that wearability can be improved through engineering at a later stage, which is certainly a valid research approach. However, this approach may overlook important insights and applications that wearables can enable in real-world contexts. In contrast, this dissertation ensures that devices are comfortable for everyday use, enabling longitudinal, in-the-wild studies and demonstrating the value of real-world deployment through three key advantages:

- **Capturing transient events:** Many health conditions, such as heart arrhythmias, are transient and can occur unexpectedly. These conditions are difficult to capture during short laboratory studies. Continuous monitoring in everyday environments increases the likelihood of detecting these transient events.

- **Minimizing behavior changes in studies:** Laboratory settings can influence user behavior and physiological responses. For example, to study emotion or stress levels, it is essential to collect the data in a natural daily environment instead of a controlled lab study.

- **Enabling longitudinal insights from larger population:** Extended deployment allows for the collection of long-term data that can reveal trends and patterns not

observable in short-term studies. This type of data provides a deeper understanding of how physiological states change over time. Additionally, the ease of deployment and user comfort make it feasible to reach a broader and more diverse population, increasing the generalizability of the findings.

1.4.3 Data analysis to unlock new insights

The third component of this research involves analyzing real-world, longitudinal data to uncover new insights from these unique data streams. These insights enable applications that were previously difficult or impossible to realize. For example, through continuous monitoring of temperature at the earlobe, we discovered that earlobe temperature could be a new indicator of daily activities such as eating, exercise, and acute stress. These findings were made possible only through the analysis of data collected in natural, everyday settings.

This dissertation also presents signal processing methods and proof-of-concept demonstrations for detecting various activities using smart jewelry. It provides a valuable foundation for future research in automatic activity recognition and wearable sensing using earring-based devices. The goal of this initial exploration is to demonstrate the potential of unobtrusive wearables to support continuous, context-aware health monitoring in daily life.

1.5 Dissertation Structure

The dissertation is organized as follows. Chapter 2 presents the background and related work. The following chapters present three novel smart wearable systems and demonstrate the new applications they enable.

1.5.1 Thermal Earring

Chapter 3 presents Thermal Earring, a first-of-its-kind wireless, smart earring that enables a reliable wearable solution for continuous temperature monitoring from the earlobe. As shown in Figure 1.4, Thermal Earring is in the form factor of real earrings, measuring a maximum width of 11.3 mm and a length of 31 mm, weighing 335 mg, and with a battery life of one month. The practical and comfortable form factor allows us to conduct the first-

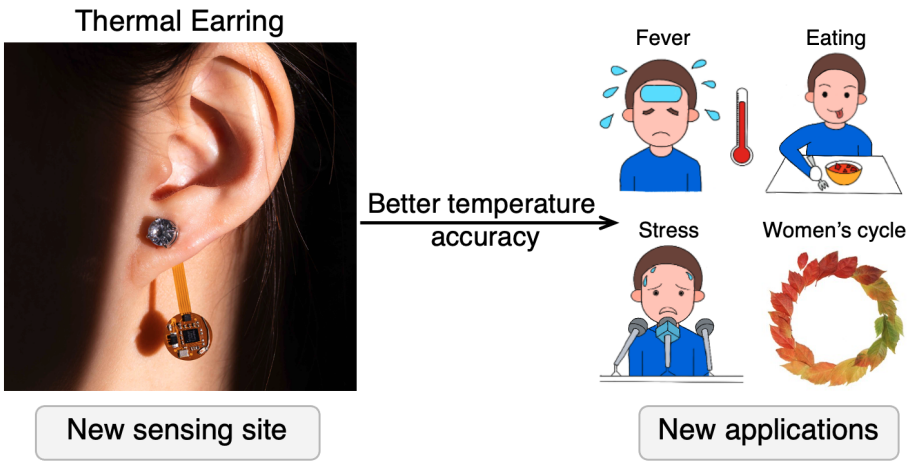

Figure 1.4: Thermal Earring: A wireless smart earring that demonstrates how leveraging a new sensing site significantly improves physiological monitoring accuracy, unlocking new applications for daily health and wellness.

ever investigation of earlobe temperature dynamics in relation to health and daily activities in the wild. The new earlobe sensing site not only demonstrates much higher accuracy than wrist-worn smartwatches because of the proximity to the head and core body, but also unlocks new applications for daily health and wellness tracking. We demonstrate Thermal Earring's effectiveness in continuous fever detection and recovery monitoring, responses to eating, exercise, and acute stress, and its potential for menstrual cycle tracking. This work highlights how exploring new sensing locations can unlock applications previously unattainable with conventional wearables.

1.5.2 PPG Earring

Chapter 4 presents PPG Earring: a wireless stud earring designed for heart health monitoring using PPG. This innovative device functions as a general health monitor, measuring what current smartwatches can measure too, including heart rate, activity levels, and body temperature. PPG Earring, as shown in Figure 1.5, measures 14 mm in diameter, weighs 2.0 g, and offers 21 hours of continuous sensing. The PPG Earring system is integrated into the earring back, allowing for different and changeable fashionable designs on the front.

PPG Earring addresses the common motion artifacts problem in wearable heart rate

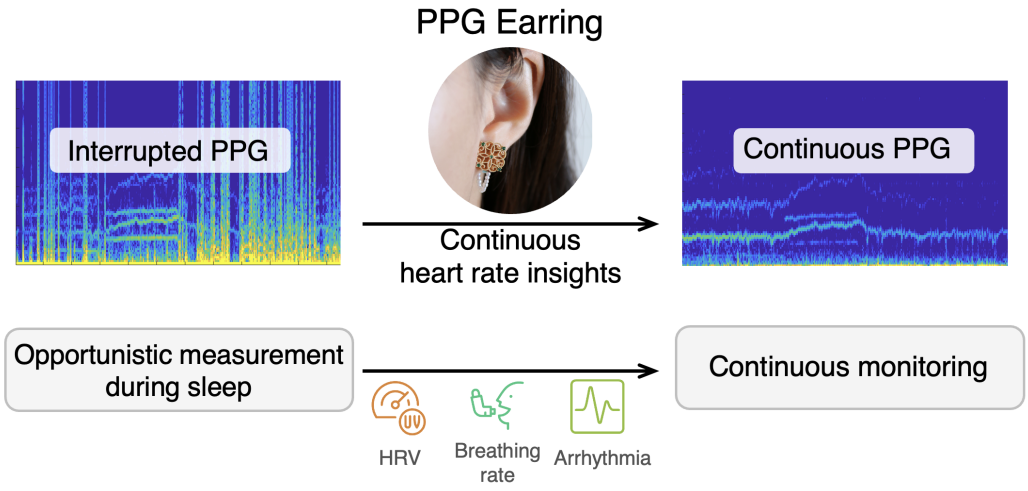

Figure 1.5: PPG Earring is a wireless stud-hoop earring designed for continuous photoplethysmography (PPG) monitoring. By optimizing the system's size, weight, and mechanical attachment, it achieves more stable and continuous PPG signals than commercial smartwatches like Fitbit (as shown in the left spectrogram). The reliable PPG enables not only uninterrupted heart rate monitoring, but also extends opportunistic measurements, such as heart rate variability (HRV), breathing rate, and arrhythmia detection, beyond sleep and into everyday activities.

monitoring by optimizing size, weight, and attachment methods. While current wearables suffer signal interruptions during motion due to the light-based nature of PPG sensing, PPG Earring leverages the earlobe's minimal motion and stable contact to deliver uninterrupted, continuous PPG signals. This enables continuous heart rate monitoring and supports advanced measurements such as HRV, breathing rate, and arrhythmia detection. In our exercise study, PPG Earring captured valid heart rate data $91.74 \pm 4.84\%$ of the time, compared to 61.76 ± 6.74 % for Fitbit. In a day-long in-the-wild study, it maintained valid readings 86.29 ± 2.96 % of the time, compared to Fitbit's 54.88 ± 4.63 %. All participants reported it to be as comfortable as their regular earrings, and most expressed a strong willingness to wear it every day.

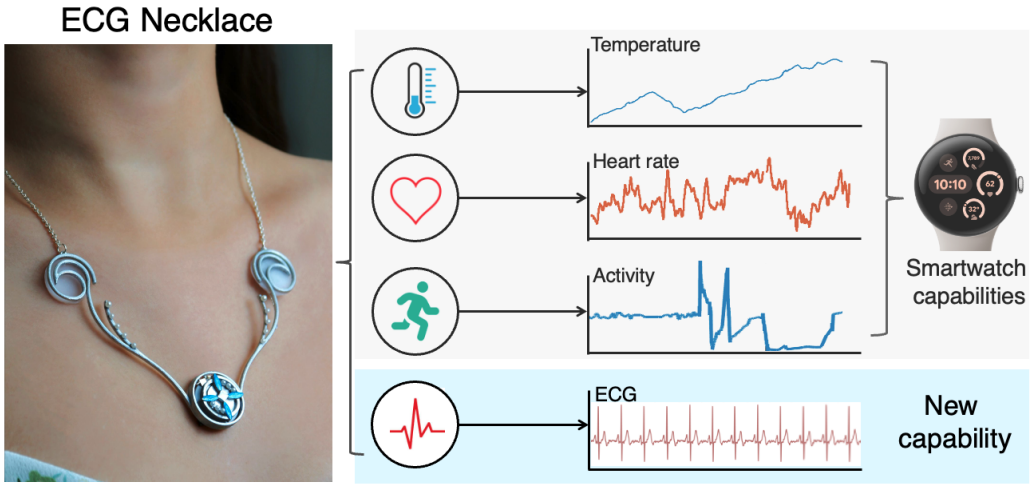

Figure 1.6: By exploring a novel wearable form factor, ECG Necklace can not only measure what existing smartwatches can do, but also enables continuous ECG monitoring, which existing wearables cannot achieve. This adds a new dimension to wearable sensing, supporting early detection of heart disease and capturing transient conditions as they evolve over time.

1.5.3 ECG Necklace

Chapter 5 presents ECG necklace, a wireless necklace for longitudinal ECG monitoring with skin moisture-enhanced electrode. Electrocardiogram (ECG) is crucial for diagnosing heart diseases, the leading cause of death worldwide. However, traditional ECGs perform intermittent monitoring, missing transient heart anomalies that occur in daily life. Continuous ECG monitoring can enable early detection of "silent" heart diseases, but cannot be performed on commodity smartwatches, which have limited space for electrode placement. Our necklace device, shown in Figure 1.6, offers continuous ECG sensing that is comparable to standard Lead I ECG using electrodes positioned under the left and right collarbones. Our compact necklace prototype has a pendant diameter of 2.2 cm and achieves a battery life of 88 hrs. We develop a custom dry electrode design that leverages natural skin moisture to achieve signal quality comparable to industry standard adhesive gels while maintaining long-term user comfort. We characterize this novel wearable design space by evaluating electrode placement and size, and assess the trade-offs between ECG signal quality, clinical

value, and aesthetic considerations. In real-world testing across everyday activities with eight users, the necklace captures valid ECG for 89.4 ± 15.21 % of the time while using a laptop, $89.3 \pm 14.42\%$ while talking, and $92.78 \pm 8.86\%$ during smartphone use. We further show through comparisons with an FDA-approved ECG monitor that ECG necklace can resolve key features of the signal such as the P, R and T waves to within 3.5-16 ms (0.5-2.5 samples at 150 Hz) in a typical 500-1000 ms heartbeat cycle, showcasing its potential as a practical solution for daily ECG monitoring.

1.5.4 Design Principles and Conclusion

At the end, in Chapter 6, we discuss the lessons learned from these research projects and the general design principles for low-power wearables. Chapter 7 concludes and discusses future directions.

Chapter 2

RELATED WORK

2.1 Smart Jewelry and Fashion-related Wearable Devices

Smart jewelry is an emerging class of wearable devices that seeks to combine fashion and function by integrating sensing into jewelry accessories. Vega et al. have highlighted the concept of integrating technology with beauty products, proposing wearable computing in forms like artificial nails and makeup [139]. Previous research in smart jewelry has explored various functional items: smart necklaces, bracelets, glasses, rings, earrings, and nails. Smart necklaces have been utilized for applications such as silent speech recognition [156], eating detection [157], medication adherence [67], and posture correction [33]. Research on bracelets has spanned areas like user interaction [51, 134], health monitoring [50, 7], and personal safety automation [106]. Smart glasses have been developed and commercialized[1, 135, 99], smart glasses have been used for interaction [81], industry training [41], and clinical applications [95]. Rings have also been explored for their interactive [12, 159, 158, 122] and health monitoring capabilities [101, 87]. However, earrings have been less explored, with limited research focusing on wellness tracking [111, 102] and audio sensing [65, 108], often featuring larger than desired form factors. The smart nail has been investigated as a gestural input surface [68] and for sensing fingernail deformation [62]. Additionally, nose rings have been developed for electrical trigeminal stimulation [23]. A significant challenge in the development of smart jewelry is maintaining the compact size typical of traditional jewelry—a goal that most of the current research has not yet achieved. Maintaining this compactness is essential for both the practical usability and aesthetic appeal of these smart jewelry devices.

Researchers have augmented human skin with stylish interfaces, such as electronics tattoos [15, 59, 16, 6] and paintings [69, 77, 124]. Other innovations that combine smart wearables with fashion include smart clothes and buttons [92, 133, 138, 43], smart textiles

[152, 132, 77], as well as novel concepts like smart hair [96] and smart makeup [86]. These developments highlight a trend towards integrating technology with stylish accessories, enhancing both functionality and aesthetic appeal.

2.2 Body Temperature Monitoring

Body temperature is a crucial vital sign that can be measured or estimated using a variety of methods. Specifically, elevated core-body temperatures were found to be the primary predictive symptom for many viral infections, including influenza and COVID-19 [20, 56, 57]. Although invasive techniques such as arterial catheters [63] or e-pills [76] provide the most accurate measurement of core body temperature by entering the body through arteries or intestines, they are not suitable for everyday use. Non-invasive thermometers, such as oral, tympanic thermistors, and infrared temporal thermometers, are more commonly used but require specialized devices that may only be used a few times a year [104].

Past research has attempted to develop more accessible and ubiquitous methods of temperature sensing by incorporating temperature sensors into wearable devices [9, 46, 60, 19], utilizing thermal cameras [146, 89], or leveraging existing temperature sensors on smartphones [22]. Wrist-mounted temperature sensors have been extensively explored for core-body temperature sensing [60, 9, 46], but they have struggled to provide accurate measurements due to noisy temperature signals from the wrist. Infrared thermopile sensors mounted on headphones have been used to monitor tympanic temperature directly and longitudinally [19], but require the user to wear their headphones to make measurements, which may not be suitable in many environments. Another approach for temperature sensing is using thermal cameras on facial video [146, 89]. However, these sensors are expensive and not suitable for personalized health sensing applications. In addition to dedicated hardware, researchers have developed software models that map smartphone temperature to core-body temperature when the phone is in contact with the user's head [22]. However, this method requires a dedicated interaction to make spot estimates rather than passively sensing temperature longitudinally.

2.3 PPG Sensing

PPG sensing provides valuable insights into heart rate and cardiovascular health, making it a popular choice for wearable health monitoring. Many commercially available devices, such as the Apple Watch and Google's Fitbit, have integrated PPG technology to track heart rate and detect anomalies like arrhythmias. More recently, wearables like the Oura Ring have also incorporated PPG sensors for heart rate monitoring from the finger. In addition to these mainstream wearables, researchers have explored PPG sensing in other form factors, such as smart glasses [38, 61]. Glabella [61] investigated PPG sensing on smart glasses and used it to estimate blood pressure. PPG sensing around the ear has also gained attention, with mainly earbuds being studied for their potential to detect heart rate signals through in-ear PPG measurements [105, 47]. There have also been prior explorations of smart earrings for PPG sensing [111, 118]. These designs often result in a significantly larger form factor, presenting challenges in terms of user comfort and signal quality due to motions caused by device weight. Besides sensing PPG using wearables, researchers have also explored PPG sensing using phone camera light [142], and there are also remote PPG sensing by capturing subtle facial color changes using cameras [110, 144, 109].

PPG sensing being affected by motion artifacts is a well-known problem and there have been a lot of explorations using various methods to address the motion artifact problems, such as using an accelerometer signal on the same wearable device to cancel out the motion signal in PPG [91, 18], or use advanced deep learning methods to recover PPG signal from heavily distorted signal [26, 17]. Besides using PPG for heart health monitoring, researchers have extended the PPG sensing capability to other activity sensing or interaction applications [151, 25].

2.4 ECG Sensing

ECG is a common medical test that measures the electrical activity of the heart. There have been numerous research efforts to make ECG sensing more accessible to common people in daily life.

ECG Holter monitors are usually hand-sized devices with wires connected to electrodes

attached to the user's body. More recently, there are patches like ECG Holter monitors with sticky electrodes attached to the chest. Frontier X2 is a chest strap continuous ECG monitor that users wear around the chest.

Apple Watch and Fitbit are commercial wrist-worn wearables that support single-lead ECG sensing by putting the finger from the other hand on the crown of the smartwatch. KardiaMobile is a portable, non-wearable, single-lead ECG with two conducting surfaces where users can place their fingers from their left and right hands to take a measurement. However, all of these above methods require users to manually initiate the ECG measurement by placing their fingers on the conducting surfaces, limiting their ability to provide long-term, continuous cardiac monitoring.

Bhattacharya et al. proposed a wireless electro-mechanical E-Tattoo for ECG and Ballistocardiogram (BCG) sensing, which leverages an adhesive layer to stick to the skin [16]. Researchers have explored reconstructing ECG signals from heart vibrations [28, 103] and UWB [145]. Vibcardiogram estimated ECG from wrist-worn wearable [28]. HeartQuake estimated ECG patterns from geophone-based sensing on a bed mattress [103].

2.4.1 ECG Dry Electrode

Traditional wet electrodes, despite providing high-quality ECG signals, are unsuitable for long-term monitoring due to issues like gel evaporation and skin irritation. Researchers have been developing gel-free dry electrodes for long-term ECG monitoring.

Smartwatches provide ECG measurements when a finger is placed on the crown [8, 2]. Devices such as the Apple Watch and Fitbit leverage the human finger, which is one of the most moisturized parts of the body, to enable ECG sensing with dry electrodes. Similarly, the KardiaMobile device requires users to touch two dry electrodes with fingers for ECG sensing [70]. Beyond leveraging finger moisture, the Frontier device employs chest strap pressure to increase the electrode-skin contact [52] with a dry electrode, although this pressure may affect comfort for some users.

Kim et al. present a detailed overview of research on soft and dry electrodes, identifying key characteristics — high conductivity, strong adhesion, stretchability, and biocompat-

ibility, which are essential for high-performance dry electrodes [73]. Material scientists have explored various conductive materials for dry electrodes, including metals, conductive carbon-based materials such as graphene [131, 78] and carbon-nanotube [83], and conductive polymers such as PEDOT:PSS [84, 42] and polypyrrole (PPy) [154]. Beyond different materials, researchers have also explored different methods for adhesion to the skin [85], including gecko-inspired microstructures [74] and octopus-like patterned structure [31, 32] to achieve adhesion through van der Waals force. To enhance skin-electrode contact and reduce the impedance mismatch, researchers have explored materials modification and micro-structure modification for achieving conformal contact. This includes altering material properties, such as adjusting the Young's modulus [155] and bending stiffness [82], and innovating structural designs like ultra-thin films and tattoos [97, 48, 66].

Chapter 3

THERMAL EARRING

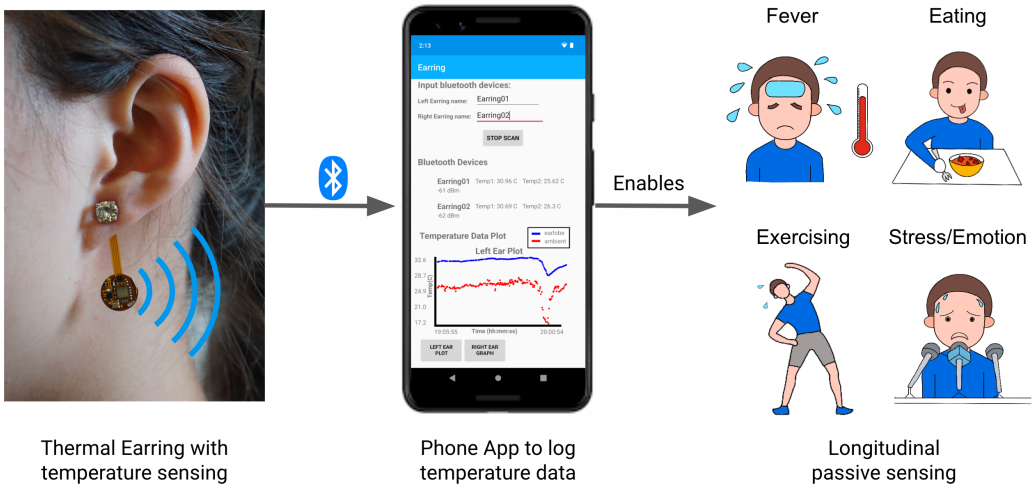

Figure 3.1: Thermal Earring is a first-of-its-kind smart wireless earring that enables a reliable wearable solution for continuous temperature monitoring. By leveraging the earring's unique position near the head, it significantly improves temperature sensing accuracy, enabling new health applications such as continuous fever monitoring, eating and exercise detection, acute stress detection, and women's cycle tracking.

3.1 Introduction

Wearable devices with sensors have gained significant popularity in recent years and are becoming a ubiquitous part of daily life. Nearly 40% of US households possess wearables like smartwatches [126]. Wearables which are often in contact with a user's body throughout the day offer unique opportunities for interaction, health sensing, and activity tracking. This has prompted exploration of various accessories for sensing, including smart rings [101, 12], smart glasses [141], fitness earbuds [105, 47], and smart clothing [138, 130]. We observe however that an entire class of common accessories worn by millions of people every day

has been largely ignored: jewelry. For example, in the United States alone, 76% of women have pierced earlobes which is nearly twice the current adoption rate of smartwatches and there is a growing trend of men embracing earrings, indicating its widespread acceptance as a fashionable choice [44].

Earrings, in particular, present a unique opportunity for continuous monitoring of physiological signals. Unlike headphones and earbuds, earrings are typically worn continuously for most of the day and could be used as a continuous sensing platform. Moreover, earrings have the further advantage of being tightly coupled to a user's body in contrast to watches which can easily move and shift against the skin. In addition to these form factor considerations, their attachment to a user's head provides key sensing advantages. Emotions such as embarrassment or other stressors can cause a person's face and ears to "turn red," inducing substantial blood flow to the head and ears. One result of these changes in blood flow is a change in temperature. Body temperature is an important vital sign but challenging to sense continuously. Traditionally, the temperature is measured with a thermometer orally, axillary, in-ear, or by skin. However, using a thermometer can only provide sporadic measurements that might miss important temperature data points. For example, a fever can be intermittent, leading to fluctuations in temperature over the course of a viral infection. Similarly, the ability to measure fine-grained temperature changes could yield new insights into the wearer's daily activities or novel health signals.

We present Thermal Earring, a first-of-its-kind wireless, smart earring that enables a reliable wearable solution for continuous temperature monitoring. As shown in Figure 3.1, the hardware prototype is in the form factor of real earrings, measuring a maximum width of 11.3 mm and a length of 31 mm, weighing 335 mg, and with a battery life of one month. We investigate the earlobe temperature's real-world use cases by gathering data from 5 febrile patients and 20 healthy participants, and demonstrate Thermal Earring's ability in fever detection. Further, we observed in our user testing that the relative change in earlobe temperature can identify activities such as eating and exercise, as well as stressful events such as public speaking and exams. Rather than attempting to convert earlobe temperature into core body temperature, which generally remains around 37 °C (98.6 °F) except during fever, our focus centered on exploring novel applications based on relative changes in earlobe

temperature within everyday contexts.

Achieving continuous body temperature sensing on wearables is challenging and remains an open problem in the research community. Although smartwatches and rings such as Apple Watch, Fitbit, and Oura Ring offer skin temperature monitoring on the wrist or finger, skin temperature data from extremities is noisy due to the distance from the core body [53] and is more susceptible to motion artifacts and contact with hot or cold surfaces. As a result, these devices only provide one average temperature reading per day, primarily from data during sleep. In contrast, Thermal Earring takes advantage of the unique position of earrings on the head and tight coupling to the earlobe to provide a reliable measurement of earlobe temperature. We find in initial trials across six users in the wild that earlobe temperature remains stable during periods of rest with a maximum standard deviation of 0.32 °C (0.58 °F) compared to a watch that varies by over 0.72 °C (1.3 °F). This is promising for future applications such as ovulation tracking which requires 0.28 to 0.56 °C accuracy [128].

Accurately measuring the earlobe skin temperature requires also isolating the effect of ambient temperature changes, which is one of the fundamental challenges in wearable body temperature measurement. One way to measure these effects would be to add a second temperature sensor solely dedicated to capturing ambient temperature. This is however not possible on a watch form factor where much of the surface area is coupled to the skin or within 1 cm. We observe that common earring designs include a dangling decorative portion that does not make contact with the body. Leveraging this observation, we propose a novel dual temperature sensors system that incorporates an additional temperature sensor in the dangling part to capture the ambient temperature. This unique design enhances the reliability and accuracy of temperature measurements from wearable devices, surpassing the temperature accuracy achieved by existing smart watch devices.

Developing a wireless sensor in an earring form factor has many sensing advantages, but presents multiple technical challenges. The system must be small and lightweight for comfortable use. These constraints on size also introduce fundamental constraints on the power consumption of the system due to the limited energy density of batteries. For example, in addition to highly limited capacity, small batteries have severely limited current

output making it challenging to support radios for transmitting the temperature data. To design a system within these strict form factor constraints we leverage the highly integrated nRF52 Bluetooth SoC which is available in a highly miniaturized 3 mm x 3 mm package and the 1.5 mm x 1.5 mm temperature sensor (TI HDC2010). We observe however that the battery and microcontroller consume a significant portion of the size, which may exceed the available space on a user's earlobe. Therefore, we positioned larger components, such as the microcontroller and battery, in the dangling part of the earring. In contrast, the small temperature-sensing unit is positioned directly on the user's earlobe. In addition, we optimize the power consumption of the system to operate on a miniaturized battery, capable of sustaining continuous discharge currents of 0.25 mA. Despite the 5 mA requirement during Bluetooth transmission, we demonstrate its ability to run continuously for a month.

To summarize, Thermal Earring has the following **contributions**:

- We design the first wireless smart earring platform for continuous temperature sensing, demonstrating a small and comfortable size (with a maximum width of 11.3 mm and a length of 31 mm), light-weight (335 mg), and ultra-low-power (14.4 uW, 28 days battery life), in a common dangling earring shape.

- We develop a novel dual temperature sensor design to differentiate human body temperature change from the environment temperature change. We further conduct experiments to demonstrate the Thermal Earring's ability to disambiguate the effects of environmental temperature change from valuable body temperature changes.

- We conduct real-world experiments in febrile patients demonstrating fever detection using earlobe temperature.

- We perform the first-ever investigation of the relationship between earlobe temperature and a variety of daily activities, demonstrating earlobe temperature changes related to eating, exercise, and periods of acute stress. In addition, we perform in-the-wild experiments and confirm the temperature changes caused by these daily activities in natural scenarios. The initial exploration results provide a basis for future

automatic activity detection.

3.2 Thermal Earring System Design

When designing a smart earring, it is crucial to consider various constraints, including size, weight, and power consumption. The earring should fit comfortably, be lightweight, and have a long battery life to avoid frequent charging or battery replacement. However, the limited battery capacity due to size and weight limitations requires careful co-design for a low-power and small-size system.

Inspired by dangling earrings, the Thermal Earring adopts a similar design. The small temperature-sensing unit is placed on the earlobe, while larger components like the microcontroller and battery are discreetly placed in the dangling part. This design ensures a compact and comfortable structure that maintains the appearance of a typical dangling earring. In this section, we introduce the key components of the Thermal Earring system, including the temperature-sensing unit, microcontroller, wireless communication, and battery. We also evaluate the system's battery life and wireless performance.

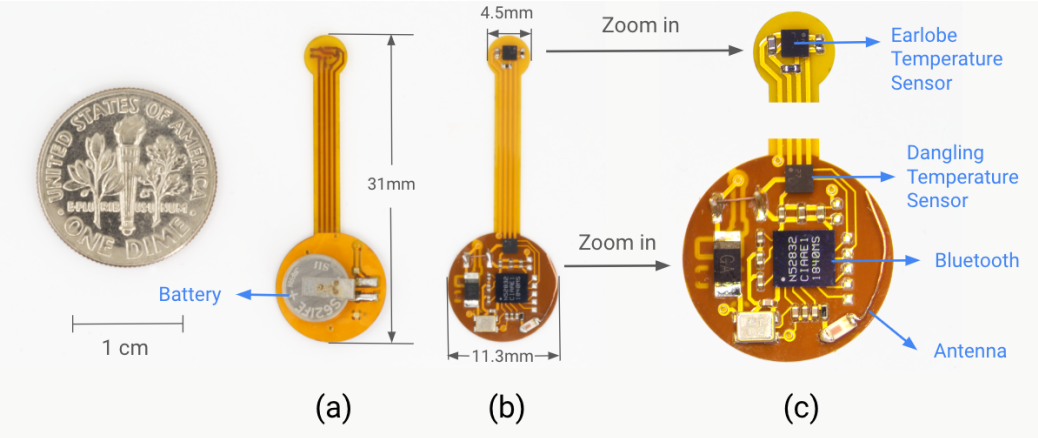

Figure 3.2: The Thermal Earring system with one dime coin as reference. (a) The back side of the Thermal Earring. (b) the front side of the Thermal Earring. (c) The zoomed-in view of the Thermal Earring components.

3.2.1 Dual Temperature Sensors Design

The Thermal Earring features a dual temperature sensor design that can sense the earlobe and the ambient air temperature simultaneously. This design helps differentiate the user's body temperature changes from environmental changes. One temperature sensor is designed to directly contact the earlobe skin for sensing earlobe temperature, while the other one is embedded into the dangling part to sense the ambient air temperature around the ear. The addition of the dangling temperature sensor provides data to differentiate environmental changes, such as walking from a temperature-controlled building to outdoor environments, from body temperature changes. This design effectively overcomes the challenge that skin temperature changes with the environmental temperature and enhances its accuracy and utility in monitoring changes in body temperature.

We implement Thermal Earring's temperature sensing using the HDC2010 temperature sensor from Texas Instruments. We choose this sensor for its small size (1.49 mm $\times$ 1.49 mm), low power consumption (0.9 uW), and high accuracy. The HDC2010 is capable of providing temperature accuracy within $\pm 0.2°C$, while consuming only 0.3 uA of average current when measuring temperature once per second. The two temperature sensors are connected to a Bluetooth microcontroller through the same I2C line but with different I2C addresses for synchronized data acquisition.

3.2.2 Microcontroller and Wireless Communication

The sensed data from the wearable requires wireless communication to a smartphone or a computing device for further computing and analysis. However, the microcontroller and wireless communication are orders of magnitude more power-intensive than the sub-microwatt temperature sensors, which can significantly impact the battery life of the wearable device. Wireless communication involves transmitting high-frequency RF signals in the GHz range, which typically constitutes the most power-consuming aspect of a wearable system. Therefore, it is critical to carefully select a wireless communication method that is both low-power and compact in size for optimal performance in the Thermal Earring system.

Previous research has explored the use of backscatter communication for sending data from the wearable or Internet of Things (IoT) device to a computer. However, this method requires a customized carrier wave transmitter or a customized radio receiver, which makes it difficult to communicate directly to a user's smartphone. In contrast, Bluetooth chips offer a longer wireless range and compatibility with commercial phones, albeit with slightly higher power consumption. Considering these factors, we chose to develop wireless communication using the NRF52832 Bluetooth chip. This ultra-compact chip is packed in a wafer-level chip-scale package, measuring 3mm by 3mm in size and weighing 6.8mg. Furthermore, it incorporates an ARM Cortex M4 processor with a floating point unit for computing tasks in the same compact package making it an ideal choice for Thermal Earring.

Bluetooth Advertising

We utilize Bluetooth in advertising mode, which is well-suited for the Thermal Earring's short-temperature data transmission needs. Bluetooth advertising mode is a feature that enables Bluetooth devices to broadcast their presence and identity to other Bluetooth-enabled devices such as smartphones. This mode allows embedding customized data of up to 31 bytes in short advertising packets. Bluetooth advertising is significantly lower power compared to establishing a continuous Bluetooth connection which requires sending a series of packets to synchronize and negotiate the frequency hopping sequence as well as regular transmissions to keep the connection alive. The series of packets needed to set up the connection requires significant energy over a short time period which is significantly greater than our small sub-centimeter battery can support. We observe the voltage begins to decrease upon transmitting a packet due to its current limitation. Operating in advertising mode with sufficient time between packets enables the battery voltage to recover prior to the next transmission. Given that each temperature data point sent by the Thermal Earring can be compressed into two bytes, it is more energy-efficient to transmit the data using Bluetooth advertising mode instead of maintaining a constant Bluetooth connection with the smartphone.

The Bluetooth chip communicates with two temperature sensors via I2C and packs the

temperature data into advertising packets. These packets adhere to the standard Bluetooth advertising structure, beginning with a fixed preamble pattern, access address, header, payload, and the Cyclic Redundancy Check (CRC). The payload of the Bluetooth packet contains the temperature data and the customized name of the Thermal Earring. Each temperature data is wrapped as service data, starting with a 2-byte Universally Unique Identifier (UUID) of 0x1809, which corresponds to health temperature data in the Bluetooth protocol. The customized name of the Thermal Earring typically ranges from four to ten bytes. For our experiments in this paper, we used names such as "Earring01" to "Earring14," which occupy nine bytes.

In the Thermal Earring system, there are several programming pins for programming the NRF52832 chip. Bluetooth can be configured to transmit advertising packets at different intervals to balance the need for visibility with power consumption. We also conducted experiments to explore how different Bluetooth advertising intervals affect the Thermal Earring's battery life. The results are presented in section 3.2.5. Overall, our approach provides an efficient way to transmit temperature data in wearable devices using Bluetooth advertising mode without draining the battery.

3.2.3 Battery

In the development of wearable devices, the power source is a critical component that must have high power capacity while being compact and lightweight. The energy limits of currently available battery technologies make batteries the largest and heaviest components in such small centimeter-scale devices. To achieve our target form factor, we select the Seiko MS621FE lithium manganese battery for Thermal Earring. This rechargeable battery offers a capacity of 5.5 mAh, with a slim 6.8 mm diameter and a weight of 0.23 grams. While hearing aid batteries offer higher capacities they are not rechargeable. Although MS621FE can generate a maximum output voltage of 3V, its standard discharge current is only 15uA with a maximum continuous discharge current of 0.25mA. While this is sufficient to support the temperature sensor and nRF52832 in sleep mode, it is not sufficient to robustly start up or transmit Bluetooth packets which both require 5 mA of current. We observe however

that both the startup and Bluetooth transmissions are transient operations that only require short pulses of high current. To address this, we add a low equivalent series resistance 100uF capacitor (F980G107MSA) in parallel with the battery. The 100uF capacitor buffers charge while the system is in sleep mode, and can then provide a pulse of mA-level current by quickly discharging itself when needed. We note that in addition to size and capacity, this capacitor presents a trade-off between low Equivalent Series Resistance (ESR, the ability to source high current) and the leakage current when it is in sleep mode. We select this specific capacitor to minimize leakage while providing a sufficient buffer to transmit Bluetooth packets reliably.

3.2.4 The Final Earring System

The final prototype of the Thermal Earring is shown in Figure 3.2. Built on a flexible printed circuit board (PCB), the final prototype of the Thermal Earring can exhibit the same level of flexibility and movement as traditional earrings. The ambient temperature sensor and Bluetooth microcontroller are located on the front side of the earring's dangling part, while the battery is placed on the backside. The earlobe temperature sensor is situated on the small segment attached to the user's earlobe. The earlobe part and the dangling part are positioned approximately 3 centimeters apart, which falls within the dangling length of common earrings (2 to 6 centimeters)[93]. It is worth noting that the dangling length of the Thermal Earring can be customized without compromising system performance. However, setting it too short may affect the accuracy of environmental temperature sensing, as it brings the dangling temperature too close to the body. The earring is attached to the back of the user's earlobe using commercial magnetic earrings, with the PCB attached to the back magnet, and another magnet positioned on the front of the earlobe to hold the earring in place. To ensure user safety and comfort, we integrated a layer of Kapton to insulate the electronic components from the user's skin. The entire earring system is compact, measuring 4.5 mm in diameter for the part attached to the earlobe, and 11.3 mm in diameter for the dangling part. The length is 31 mm including the thread in between, while the thickness is 3.46 mm. With a weight of just 0.335 grams, the Thermal Earring is significantly lighter

than the average weight of a commercial earring (around 3 grams) [64], which allows for the integration of artistic enclosures and gemstones in future designs. In section 5.8.1 we also showcase an example of fashion design for the Thermal Earring.

3.2.5 System Evaluation

Battery Life

Transmitting Period	Average Current	Battery Life
1s	11.8 uA	5 days
5s	6.1 uA	17 days
10s	4.8 uA	28 days

(a)

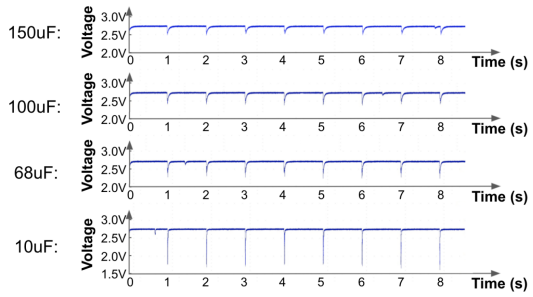

(b)

Figure 3.3: (a) The table of average current and battery life with different Bluetooth transmitting periods. (b) The plot of battery voltage drop during transmission with four different capacitors connected in parallel.

We investigate the impact of different transmission frequencies on the battery life of the Thermal Earring. Three Thermal Earrings were programmed to transmit temperature data at intervals of one second, five seconds, and ten seconds, respectively. The battery life was tested using the MS621FE coin battery as previously discussed, and the average current drawn by each Thermal Earring was measured using a Keysight U1282A multimeter over one hour. The time duration between the reception of the first and last Bluetooth packets on the smartphone was counted as the battery life, and the results were summarized in Figure 3.3 (a).

The average current compromises periodic high pulses (approximately 5 mA for 400 us) during Bluetooth transmission and sleep current (approximately 2.4 uA). A lower transmission frequency reduces the instances of high current, bringing the average current closer to

the sleep current. Nevertheless, even with the parallel capacitor, the system still draws up to 0.8 mA from the battery during transmission, surpassing the battery's maximum continuous discharge. The battery can still source it due to the very short duration (400 us), but it reduces the actual capacity[148], resulting in a shorter battery life than ideal.

Moreover, to assess the parallel capacitor's effectiveness and provide design insights for capacitor selection, we also demonstrate the battery's voltage change during high current pulses. Figure 3.2.5 (b) illustrates the battery voltage with four different capacitors. During Bluetooth transmission every second, the battery with larger capacitors (150 uF, 100 uF) exhibited a temporary up to 0.3V drop, which quickly recovered after the transmission was completed. Conversely, the 10uF capacitor led to a significant battery voltage drop to 1.5V, making the battery unable to recover and power the system after approximately 20 seconds. Despite better current supply, larger capacitors are larger in size and weight. After careful trade-off consideration, we chose the 100 uF capacitor (Kyocera F980G107MSA) for our final design.

Overall, the results presented in Figure 3.3 provide valuable insights into the trade-off between transmission frequency and battery life in wearable devices, and suggest that slower temperature sensing and transmission rates, such as every ten seconds, can significantly extend the battery life of the device. In addition, we also explored the trade-off between the parallel capacitor's performance and its size, and hope to provide design insights for future research when designing wearable systems with limited-capacity batteries.

Wireless Range

We conducted several experiments in an indoor natural environment to test the Thermal Earring's wireless range. Miniaturization of the antenna and ground plane is known to affect antenna performance, and placement close to the body further detunes antennae by shifting their resonant frequency and reducing radiation efficiency. To evaluate whether our miniaturized earring can robustly send data to a phone, we evaluated the Received Signal Strength (RSSI) and packet loss rate of the Thermal Earring at distances ranging from 0 meters to 30 meters from two Bluetooth receivers: a Google Pixel 6 phone and an nRF52840

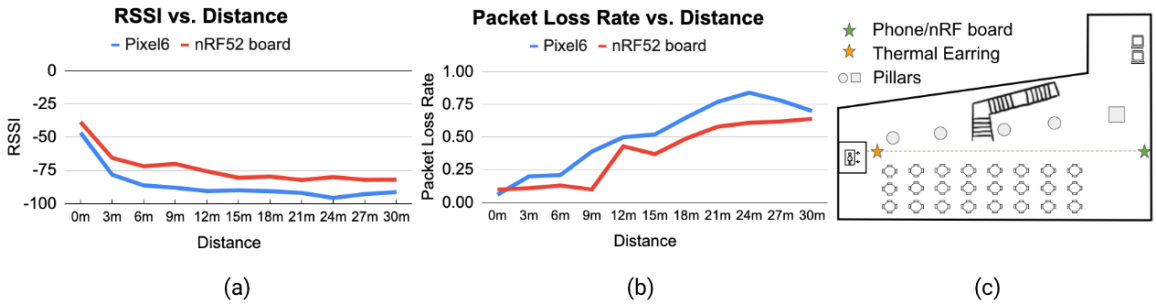

Figure 3.4: (a) The Received Signal Strength Indicator (RSSI) of the Thermal Earring Bluetooth packets. (b) The Thermal Earring's Bluetooth packet loss rate using Bluetooth receiver. (c) The floor plan of the space where we conducted the experiment.

development board. The Google Pixel 6 represents a practical Bluetooth receiver while the nRF board represents an ideal but less practical one illustrating a practical upper bound on the achievable range. To conduct the experiments, we placed the Bluetooth receivers at a fixed position marked as a green star in Figure 3.4 (c) and had a person wear the Thermal Earring, who moved away from the receiver at various distances. The Thermal Earring transmitted one Bluetooth packet per second, and we calculated the packet loss rate based on the number of packets received during a continuous 100-second interval.

Figure 3.4 presents the results of the experiments, showing the average RSSI and packet loss rate. The RSSI for the Google Pixel phone decreased to approximately -90 dBm at a distance of 12 meters and reached its lowest RSSI of -95.6 dBm at 24 meters. In contrast, the nRF52 board's RSSI dropped to -80 dBm at 15 meters and reached its lowest RSSI of -82 dBm at 30 meters. Similarly, the packet loss rate for the Google Pixel phone increased to 50% at a range of 12 meters, while the nRF52 board's packet loss rate exceeded 50% at 21 meters. The packet loss rate even at 0 meters is 0.06 and 0.10 for the Pixel phone and nRF board respectively. This is expected since the experiment environment had tables, pillars, and other Bluetooth devices causing interference. These factors contribute to the non-ideal change in packet loss rate over distance. Overall, our experiment results demonstrated that Thermal Earring could provide reliable wireless connectivity in indoor environments, especially in our close-range target use cases where the receiving smartphone is on the user.

Wireless Performance in Daily Scenarios

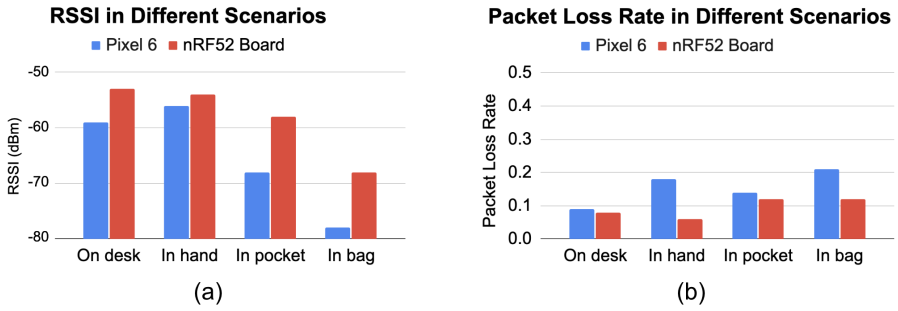

Figure 3.5: (a) The Received Signal Strength Indicator (RSSI) of the Thermal Earring Bluetooth packets. (b) The Thermal Earring's Bluetooth packet loss rate using Bluetooth receiver.

To assess Thermal Earring's wireless performance in real-life situations, we conducted experiments to investigate the RSSI and packet loss rate when the Bluetooth receivers (Google Pixel 6 and nRF52840 board) were positioned in various scenarios, including being placed on a desk, held in hand, kept in a pocket, or stored in a bag (backpack). Consistent with our prior wireless experiments, The Thermal Earring was worn by a user and was programmed to transmit one Bluetooth packet per second. We calculated the packet loss rate based on the number of packets received during a continuous 100-second interval.

Figure 3.5 shows the RSSI and packet loss rate results. Both Google Pixel 6 and nRF board had RSSI exceeding -60 dBm on the desk or in hand, and further decreased when obstructed in the pocket or bag. Google Pixel 6's packet loss rates were 0.09, 0.18, 0.14, and 0.21 for desk, hand, pocket, and bag, respectively. Higher loss when held in hand could be due to human body interference. In contrast, the nRF board consistently had lower packet loss, with highest (0.12) when in the pocket or backpack likely due to its better antenna performance. While phone antennas cannot be changed, this suggests a path to improving the link budget by improving the earring's transmit antenna. It is important to acknowledge that the experiments were conducted in a real-world office environment, with factors like desks, people moving, and other actively transmitting Bluetooth devices introducing possible interference. Additionally, it is worth noting that the loss of some data points does not

significantly impact our temperature sensing applications because temperature data does not fluctuate rapidly, as discussed in Section **??**. Overall, the experiments confirm Thermal Earring's robust wireless communication in daily scenarios, even with smartphones in pockets or bags.

3.3 Lab-controlled Experiments

In this section, we present the results of several real-world experiments conducted to investigate the effects of fever, eating, exercising, and environmental changes on earlobe temperature. All the experiments were conducted under Institutional Review Board (IRB) approval, and the participants were compensated differently depending on the experiments they were involved in. Table 3.1 summarizes the demographic information about the participants who were involved in each experiment. Throughout these experiments, participants were instructed to wear the Thermal Earring on their preferred ear, while the Thermal Earring was programmed to measure the temperatures every second to capture comprehensive information. The results demonstrate that Thermal Earring is capable of distinguishing between changes in body temperature and environmental temperature. Our findings show that the Thermal Earring is a promising platform for a wide range of applications, including monitoring fever and detecting daily activities such as eating and exercising.

Table 3.1: Table of the demographic information about the participants involved in the experiment.

Experiment	**Gender**	**Average Age**	**Race**
Fever Experiment Febrile	2 male, 3 female	39.6 ± 18.20	1 Asian, 1 Latino, 3 White
Fever Experiment Healthy	10 male, 10 female	23.55 ± 4.03	14 Asian, 1 Black, 5 White
Eating Experiment	3 male, 3 female	25.7 ± 1.6	4 Asian, 2 White
Exercising Experiment	3 male, 3 female	23.67 ± 3.01	4 Asian, 1 Black, 1 White
Ambient Change Experiment	2 male, 2 female	25.75 ± 2.06	3 Asian, 1 White

3.3.1 Effect of Fever on Earlobe Temperature

Fever is a common physiological response to a variety of medical conditions, including infectious diseases such as COVID-19 and influenza, characterized by a core body temperature above nominal 37° C [57]. Clinically, fever is defined as an elevated core body temperature exceeding 37.8°C (100°F) when measured orally. This experiment aimed to investigate the effects of fever on earlobe temperature and explore the feasibility of using the Thermal Earring to detect and monitor fever.

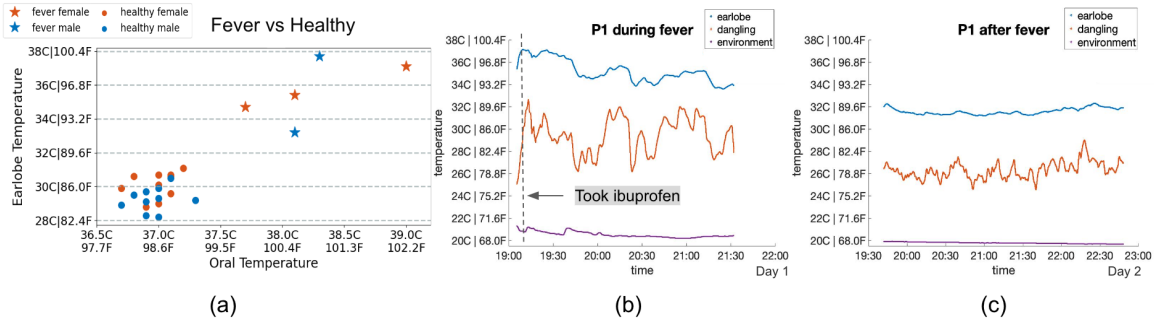

Figure 3.6: (a) The Thermal Earring's earlobe temperature data on healthy and febrile people. (b) Day 1 when the participant was having a fever with an oral temperature of 39C (102.2F) at 19:10. (c) Day 2 after the fever was gone. The participant's oral temperature was 37.2C (98.96F) at 22:30.

We recruited a total of twenty-five participants, including four febrile individuals with a core body temperature higher than 37.8 °C (100 °F), one individual (female) with a slightly elevated core body temperature of 37.6 °C (99.7 °F) in close proximity to fever, and twenty healthy individuals with a core body temperature around 37 °C (98.6 °F). The demographic information of the participants is shown in Table 3.1. During the data collection process, each participant wore the Thermal Earring for a duration of five minutes to obtain earlobe temperature readings. Additionally, their oral temperature was measured while wearing the Thermal Earring. The measurements were conducted in a similar room environment with a temperature ranging from 20 °C to 22 °C (68 °F to 71.6 °F). Figure 3.6 (a) presents the results of the earlobe temperature measurements obtained from each participant. The febrile participants have an average earlobe temperature of 35.62 ± 1.8 °C (96.12 ± 3.24

°F), which is significantly higher than healthy participants' average earlobe temperature of 29.7 ± 0.74 °C (85.5 ± 1.33 °F). It was also observed that in general, healthy female participants have a higher earlobe temperature of 30.11 ± 0.78 °(86.2 ± 1.4 °F) than healthy male participants' average earlobe temperature of 29.26 ± 0.70 °C (84.67 ± 1.26 °F). The results are expected since women have slightly higher body temperatures in general. We also note that the lowest temperature among febrile patients was observed in an older study participant (age 71) who is known to have a lower body temperature baseline.

In addition to the aggregated results, we also present the Thermal Earring results of a participant (P1) over time during fever and after fever. Figure 3.6 (b) shows the Thermal Earring data of P1 during fever, including the changes observed after taking a common antipyretic to reduce fever. P1's oral temperature was initially recorded at a high fever of 39 °C (102.2 °F) at 19:10 on day 1, with a corresponding high earlobe temperature of 37.1 °C (98.8 °F). At 19:20 on day 1, the participant took a capsule of ibuprofen, a common antipyretic, which resulted in a gradual decrease in earlobe temperature from 37.1 °C (98.8 °F) at 19:10 to 33.9 °C (93 °F) at 21:30. On day 2, the participant's earlobe temperature stabilized at around 31.4 °C (88.5 °F), which was significantly lower than her earlobe temperature during fever. The participant's oral temperature was measured at 37.2 °C (98.96 °F) at 22:30 on day 2, indicating a return to the normal temperature range. The limited oral temperature measurements were due to the participant's illness and unwillingness to move. These results suggest that Thermal Earring temperature data could serve as a convenient and effective method for monitoring fever at home and in clinical settings, providing valuable information on the effectiveness of fever treatments.

In conclusion, the findings of this experiment suggest that the Thermal Earring is a promising tool for detecting and monitoring fever non-invasively. Our study provides evidence that the Thermal Earring has the potential to be used in a variety of clinical and home-based settings to aid in the diagnosis and management of fever, particularly during outbreaks of infectious diseases. However, further research is needed to validate the performance of the Thermal Earring in larger and more diverse populations.

3.3.2 Effect of Eating on Earlobe Temperature

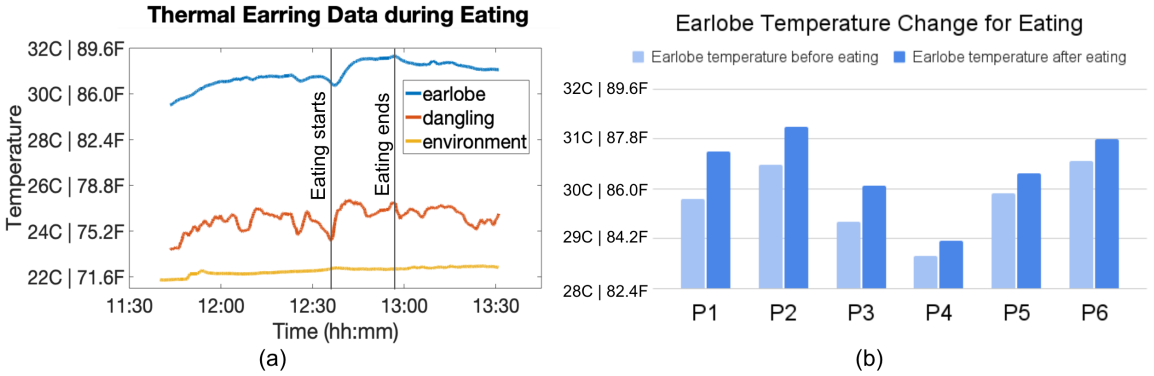

Figure 3.7: The Thermal Earring temperature results for six participants during the eating study.

Eating is an important daily activity that is known to slightly increase body temperature. Generally, the core body temperature starts to rise within thirty minutes to an hour after eating a meal due to the increased metabolic rate associated with the digestive process. Furthermore, the act of chewing and the heat from the food can also elevate the earlobe temperature since the Thermal Earring is located close to the mouth.

In this experiment, we investigated the effect of eating on earlobe temperature. We recruited six participants (three males and three females, with an average age of 25.7 $\pm$ 1.6) to participate in a semi-controlled lunch setting. The study began at 11:30 a.m., with participants sitting until 12:30 p.m. to establish a resting baseline temperature. The lunch session began at approximately 12:30 p.m., with slight variations in duration across the participants. During lunch, all participants ate warm food that they chose.

Figure 3.7 (a) illustrates a representative example of Thermal Earring data obtained from a participant during the eating session. The temperature data of all six participants exhibited a similar pattern as depicted in Figure 3.7 (a), wherein the earlobe temperature exhibited a slight increase upon initiating the act of eating. Notably, some participants experienced a continued rise in earlobe temperature after finishing their meal, while others observed a stabilization or a slight decrease.

To provide an overall analysis, Figure 3.7 (b) presents the aggregated results of the

average earlobe temperature for all six participants before and after 12:30 pm (the start of eating activity). The earlobe temperature showed an average increase of 0.60 ± 0.25 °C (1.08 ± 0.45°F) from the pre-eating resting baseline (11:30 am to 12:30 pm) to the post-eating (12:30 p.m. to 1:30 p.m.) average temperature. Furthermore, the earlobe temperature exhibited an average rise of 1.04 ± 0.30 °C (1.87 ± 0.54 °F) from the pre-eating temperature to the maximum temperature observed after the initiation of eating. We conducted a paired t-test on the average earlobe temperature before and after eating starts. The test statistic is 5.67, and the corresponding p-value is 0.0024, which proves the earlobe temperature is very statistically different before and after eating starts. These experimental findings confirm the body temperature change associated with the act of eating and demonstrate the potential of utilizing Thermal Earring as a non-invasive detector of eating activities.

3.3.3 Effect of Exercise on Earlobe Temperature

Exercise is another common activity that significantly impacts human core body temperature and skin temperature. During exercise, the core body temperature rises due to the increased metabolic activity of muscles. The thermoregulatory system is activated to dissipate heat and maintain a stable core body temperature through mechanisms such as vasodilation and sweating. Among these mechanisms, sweating plays a critical role in maintaining a relatively stable core body temperature. As sweat evaporates from the skin, it carries away heat, resulting in skin cooling and the maintenance of core body temperature.

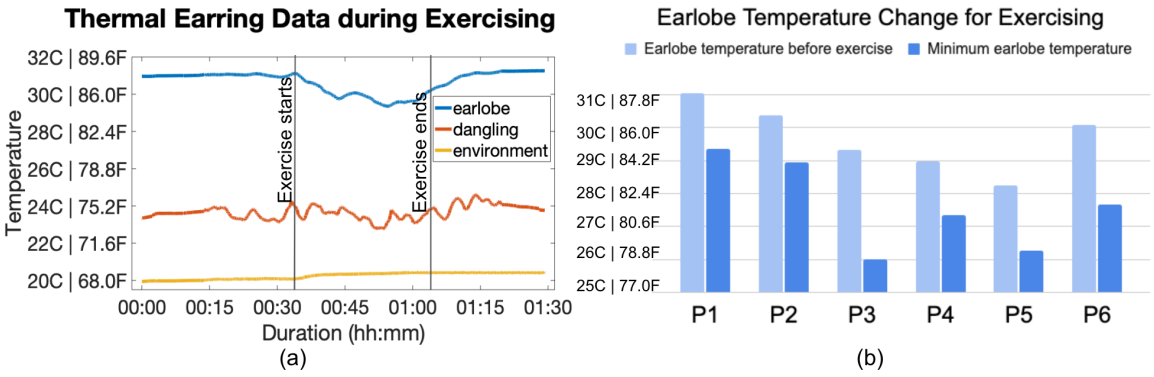

Figure 3.8: The Thermal Earring temperature results for six participants during the exercise study.

The exercise experiment aimed to investigate the effect of exercise on earlobe skin temperature. We recruited six participants (three females and three males, with an average age of 23.7 ± 3.0) to complete a 30-minute cardiovascular workout (with 4-minute stretching at the end) following a YouTube video in a controlled room. Two of the six participants also participated in the previous eating experiments. The exercise study lasted for 90 minutes in total, which included a 30-minute rest before and after the exercise. Similar to the eating study, the participants were asked to rest or engage in sedentary activities during the rest periods to establish a baseline earlobe temperature in the room.

Figure 3.8 (a) shows a representative example of Thermal Earring data obtained from a participant during the exercise session. Consistent with our hypotheses, all six participants experienced a decrease in earlobe temperature during exercise, followed by a gradual recovery to their resting earlobe temperature after the exercise ended. Notably, one participant continued to experience a decreasing earlobe temperature for approximately ten minutes after the workout ended, likely due to ongoing sweating.

Figure 3.8 (b) presents the aggregated results of the six participants' average earlobe temperature before exercise and their minimal earlobe temperature during exercise. The earlobe temperature showed an average decrease of 2.08 ± 0.70 °C (3.74 ± 1.26 °F) from the pre-exercising resting baseline (duration 00:00 to 00:30) to the lowest earlobe temperature during exercise. We conducted a paired t-test on the average earlobe temperature before and during the exercise. The test statistic is 6.52, and the corresponding p-value is 0.0013, which proves the earlobe temperature is very statistically different before and during exercise. These findings provide valuable insights into the influence of exercise on earlobe temperature and show the potential application of using earlobe temperature as a non-invasive biomarker for monitoring physiological responses to exercise.

3.3.4 Effect of Environment Temperature Change

This section focuses on evaluating the ability of the Thermal Earring's dual temperature sensor design to detect changes in environmental temperature. To achieve this, we conducted an experiment involving four participants (two males and two females, with an average age

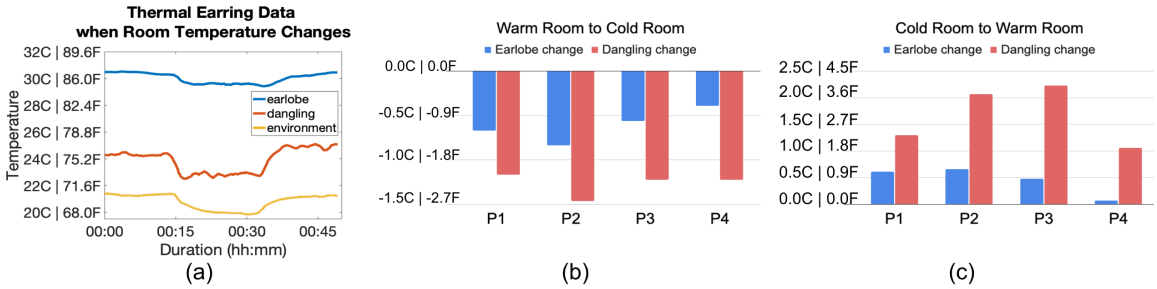

Figure 3.9: The Thermal Earring temperature results when room temperature changes.

of 25.8 ± 2.1) to investigate the effects of slight indoor temperature changes. All of the four participants also participated in either the experiment for eating or exercising. Specifically, we examined the transition from a warm room to a cold room and vice versa, which are typical scenarios encountered in daily life.

The two temperature change experiments were conducted in a continuous manner. Participants were instructed to spend 15 minutes in a warm room with an ambient temperature of 21.4 °C (70.5 °F), followed by 15 minutes in an adjacent colder room with an ambient temperature of around 19.9 °C (67.8 °F), and then return to the warm room for another 15 minutes.

Figure 3.9 (a) presents an example of temperature data obtained from one participant during these sessions, demonstrating a consistent pattern observed across all participants. When the environment temperature changed, the dangling temperature exhibited a similar change as the environment, while the earlobe temperature stayed relatively stable.

Figure 3.9 (b) presents the aggregated results from the amount of change in the earlobe and dangling temperature change when entering from a warm room to a cold room. Figure 3.9 (c) presents the aggregated results of the amount of temperature change in the earlobe and dangling data when the participants enter from a cold room to a warm room. All participants' data showed significantly higher dangling temperature change than the earlobe temperature change. When participants entered the warm room from the cold room (the environment temperature decreased by 1.5 °C), the dangling temperature increased by an average of 1.60 ± 0.50 °C (2.88 ± 0.90 °F), while the earlobe temperature only increased

by 0.46 ± 0.27 °C (0.83 ± 0.48 °F). Conversely, when participants entered the cold room from the warm room (environment temperature increased by 1.6 °C), the dangling temperature experienced an average decrease of 1.27 ± 0.13 °C (2.29 ± 0.23 °F), while the earlobe temperature decreased only 0.61 ± 0.19 °C (1.10 ± 0.34 °F) on average.

These results indicate that the Thermal Earring's dangling temperature tends to mirror the changes in environmental temperature, while the earlobe temperature remains relatively stable with a consistent offset from the core body temperature. Therefore, the Thermal Earring demonstrates its effective ability to detect variations in environmental temperature. The subsequent section will delve into further analysis, showcasing how the Thermal Earring can differentiate between changes in environmental temperature and those related to human body temperature, such as during eating and exercising activities.

3.3.5 Summary of Thermal Earring Results

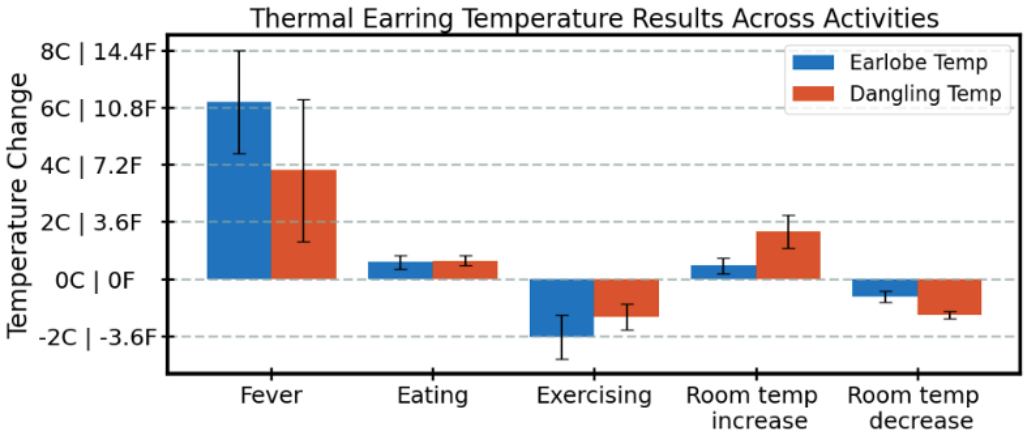

Figure 3.10: The Thermal Earring temperature results across activities.

This section provides a comprehensive summary and comparison of the results obtained from the previous experiments investigating the effects of fever, eating, exercising, and environmental changes. Figure 3.10 presents the temperature change patterns captured by the Thermal Earring across these different factors. The combined statistical results indicate that environmental changes, such as room temperature increasing or decreasing, exerted a

more significant impact on the dangling temperature compared to the earlobe temperature. Conversely, alterations in body temperature because of fever, eating, and exercising result in larger or comparable changes in the earlobe temperature, with the dangling temperature exhibiting a lesser impact.

Furthermore, the amplitude of temperature change is another informative metric. Our findings demonstrate that fever prompts a substantial increase in both earlobe and dangling temperatures, resulting in a significantly larger temperature rise compared to other activities such as eating.

Overall, our study provides valuable insights into the human body's earlobe temperature change patterns across various reasons and can have potential applications for detecting activities in daily natural settings.

3.4 In-the-Wild Results

The Thermal Earring's compact form factor enables longitudinal temperature sensing in real-world settings. We conducted an in-the-wild exploration with six participants. The six participants are 3 male and 3 female, with an average age of 24.83 ± 2.86. The racial composition consisted of five individuals identifying as Asian and one as White. Five of the six participants have also participated in either the eating experiment or the exercising experiment in Section 3.3. The six participants conducted the in-the-wild experiment on different days without any overlap. We asked the participants to wear the Thermal Earring for one day in their natural daily routine. The participants were asked to remove the Thermal Earring when sleeping, taking a bath, or any time they did not want to wear it. We also requested the participants to wear an Empatica EmbracePlus smartwatch [46], which provides raw data on continuous wrist temperature every second. To gather ground truth on activities, participants were further asked to self-report their activities using the Thermal Earring Android App when they did any activity or went outside.

Figure 3.11 shows an example of temperature data captured by the Thermal Earring and Empatica Watch over a day, with the participant's self-reported activity log as labels.

For the Thermal Earring data, there are three time periods of time showing significant effects from ambient temperature change: 1) going outside and taking a bus, and 2) during

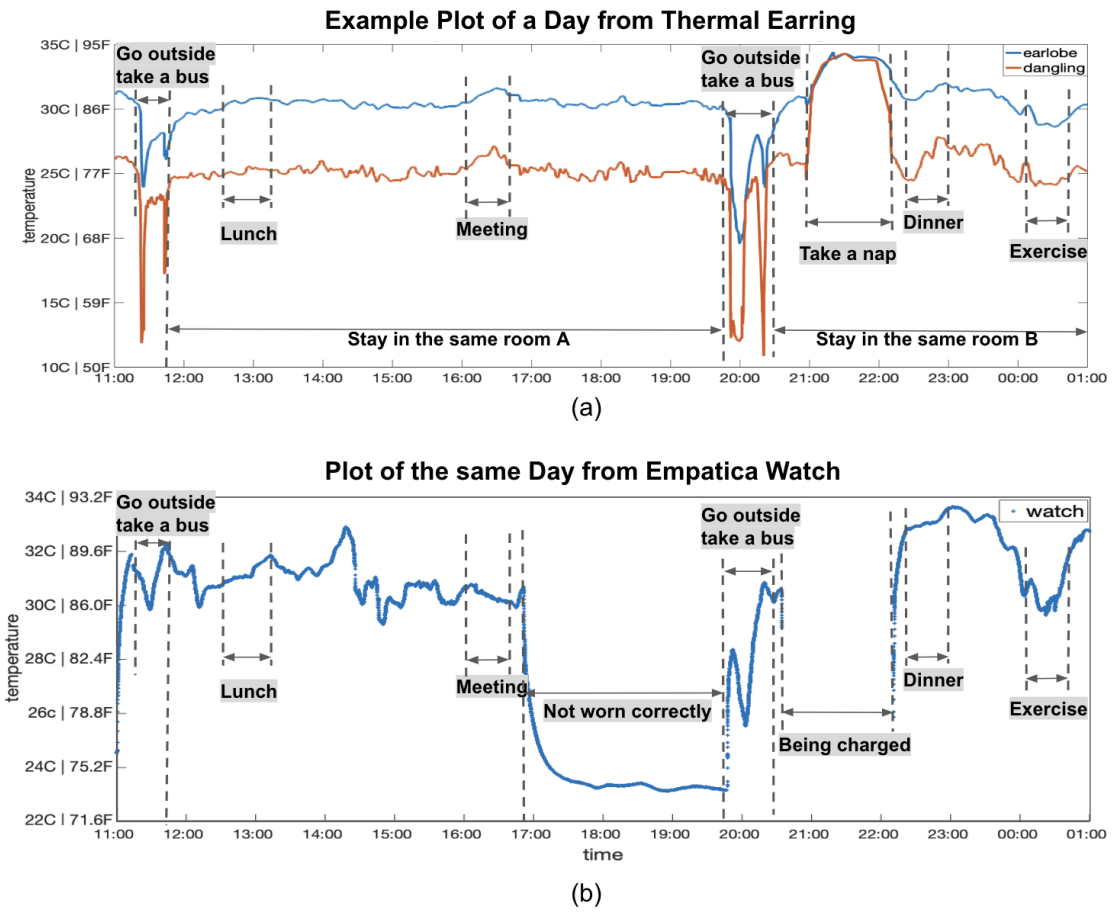

Figure 3.11: An example of the Thermal Earring's data on a participant for a day: (a) from Thermal Earring, (b) from Empatica Watch.

a nap. During the napping period, both the earlobe and dangling temperature sensors were covered by a blanket which formed a warm chamber. As a result, the earlobe and dangling temperatures became almost the same and also higher than their usual values during indoor conditions. These periods can be identified by comparing the amount of dangling change with the corresponding earlobe temperature change, which we will show a heuristic detecting algorithm in the next section. After excluding the periods heavily affected by the ambient change, the participant's temperature data is relatively stable during indoor periods throughout the day. During the indoor time, the participant's earlobe temperature shows a similar pattern to our previous lab-controlled experiments on eating and exercising.

The participant's earlobe temperature increased by 1.0 °C (1.8 °F) when eating lunch, and 1.3 °C (2.3 °F) when eating dinner. During the exercise, the participant's earlobe temperature decreased by around 2.1 °C (3.8 °F) and then gradually recovered after the exercise ended. In addition to the changes caused by eating and exercising, there is an additional noticeable earlobe temperature increase from 16:00 to 16:30, when the participant was in a stressful meeting with two professors. In the next section, we will present a heuristic algorithm to detect these events.

3.4.1 Heuristic Algorithm on Thermal Earring Data

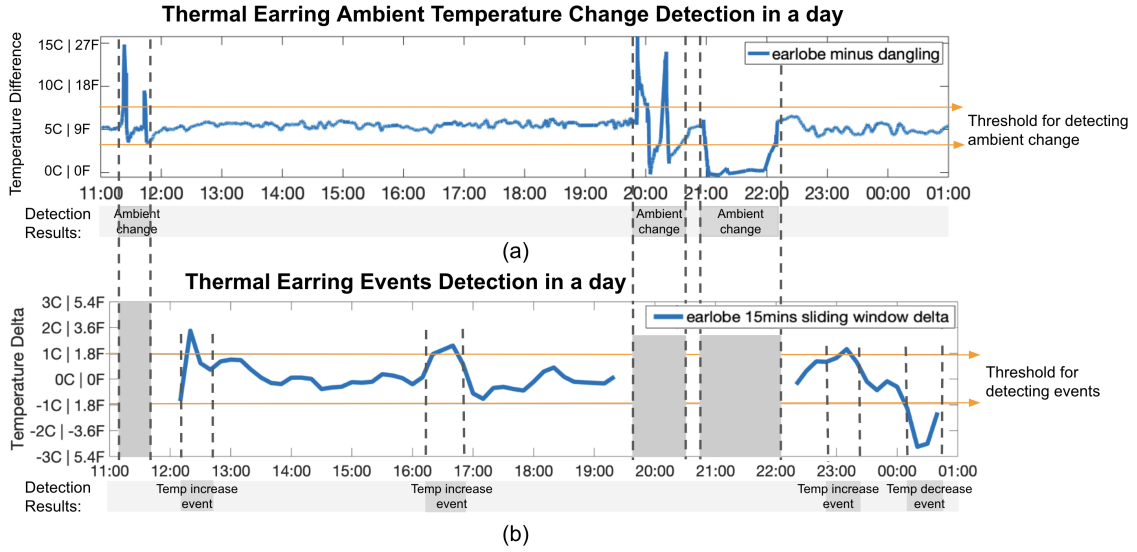

Figure 3.12: (a) A heuristic ambient temperature change detection model using a threshold. The empirical threshold is applied on the earlobe temperature minus dangling temperature. (b) A heuristics event detection model using the user-specific model. The plot shows the earlobe temperature delta over time computed using the average in a 30-minute sliding window minus the average in the window 30 minutes prior. The threshold is then applied to the computed results to detect various events.

Based on insights from this real-world data, we propose a threshold-based heuristic algorithm for activity events detection using the combined temperature data from the Thermal Earring's earlobe and dangling sensors. We will first explain this heuristic algorithm on

the example participant's data, then present the heuristic algorithm results on all six participants. The algorithm consists of two stages, as illustrated in Figure 3.12. In the first stage (Figure 3.12 (a)), we identify periods when the environment's ambient temperature is rapidly changing and exclude these periods. To achieve this, we compute the temperature difference between the earlobe and dangling temperature and use an empirical threshold of ±2 °C (3.6 °F) on the computed temperature difference. This approach is guided by the insights highlighted in Section 3.3.4, which suggests that the magnitude of the dangling temperature change exceeds that of the earlobe temperature during changes in ambient temperatures. The empirical threshold was determined leveraging the significant environment temperature change (¿10 °C) observed in the experiment while ensuring it remained higher than the maximum fluctuation induced by activities like eating or exercising. This approach successfully detected all rapid ambient temperature changes for this participant shown in the example, such as when the participant transitions from indoors to outdoors. Furthermore, we merge the detected ambient temperature change events occurring within a 15-minute time frame, since the second stage of the algorithm requires a 15-minute window during a stable indoor environment. These detected periods of unstable environmental temperature were excluded from further analysis.

In the second stage of the algorithm, we focus on identifying user activity related events occurring while users were indoors. We achieve this by computing the temporal changes in earlobe temperature using a 15-minute sliding window. For each window, we consider the average earlobe temperature during the window 30 minutes ago as the baseline temperature for the current window to account for changes in the room or slow changes in body temperature. By subtracting the corresponding baseline from the current window's average earlobe temperature, we obtain the temperature delta. The computed sliding window results are shown in Figure 3.12 (b). We then apply a threshold of ±0.96 °C (±1.7 °F) to the computed data. The threshold was determined by calculating three times the average standard deviation (0.32°C) of earlobe temperature during non-activity periods across all six users, which we will discuss in the next section 3.4.2. We note that future studies with larger scale datasets can explore more complex methods. In this way, we were able to detect temperature-increasing events (e.g., eating, stress) and temperature-decreasing events (e.g.,

exercising) throughout the day.

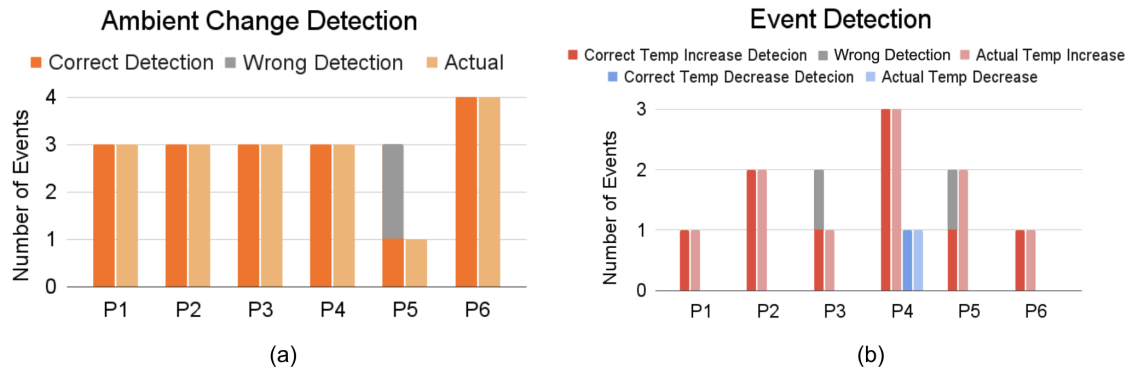

Figure 3.13: (a) Heuristic algorithm results on detecting ambient temperature change. (b) Heuristic algorithm result of detecting temperature-increasing events (eating and stress), and temperature-decreasing events (exercising).

We employed our heuristic algorithm on the six participants, utilizing consistent window lengths and thresholds as described above. Figure 3.13 (a) shows the aggregated results of detecting ambient temperature change events among the six participants. Most changes were accurately identified, while two false positives were observed in participants P3 and P5, along with one false negative in participant P5. We followed up with P5 and the participant explained that she occasionally sat on her bed covered by a blanket, potentially leading to temperature fluctuations that were attributed to the Thermal Earring errors. Figure 3.13 (b) shows aggregated results for detecting temperature-increasing (eating or stress) and temperature-decreasing (exercising) events across participants. Notably, only one participant exercised during the experiment, and it is possible that certain participants might not have worn the earring while eating, leading to fewer than three actual eating events per day. For P3, a distinct earlobe temperature increase lasting approximately 40 minutes, peaking at 1.8°C (3.24°F), was observed. However, no user activity log was provided for this period, potentially implying additional factors contributing to earlobe temperature changes that were not logged. For P5, there were two eating events logged, with only one being correctly detected, and the other remaining undetected. In addition, there is also a falsely detected temperature increase event for P5 where the participant self-reported as having no

activity.

In summary, our results demonstrate the Thermal Earring's ability to detect temperature changes triggered by eating, stress, and exercise in dynamic real-world scenarios. However, instances of temperature increases not directly related to known events require further exploration. Furthermore, the Thermal Earring's threshold-based heuristic algorithm demonstrates limitations, occasionally miss-identifying eating-related events. It is important to note that this heuristic algorithm serves as a simple proof of concept method. The algorithm can be further improved by utilizing pattern matching on the time-series temperature data or employing a machine learning classification model. However, a more extensive dataset is required for a robust model. By integrating the heuristic algorithm with the hardware system and our exploratory experiment, we establish a foundation for future endeavors in earring-based activity recognition.

3.4.2 Thermal Earring vs. Smartwatch

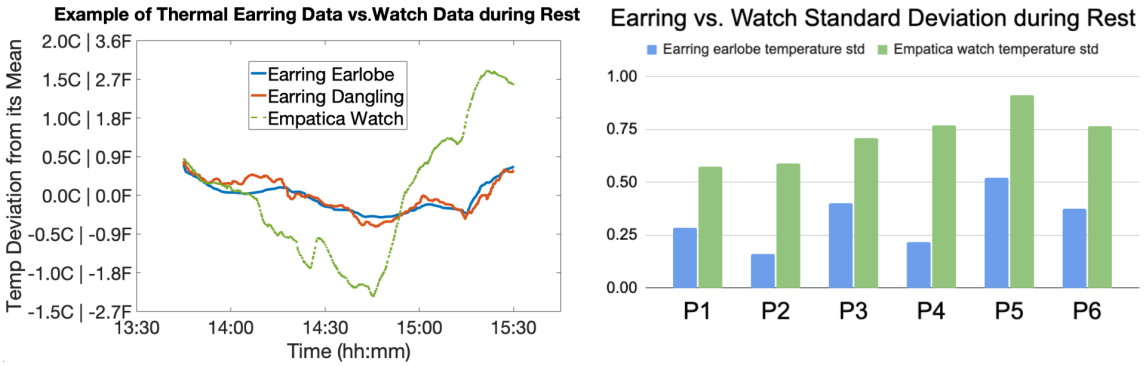

Figure 3.14: Thermal Earring temperature data vs. Empatica Watch temperature data during resting time.

As expected, the temperature data obtained from the wrist using a smartwatch tends to be noisier compared to the data collected from the earlobe using the Thermal Earring. This is potentially due to the effects of hand motions on the wrist temperature. The watch lacked data during the napping period because it was being charged during that time.

As shown in Figure 3.11 (b), the Empatica Watch data appears significantly noisier than the Thermal Earring data on the same day. Firstly, because of the lack of a secondary ambient temperature sensor, the watch data cannot differentiate ambient temperature changes. Secondly, even during indoor periods, the watch data exhibits fluctuations of up to 3.6 °C without any apparent correlation to the participant's provided activity labels. Thirdly, the watch data is occasionally shown as "not worn correctly", potentially because of loose contact with the wrist, resulting in data reflecting the environmental temperature rather than the participant's skin temperature. Besides those limitations, the watch data demonstrate a similar pattern of temperature increase during meals and temperature decrease during exercise. However, these patterns are obscured by the noise in the watch data, making them difficult to identify.

To further analyze the noise levels of the smart watch temperature compared to the Thermal Earring's, we compared the data from the Thermal Earring and the Empatica Watch during six participants' resting periods, when no activity was recorded. Figure 3.14 (a) shows the temperature deviation of Thermal Earring data and Empatica watch data from its average temperature during a participant's resting period, where the participant was not engaged in activities like eating, exercising, or talking. It is observed that the Thermal Earring data is more stable since the earlobe is less susceptible to motion effects, with a standard deviation of 0.18 °C (0.32 °F), whereas the watch data showed significant fluctuations for unknown reasons, resulting in a standard deviation of 0.82 °C (1.48 °F). Figure 3.14 (b) summarizes the aggregated results of the standard deviations for the Thermal Earring and Watch data during indoor resting periods from six participants. The average standard deviation from the Thermal Earring is 0.32 °C (0.58 °F), while the average standard deviation from the watch temperature is 0.72 °C (1.3 °F).

The Thermal Earring's reliable temperature readings have the potential to enable applications such as ovulation tracking, surpassing the capabilities of current smart watches. During ovulation, a woman's body temperature typically rises by approximately 0.28 to 0.56 °C (0.5 to 1.0 °F) [128]. However, smart watches struggle to accurately detect this temperature increase since their noise level exceeds the temperature change caused by ovulation. In contrast, the Thermal Earring provides a more reliable temperature reading, with

a standard deviation close to the lower range of ovulation temperature rise. As a result, the Thermal Earring shows its theoretical potential for tracking ovulation.

In conclusion, Thermal Earring surpasses smart watches in terms of noise levels and the ability to disambiguate ambient temperature changes. These advantages enable Thermal Earring to detect user activities effectively, and potentially support ovulation tracking.

3.4.3 Acute Stress Exploration

In our preliminary pilot experiments, we discovered significant changes in earlobe temperature during stressful events, such as public speaking. This temperature increase might be caused by the blood flow change within the superficial temporal artery and the posterior auricular artery during stressful events. While stress has been investigated using various physiological signals like heart rate, heart rate variability, blood pressure, and skin conductance, these metrics often struggle to differentiate between various types of events. For example, it is hard to differentiate stress from exercising solely based on an elevated heart rate. However, the measurement of earlobe temperature introduces a promising additional dimension that effectively aids in differentiating events.

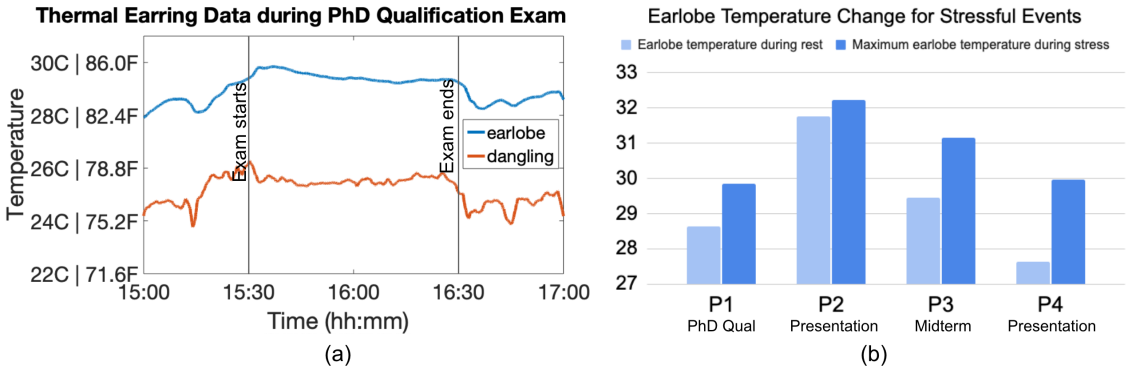

Figure 3.15: The Thermal Earring temperature results from stressful events.

Besides the stressful meeting event shown in Figure 3.11, we extracted one more stressful event (P1 taking PhD qualification exam) from the in-the-wild experiment and further recruited three participants (P2, P3, and P4) who were known to experience potentially stressful events. The four participants are two male and two female, with an average age of

22±3.65. The racial composition consisted of three individuals identifying as Asian and one as Black. For the specific stress experiment involving P2, P3, and P4, they were instructed to begin wearing the Thermal Earring at least thirty minutes before the stressful event and to continue wearing it for at least thirty minutes after the event ended.

In Figure 3.15 (a), we present a representative example of the data obtained from one participant during their PhD qualification exam. The data clearly show a sustained increase in earlobe temperature throughout the exam. This pattern was consistently observed in all four participants, with the rise in temperature slightly prior to the stressful events and a subsequent decrease at the end.

Figure 3.15 (b) provides the aggregated results of all participants who wore the Thermal Earring during various stressful events, including PhD qualification exam, public presentation, and midterm. An average of 1.42 ± 1.07 °C (2.56 ± 1.93 °F) increase between the average earlobe temperature during rest and the maximum earlobe temperature during stressed time demonstrated the response related to the stressors. We conducted a paired t-test to compare the average earlobe temperature before and during the stress condition. The results showed a statistically significant difference in temperature, $t(n\text{-}1) = 3.55$, $p = .038$, indicating that earlobe temperature changed significantly during acute stress events. Aligned with our hypothesis, these exploration results show promising potential for using the earlobe temperature as an indicator of stress or emotion-related changes. Further studies can be conducted in future work to extensively explore the relationship between earlobe temperature and stress or emotions.

3.5 Discussion

3.5.1 Fashion Design

It is also important for the Thermal Earring to be fashionable as smart jewelry. The small size and light weight of the Thermal Earring make it compatible with various fashion designs. We showcase an example of fashion design here to indicate that the Thermal Earring can be both functional and fashionable. We chose to design a cherry blossom earring with resin, a popular material for making earrings due to its ability to be molded into various shapes and

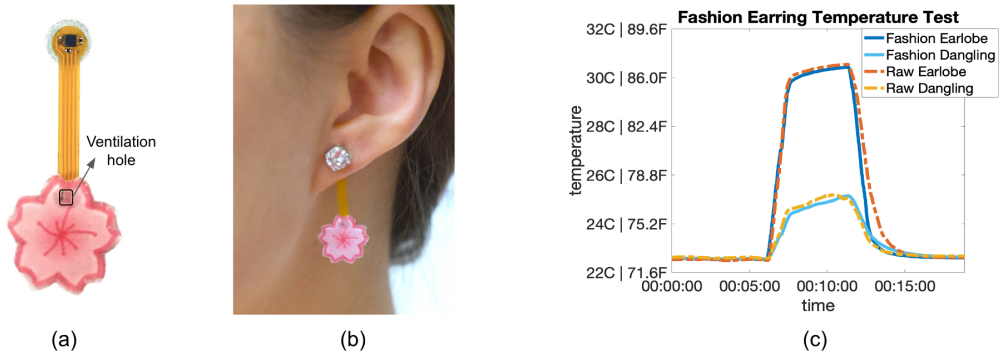

Figure 3.16: An example of Thermal Earring with fashion design.

mixed with different pigments. Thermal Earring is flat, thin, and flexible, which makes it easy to be submerged in a resin pour. Figure 3.16 (a) and (b) demonstrate the final design. The resin was poured into a cherry blossom-shaped silicone mold, encasing the Thermal Earring. We incorporated a ventilation hole around the dangling temperature sensor to ensure precise ambient temperature sensing. The dangling temperature sensor was covered by a piece of pink paper instead of resin. Future works could also use alternative coverings such as gas-permeable membranes in air quality sensors [40].

To validate the functionality of the Thermal Earring after integrating the resin fashion design, we conducted a comparative test. A Thermal Earring with the fashion design was placed alongside an uncovered Thermal Earring on a table for approximately seven minutes. Subsequently, they were placed on a person's left and right ear for approximately six minutes and then returned to the table. The temperature data results, shown in Figure 3.16 (c), prove that the Thermal Earring with the resin design performs temperature sensing as effectively as an uncovered Thermal Earring.

It is worth noting that this resin-based design represents a simple showcase of the Thermal Earring's compatibility with diverse fashion concepts. There are numerous alternative methods for incorporating fashion design into Thermal Earring. For example, techniques like welding or attaching precious metals can be explored. By employing molds of varying shapes and utilizing materials (whether resin or metal) in different colors, the Thermal earring can be personalized to various designs or styles and even incorporate gemstones like

normal jewelry.

3.5.2 Estimating Core Body Temperature from Earlobe Temperature

While we have shown that an increase in core body temperature can be reflected in earlobe temperature measurements made by Thermal Earring in section 3.3.1, directly estimating the core body temperature from the earlobe temperature requires further study. It is known that skin temperature, including earlobe temperature, is affected by a number of factors beyond core body temperature such as ambient temperature, gender, age, metabolic rate, body mass index, etc. While the Thermal Earring can provide information to exclude the ambient temperature effect, resolving these other factors such as user dependence or metabolic rate remains an open challenge. We expect that with a larger and more representative data set, it would be possible to develop a model to predict user's core body temperature using their earlobe temperature and corresponding demographics. In future work, Thermal Earring may be deployed in a larger study in conjunction with other physiological sensors to build a model for computing the core body temperature from the earlobe temperature.

3.5.3 Power Harvesting

The Thermal Earring is currently powered by a lithium coin cell battery, which can provide continuous temperature monitoring for a month. However, to address the inconvenience of battery charging and replacement, alternative power sources can be explored. One promising option is to harvest energy from the ambient environment, leveraging the motion of the earring while it is naturally dangling when the user is moving. By harvesting kinetic energy from the earring's motion, a piezoelectric harvester can convert the vibrations into electrical energy to power the earring. Additionally, solar energy can also be used as an alternative power source by harvesting it from the ambient light. Even a small solar cell can provide microwatts of power for trickle charging compatible with Thermal Earring's low-power design.

3.5.4 Limitations

The earlobe temperature appears to be user dependent, which is expected as age, gender, body weight, and composition can all affect skin temperature. Similar to existing smartwatch temperature sensors [49, 10], Thermal Earring could leverage a calibration phase to identify a user's nominal earlobe temperature before making inferences.

Recent smartwatches like the Apple Watch Series 8 also feature a dual temperature sensor design that offers improved accuracy of 0.1°C. However, the components of the smartwatch are primarily confined to the skin surface or within the watch's thickness (approximately 15 mm). In contrast, the Thermal Earring's unique form factor detects environmental temperature differently, providing better isolation from body heat.

During the evaluation of the Thermal Earring, the majority of tests were conducted indoors under normal air conditions, with temperatures ranging from 20 to 23 degrees Celsius (68 to 73.4 degrees Fahrenheit). For simplicity, outdoor measurements are disregarded. In future work, it would be valuable for future research to explore how the Thermal Earring performs in outdoor and extreme environments.

The Thermal Earring is currently only evaluated during daytime, to prevent participants' unconscious movement during sleep from harming the Thermal Earring or leading to noisy results. However, a more robust casing for Thermal Earring could enable studies during sleep to measure basal body temperature, which can be further used to track and predict menstrual cycles.

Regarding eating detection, the observed earlobe temperature rise results from factors like increased metabolism during digestion, food temperature, and chewing movements. Mouth motion, inherent to eating, also occurs in other activities, e.g., talking. To further delve into the effect of mouth motion on eating events, a future experiment comparing natural speech and dedicated eating sessions could offer insights.

While the Thermal Earring signifies temperature changes, it faces challenges in distinguishing events causing temperature elevation, like eating vs. public speaking. Integrating physiological signals like heart rate in the future could enhance its ability to differentiate these events more effectively.

3.6 Summary

We present Thermal Earring, a novel smart earring system designed for longitudinal temperature sensing from the earlobe. The Thermal Earring overcomes the challenges associated with developing a wireless smart wearable device in the form of an earring, resulting in a compact size (with a maximum width of 11.3 mm and a length of 31 mm), lightweight (0.335 grams), and a battery life of 28 days. Leveraging its proximity to the head and dual temperature sensor design, the Thermal Earring demonstrates reliable temperature sensing capabilities. We conducted extensive real-world evaluations to investigate the effects of fever, eating, exercising, and changes in ambient environmental temperature on the Thermal Earring's data. Our results proved that the Thermal Earring can successfully disambiguate the temperature changes caused by the body from those caused by the environment. Moreover, our results demonstrate significant earlobe temperature changes related to eating, exercise, and periods of acute stress. The initial exploration results provide a basis for future automatic activity detection. We evaluated the advantages of Thermal Earring over existing wrist-worn smartwatches. Overall, Thermal Earring is a promising platform for continuous earlobe temperature sensing, which shows the potential in applications of fever monitoring, activity detection, and stress assessment.

Chapter 4

PPG EARRING

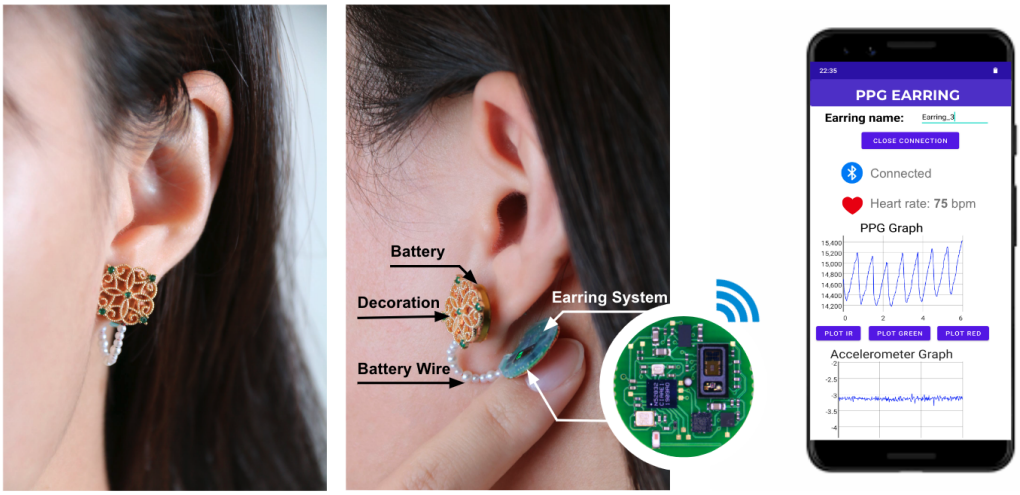

(a) PPG Earring front view (b) PPG Earring side view (c) PPG Earring App

Figure 4.1: (a) (b) The front and side view of PPG Earring with fashion design. (c) The smartphone app that connects to PPG Earring through Bluetooth and displays a real-time PPG signal.

4.1 Introduction

Integrating heart rate monitoring into daily routines using wearable technologies can empower individuals to stay proactive about their health. Heart rate provides numerous insights into cardiovascular health. Abnormal heart rates, whether too fast (tachycardia) or too slow (bradycardia), can signal a variety of underlying health conditions. The ability to track heart rate during exercise could also help maintain controlled intensity and optimize fitness benefits or even provide warnings of dangerous overexertion for individuals with cardiovascular disease. While heart rate monitoring is now widely available through devices like smartwatches and smart rings, their underlying sensing principle makes it challenging

to produce accurate, continuous measurements during exercise.

These devices use photoplethysmography (PPG) to measure the heart rate by shining a light into the skin and capturing the light reflected by the blood vessels. One of the biggest challenges of using PPG for continuous heart rate sensing on wearables is dealing with motion artifacts. Because PPG measures reflected light to detect blood volume changes caused by heartbeats, any small movement or pressure change between the skin and the PPG sensor can cause a change in the light path. This results in substantial noise in the sensed PPG signal, making it extremely challenging to measure heart rate during activities ranging from intense exercise to walking. Current wearables like smartwatches and smart rings often address this issue by either discarding noisy data or applying advanced processing methods to estimate or interpolate the heart rate [11, 115, 27, 119]. Although various processing methods, such as using motion sensor data to compensate for PPG motion artifacts [29, 80], have been explored, their estimation accuracy remains very limited due to the inherently poor quality of PPG data during motion [114, 90, 5].

In this work, we propose an alternative wearable heart rate monitoring solution that addresses this problem: smart earrings. The earlobe, like the fingertips, is a well-known site for clinical PPG measurement due to its rich blood flow near the skin's surface. The thin skin of the earlobe allows PPG light to penetrate more easily, enhancing signal quality. Additionally, humans have evolved sophisticated sensory-motor mechanisms to stabilize the head, even during exercise and motion [71]. This, combined with the constant, stable contact between the PPG sensor and the earlobe enabled by the earring, results in substantially lower motion artifacts compared to loosely worn watches and rings.

However, developing smart earrings requires overcoming multiple challenges. Earrings are significantly smaller than watches, leaving much less space for the sensing electronics and a battery. In addition to fitting within the limited dimensions of the earlobe, weight is also a critical constraint for earring form-factor devices. A heavier earring not only causes discomfort but also increases movement, which degrades the PPG signal quality. This introduces strict constraints on the battery, typically the heaviest component in the system, which must be small and lightweight while supporting continuous system operations. This is particularly challenging for PPG sensing, which requires 10-50 mA of current to produce

sufficiently bright light for reliable signal acquisition.

In this paper, we address these challenges and develop PPG Earring: the first compact smart earring capable of monitoring the user's heart rate through PPG on the earlobe. As shown in Figure 4.1, the PPG Earring prototype mimics the form factor of standard earrings, measuring 14 mm in diameter and weighing 2.0 g. Our sampling strategy, which only emits light in brief microsecond pulses to capture each PPG sample, enables 21 hours of *continuous* PPG and motion sensing at a sampling rate of 50 Hz. This can be further extended to roughly 17 days when performing opportunistic sensing—for example, monitoring PPG and motion for 30 seconds every 10 minutes. Beyond heart rate, the PPG sensor can also measure heart rate variability (HRV) for stress insights and blood oxygen saturation (SpO2). Additionally, the earring includes a temperature and an accelerometer sensor, making the PPG Earring a versatile health monitoring platform.

We systematically evaluate PPG sensing signal quality at the earlobe, compared to the wrist and finger, with the same PPG light strength settings. Our experiment results demonstrate that the earlobe provides up to 6.3x (8.0 dB) higher signal quality than the wrist across various light settings and up to 2x (3.3 dB) better than the finger. Notably, earlobe-based PPG sensing proved particularly more effective than hand-based sensing for users with cold hands. In our exercise study, we compared PPG Earring's performance with a commercial Fitbit during walking, running, and weightlifting. The results revealed that the PPG Earring captured valid heart rate data for an average of 91.7% of the exercise time, significantly higher than the Fitbit's 67.2%.

In addition to controlled studies, we conducted a real-world study involving six participants wearing the PPG Earring and a Fitbit for a day (around 8-12 hours during the daytime) while continuing their natural activities. PPG Earring captured valid heart rate signals $86.29 \pm 2.96\%$ of the time, while Fitbit only captured $54.88 \pm 4.63\%$ time. All participants found PPG Earring to be as comfortable as their regular earrings. Five out of six participants expressed a strong willingness to wear the PPG Earring daily. Four participants showed a strong preference for the PPG Earring over the Fitbit, describing the earring as so comfortable that they "didn't even feel it", while the smartwatch was perceived as "bulky and uncomfortable." This in-the-wild study validated the comfort level of the PPG Earring

and highlighted its potential as a reliable daily health monitoring device.

In summary, we present the following **contributions** in this paper:

- We designed the first smart earring for heart rate monitoring that is in a form factor similar to normal earrings. The PPG Earring has a 14 mm diameter, weighs just 2.0 grams—comparable to typical earrings—and provides a battery life of 21 hours with continuous PPG sensing and Bluetooth transmission.

- We compared the earring's PPG signal quality to wrist- and finger-based sensing, demonstrating that the earring achieved 2-6.3 times (3.3-8.0 dB) better signal quality with lower power consumption and was affected by motion artifacts for 10%-37% less time during activities.

- We compared PPG Earring with a commercial Fitbit smartwatch during exercise and a whole-day in-the-wild study. PPG earring was able to capture heart rate data for 91.74 ± 4.84 % of the time during exercise, which is 24.5% higher than Fitbit. PPG Earring captured valid PPG for 86.29 ± 2.96% of time during in-the-wild study, which is 32% higher than Fitbit and has a 2.2 times (3.4 dB) higher SNR.

- The PPG Earring was rated as highly comfortable by all six participants in the whole-day in-the-wild study. All participants found it as comfortable as their regular earrings, with five participants expressing a strong willingness to wear it all the time every day.

4.2 PPG Earring System Design

Creating compact, low-power wearables like smart jewelry brings unique advantages and significant challenges due to their need for comfort and wearability. Key considerations include managing size, weight, and power consumption, all of which are often tightly interrelated and critical for ensuring comfort. We summarize the goal of our system design here: 1)

- **Compact Size:** The earring must be small enough to fit comfortably on the earlobe.

- **Lightweight:** The earring should be light to avoid any discomfort during long-time wear.

- **Reasonable Battery Life:** Despite form factor constraints, the earring should offer a reasonably long battery life without frequent recharging.

- **Universal Design:** Instead of customizing the system with various fashion designs, we developed the PPG Earring system into a universal earring backing design that can be worn together with any fashion design in the front.

PPG Earring achieves these design considerations and presents a practical wearable platform for longitudinal health sensing, offering typical health monitor capabilities such as heart rate, activity level, and body temperature. Next, we will detail the key components of the PPG Earring system, including the PPG sensor, motion sensor, microcontroller, and battery.

4.2.1 PPG Sensing

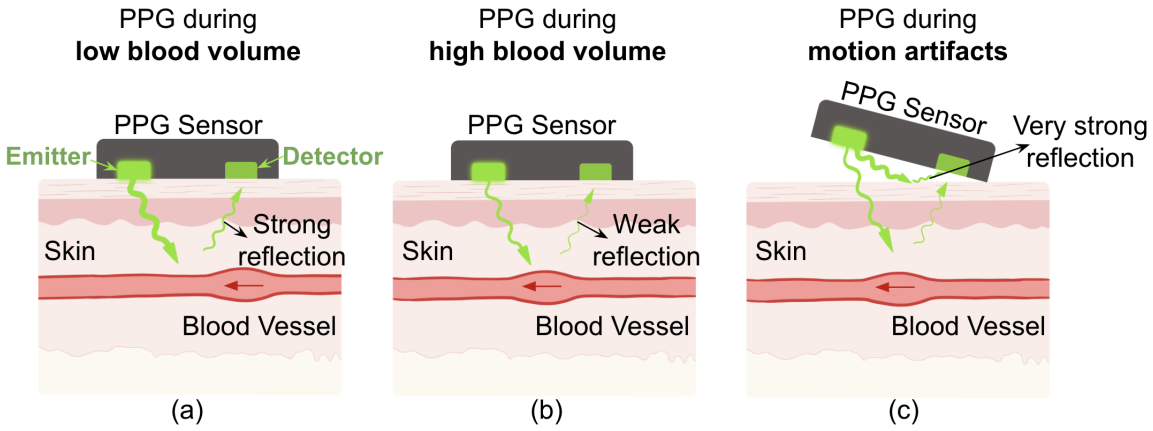

Figure 4.2: Demonstration of how PPG light reflects under different conditions: (a) when the emitted PPG light is not on the blood pulse (low blood volume, absorbing less light), (b) when the emitted PPG light is on the blood pulse (high blood volume, absorbing more light), and (c) when motion artifacts cause a portion of the PPG light to be directly reflected by the skin.

PPG is a noninvasive and low-cost optical measurement method that is often used for heart rate and SPO2 monitoring. As shown in Figure 4.2 (a)(b), a PPG sensor contains a light source and a photodetector and is placed in contact with the skin. When the light source emits light, the amount of light received by the photodetector varies as the blood volume in the vessels changes. This variation in blood volume affects the amount of light absorbed by the tissue, which in turn changes the amount of light received by the photodetector. The PPG sensor captures this signal, which can then be analyzed to derive useful information about cardiovascular health. PPG sensors typically use green (500–570 nm), red (600-750 nm), or infrared (IR, 850-950 nm) light to measure the blood volume change. Shorter wavelengths, like green light, have shallow skin penetration but are less affected by motion artifacts due to the shorter light path [80]. This makes the green light ideal for areas with good blood perfusion near the skin. In contrast, red and IR light penetrates deeper into tissue and can provide better signal quality when stable. They are also more suitable for oxygen saturation measurement.

Several factors can affect the PPG signal quality. One of the main factors is motion artifacts and the contact pressure between the sensor and the skin. As shown in Figure 4.2 (c), when a small movement happens, the PPG sensor can be slightly shifted from the skin which largely changes the optical path, resulting a significant different signal reflected to the photodetector. The appropriate amount of pressure between the PPG sensor and the skin is crucial, as too much pressure can reduce blood flow, while too little pressure may lead to poor contact and a lot of movements.

We implemented the PPG sensing on the earring using MAX30101 from Analog Devices, as shown in Figure 4.3. The MAX30101 senses the PPG signal through reflective PPG and is an integrated pulse oximetry and heart-rate monitor module that includes internal LEDs, photodetectors, optical elements, and low-noise electronics with ambient light rejection. In addition, the sensor has an integrated cover glass for optimal and robust performance. MAX30101 comes in a tiny package of 5.6 mm x 3.3 mm x 1.55 mm and features a low power consumption of less than 1 mW (varies with light intensity setting). The MAX30101 integrates red, green, and IR LEDs with programmable light strength from 0 to 50 mA. The LED pulse width can be programmed from 69 µs to 411 µs to allow balancing PPG

accuracy and power consumption based on use cases. In our setup, we experimented with all lights and different light power settings in later Section.4.4.1. The MAX30101 PPG sensor is connected to the system microcontroller through an I2C line and is programmed to a sampling rate of 50 Hz.

Beyond PPG, the MAX30101 sensor can also measure blood oxygen saturation (SpO2), similar to many pulse oximeters. Low SpO2 levels may signal respiratory or circulatory issues, with readings below 92% often requiring immediate treatment to prevent organ damage [36]. The SpO2 monitoring from the earring can provide timely assessments to help verify if the respiratory and circulatory systems are working properly. However, a comprehensive evaluation of SpO2 accuracy would require extensive experiments and is, therefore, beyond the scope of this paper.

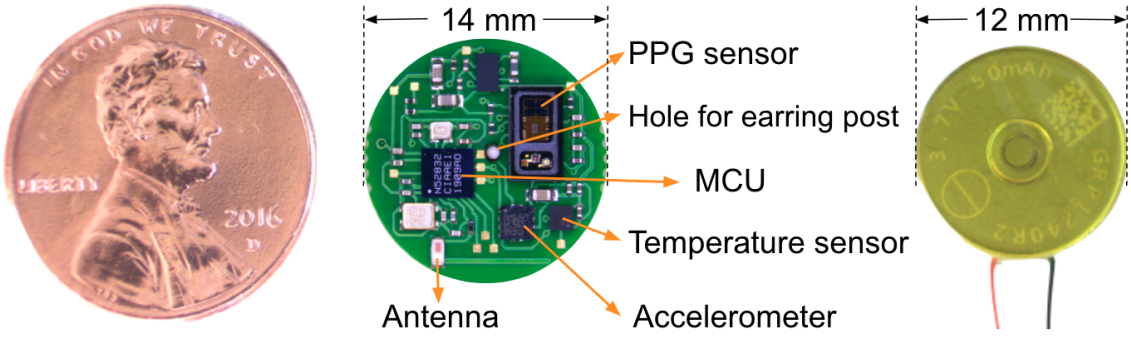

Figure 4.3: The PPG Earring system PCB with a US penny coin as reference, and the battery for PPG Earring.

4.2.2 Motion and Temperature Sensing

Although this paper primarily focuses on heart rate monitoring, we envision the PPG Earring to be a versatile health monitoring platform, just like a smartwatch fitness tracker. We have integrated motion and temperature sensing into the earring to capture user activities and monitor body temperature. We implement the motion sensing part using the LIS2DW12 3-axis low-power accelerometer from STMicroelectronics.The LIS2DW12 sensor features a programmable acceleration sensing range, sensitivity, and sampling rate. LIS2DW12 is

available in an ultra-compact 12-LGA package that measures 2.0 x 2.0 x 0.7 mm, with less than 2 uW power consumption during active sensing in low-power mode. In addition, the LIS2DW12 sensor has a built-in internal engine to process motion and acceleration detection, including fall detection, stationary/motion detection, tap gesture recognition, etc., which enables potential acceleration-triggered system wake-up to further optimize system power efficiency. The LIS2DW12 accelerometer is connected to the microcontroller with I2C lines. The accelerometer is set to a sampling rate of 50 Hz in low power mode, with a sensing range of ± 2 g and sensitivity of 0.244 mg/digit. The temperature sensor is implemented using HDC2010 from Texas Instruments. This temperature sensor was chosen because of its small size ($1.49mm \times 1.49mm$), low power consumption (0.9 uW), and high accuracy ($\pm 0.2C$). The HDC2010 is connected to the microcontroller through an I2C line, with a sampling rate of once every second.

4.2.3 Wireless Communication and MCU

The sensed data from the wearable device should be processed and presented to the user via a smartphone or computer. Wireless communication, which involves high-frequency RF signals in the GHz range, typically consumes around 5 mW of power during transmission and is often the most power-intensive component of the wearable system. As a result, selecting a wireless communication method that is both energy-efficient and suitable for compact integration is crucial for optimizing the performance of the earring.

Bluetooth Low Energy (BLE) is the preferred choice for many wearable devices due to its low power consumption, suitable wireless range, and compatibility with smartphones and laptops. Given that most people have smartphones with them most of the time, BLE offers convenient data exchange between the smart earring and the smartphone. BLE connection mode is ideal for streaming data and provides high data throughput, which supports up to 251 bytes of data in each packet.

Considering these factors, we chose the nRF52832 microcontroller chip with built-in BLE capability for smart earring computing and wireless communication. This ultra-compact chip is packaged in a wafer-level chip-scale package, measuring 3.0 x 3.2 x 0.5 mm and

weighing 6.8 mg. It incorporates an ARM Cortex M4 processor for computing tasks and has built-in Bluetooth low-energy transceivers with configurable transmitting power, making it an ideal choice for the earring wearable system.

Although the nRF52832 microcontroller is designed to be power-efficient, it still consumes around 3 mA in active mode and about 5 mA in Bluetooth transmitting mode, which is still very power-consuming for wearables with minimal battery capacity. In contrast, the nRF52832 chip consumes only 1 µA in deep sleep mode, significantly saving power. So, we configured the nRf52832 microcontroller to wake up only when needed to interface with the sensors or transmit BLE packets. Both the PPG and accelerometer sensors can store up to 32 samples of data in their FIFO, reducing the frequency at which the microcontroller needs to wake up to read sensor data.

When using a single light in the PPG sensor, each PPG sample consists of 3 bytes, each accelerometer sample (per axis) is 2 bytes, and each temperature reading is 2 bytes. To pack the measured data into a BLE packet (maximum size: 251 bytes), the earring system aggregates 25 samples of PPG and accelerometer data, along with 1 sample of temperature data, resulting in a total packet length of 25 samples x 3 bytes + 25 samples x 2 bytes x 3 axes + 1 samples x 2 bytes = 227 bytes. With both the PPG sensor and accelerometer configured to a 50Hz sampling rate, the microcontroller only needs to wake up every 25 samples x (1000ms/50Hz)=500ms to read the sensor data and send it via BLE. This approach minimizes the microcontroller's active time, significantly reducing its average current consumption. Further optimizations can be achieved by reducing the number of accelerometer samples sent or enabling accelerometer data streaming only during specific activity triggers.

4.2.4 Battery and Power Consumption

For wearable devices, and specifically smart earrings, the power source is a critical component that must have high power capacity while being compact and lightweight. As discussed before, wireless communication and powering the PPG sensor light consume the most power. On average, the total power requirement of the earring system is 2.2 mW when sensing and

wirelessly transmitting PPG and accelerometer data at a 50Hz high sampling rate.

The energy limits of currently available battery technologies make batteries the largest and heaviest components in such small centimeter-scale devices. To achieve our target form factor, we chose the high energy density GRP1240 battery from Grepow. The GRP1240 rechargeable Lithium-ion battery offers a high capacity of 50 mAh with a diameter of only 12 mm and height of 4 mm. With the 50 mAh battery, the PPG Earring can achieve a battery life of 21 hours of continuous PPG sensing (single light) and accelerometer sensing both at 50 Hz. In addition, the battery life can be further extended to reduce the sensor sampling rate, we set both sensors to high sampling rate just to collect comprehensive data. In real-world scenarios, the PPG sensor can be set to opportunistic mode instead of continuous mode, such as only sensing for 30 seconds every ten minutes unless some specific activity happens. In theory, this can extend the battery life about 20 times longer, which makes a battery life of 17 days. The accelerometer can also be set to triggering mode, which only triggers when some interesting activities happen instead of continuously streaming accelerometer data.

4.2.5 The Final Earring System

As shown in Figure 4.3, the PPG Earring system is designed on a 14 mm diameter printed circuit board (PCB), making it smaller than a US penny. Since the average human earlobe measures around 19.6mm×18.8mm [24], PPG Earring can comfortably fit into most people's earlobe. None of our participants experienced any fit issues during the study. To ensure user comfort, as the device directly contacts the skin, a thin layer of skin-friendly silicone is applied to the surface of the PCB. This silicone layer is molded and cured at room temperature, providing a soft and comfortable interface for the user. Additionally, the silicone compensates for the height difference between the PPG sensor and other components on the PCB, creating a flat surface. The flat contact surface is essential not only for comfort but also to ensure consistent contact between the PPG sensor and the skin, which is critical for maintaining high signal quality. The entire earring system weighs just 2.0 grams, which is less than the average weight of normal earrings (around 3 grams)[64]. The individual component weights of the PPG earring are detailed in the table below.

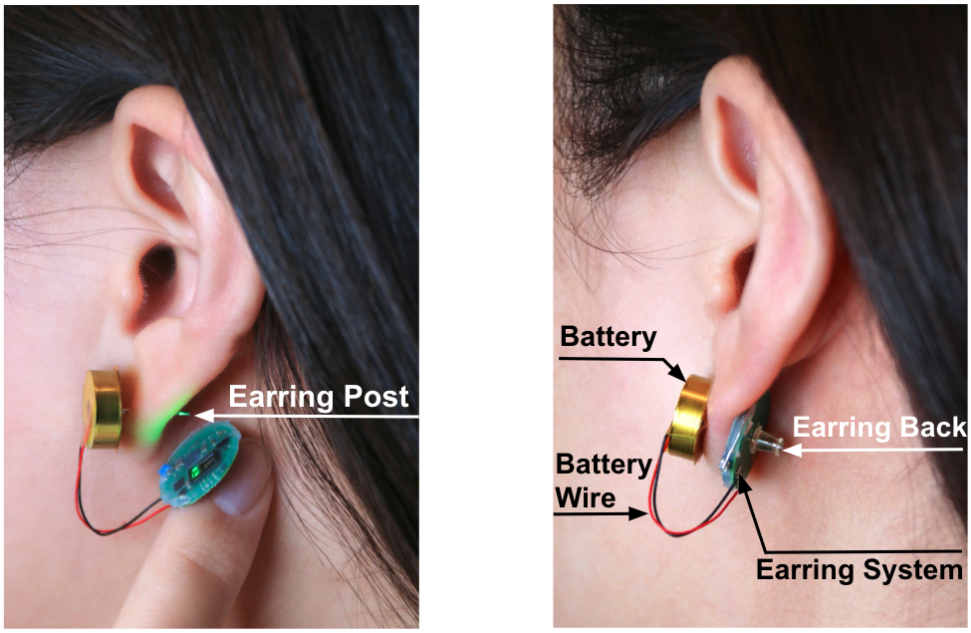

Figure 4.4: Demonstration of how to wear the PPG Earring (without the decorative components).

The PPG Earring is worn similarly to a standard stud or hoop earring. As illustrated in Figure 4.4, the battery is positioned at the front of the earlobe like a traditional stud. A commercial earring post is attached to the battery, passing through the earlobe and the earring PCB. To maintain constant contact between the PPG sensor and the earlobe, a friction earring back is added behind the PCB to ensure optimal performance. Since the earlobe has good blood perfusion, placing the PPG sensor anywhere on the earlobe typically yields a reasonable PPG signal. To maintain a consistent setup in our studies, we instructed the participants to wear the earring with the PPG sensor positioned between the earring post and the head by rotating the earring system.

Component	**Weight**
Earring PCB and electronics	0.3 g
Silicone layer	0.3 g
Battery	1.4 g
Total	2.0 g

4.3 Signal Processing

We describe the signal processing pipeline for PPG signals, along with the definitions of the metrics reported in later sections. During the study, PPG Earring data is streamed to a smartphone app and stored in a local file with timestamps, while Fitbit data is recorded on the device and later transferred to a laptop for processing. All PPG signals from the PPG Earring and Fitbit are processed offline through the same pipeline using Matlab and Python. First, the PPG signals are segmented using a 10-second sliding window with a 5-second overlap. For each 10-second window, we compute the frequency distribution using a fast Fourier transform (FFT). Figure 4.5 shows examples of valid and invalid 10-second window signals with their corresponding FFT results. The FFT results are used to determine whether this 10-second window is a valid PPG signal or not and compute the Signal-to-Noise Ratio (SNR).

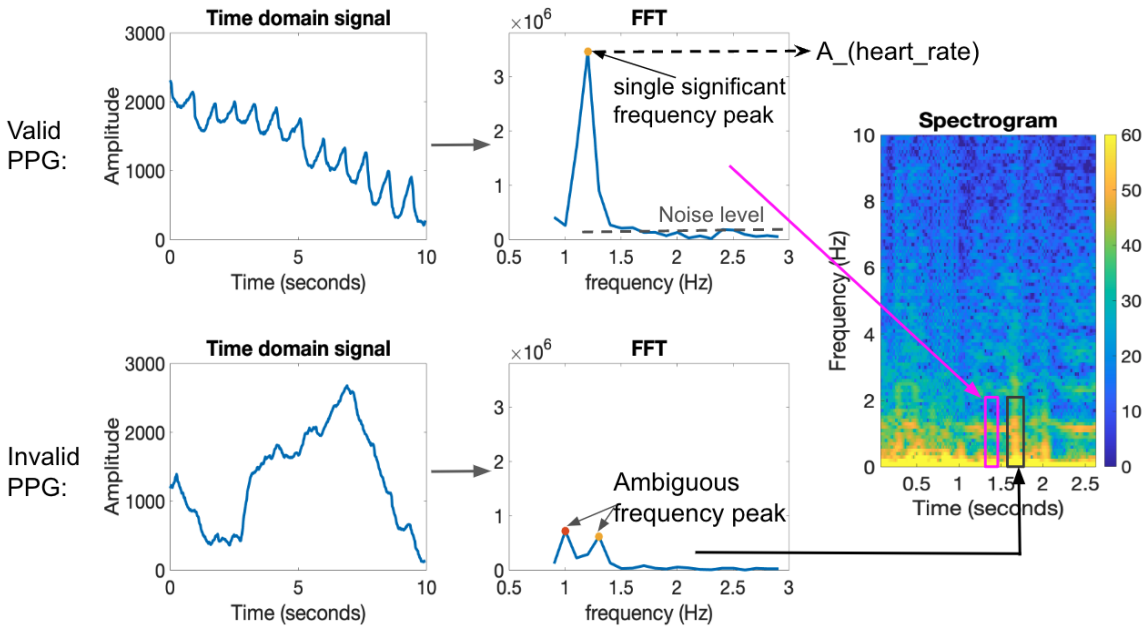

Figure 4.5: An example of a valid PPG signal window and its FFT results, an invalid PPG signal window and its FFT results, and their corresponding representations in the spectrogram.

4.3.1 Valid PPG definition

The top of Figure 4.5 shows an example of a valid PPG signal and its corresponding FFT results. The valid PPG signal demonstrates a clear periodic pattern in the time domain, with a single dominant frequency peak in the possible heart rate range (50-180 bpm during daytime [113], corresponding to 0.8-3.0 Hz). The bottom of Figure 4.5 shows an example of an invalid PPG signal, which does not show a periodic pattern in the time domain and thus does not have a single significant frequency peak in the FFT results.

Based on the observation, We define and classify whether a 10-second window is valid PPG or not using the following criteria: 1) The FFT must have a single dominant peak, with an amplitude at least twice that of the second-highest peak. 2) The peak must be significant, at least twice the mean and median power of frequencies within the 0.8 Hz to 3.0 Hz range.

The right of Figure 4.5 shows a 2.5-minute spectrogram computed using STFT (where the FFT results are stacked vertically). The continuous line in the spectrogram reflects the heart rate over time, as the heart rate always changes gradually. Thus, a third criterion is applied based on this observation: during non-exercise periods, the current window's heart rate should be within 10 bpm (0.17 Hz) of the previous window's heart rate and within 20 bpm (0.33 Hz) during exercise.

The valid percentage of the PPG signal is the ratio of the number of 10-second windows that can be used to compute a valid heart rate to the total number of 10-second windows in the whole signal.

4.3.2 SNR definition

Signal-to-Noise Ratio (SNR) is a common metric to measure the level of the target signal compared to the level of background noise. In this paper, the SNR of the PPG signal is defined as the ratio of the power of the heart rate frequency bin to the average power of the frequencies within the possible heart rate range. Since our study only focuses on daytime conditions, we consider the typical human heart rate range of 50 to 180 bpm [113], corresponding to a frequency range of 0.8 Hz to 3.0 Hz. The SNR of the PPG signal is

given by:

$$SNR = \frac{P_{heart-rate}}{P_{other-frequency}} = \frac{P_{heart-rate}}{(P_{0.8-3.0Hz} - P_{heart-rate})}$$

where $P_{heart-rate} = A^2_{heart-rate}$ represents the power of the detected heart rate frequency and $A_{heart-rate}$ is its FFT amplitude. $P_{other-frequency}$ refers to the average power of the noise floor, which is all frequencies within the 0.8 Hz to 3.0 Hz range excluding the heart rate frequency. The computed SNR result is then converted to decibels using $SNR_{dB} = 10 \times log_{10}(SNR)$.

4.4 Lab controlled studies

In this section, we present the results of the user studies, which validate the effectiveness and reliability of the PPG Earring. In the first study, We compared the performance of the sensing PPG from the earlobe with two common PPG measurement sites: the finger and wrist. The results show that sensing PPG on the earlobe provides much better signal quality than on the wrist and slightly better signal quality than on the finger. In addition, sensing PPG on the earlobe is not likely to be affected by motions, making earrings a much more reliable monitoring method than smartwatches and smart rings.

In the second study, we evaluated the PPG Earring's performance against a commercial Fitbit smartwatch during exercise. Our findings demonstrate that PPG Earring provides significantly more reliable heart rate monitoring during exercise compared to the Fitbit smartwatch.

All studies were conducted with approval from the Institutional Review Board (IRB), and users were compensated based on the specific studies in which they participated.

4.4.1 Earring vs. Ring. vs. Watch Study

The earlobe and finger are clinically optimal locations for measuring PPG due to their good blood perfusion, and the wrist has been a popular location on wearables, too, because it is convenient. In this study, we aim to compare these three measurement sites to determine if the earlobe offers a more efficient and reliable location for PPG heart rate monitoring than the finger and wrist.

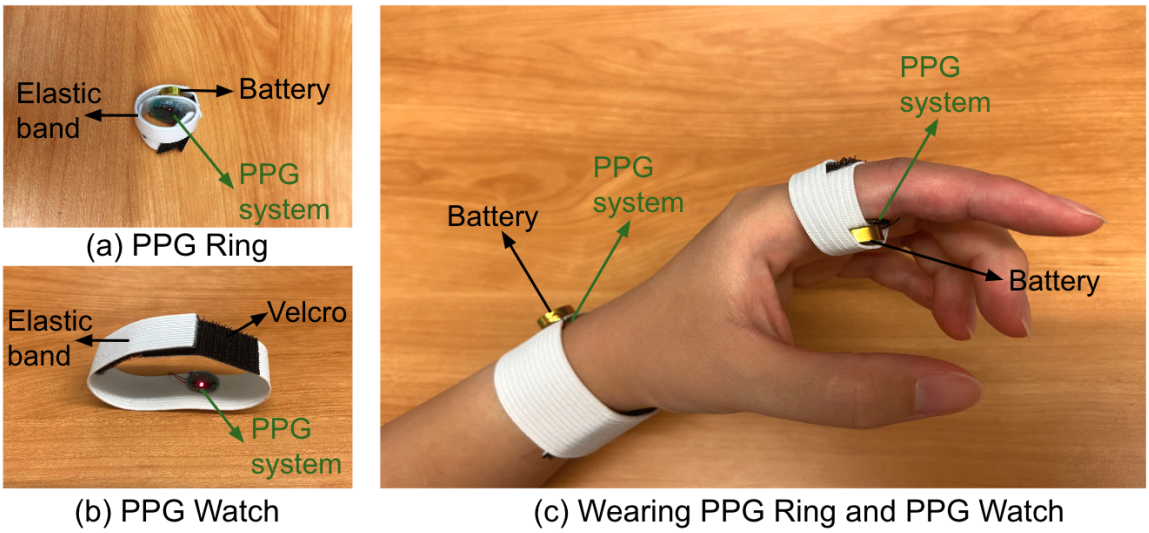

Figure 4.6: (a) The PPG Ring is made from the same system as PPG Earring. (b) The PPG Watch is made from the same system as PPG Earring. (c) The demonstration of how users wear the PPG Ring and PPG Watch during the study. Both the PPG Ring and PPG Watch are attached to the user using an elastic band with velcro to adjust tightness.

We recruited eight participants to collect PPG data in a lab-controlled environment. The participants included six females and two nonbinary individuals, with an average age of 31.1 ± 12.4 years. Their skin tones ranged from Type I to Type IV on the Fitzpatrick scale. Participants were asked to wear three devices: the PPG Earring, PPG Ring, and PPG Watch. All of these devices were made by the same PPG system so we can control light intensity. Figure 4.6 shows how the participants wear the PPG Ring and PPG Watch using an elastic band with velcro, which allows for adjustable, comfortable tightness. The participants wear the PPG Earring as shown in Figure 4.4.

The PPG Earring, Ring, and Watch were configured to the same light intensity settings and programmed to collect PPG data using green, infrared (IR), and red lights simultaneously throughout the experiment. Additionally, we examined how different PPG light intensities affected signal quality. The minimum light intensity for all wavelengths was set to 3 mA, while the maximum intensity was either the highest level that did not saturate the sensor on participants' skin or the sensor's maximum capacity: 50 mA for green light,

24 mA for IR, and 30 mA for red light. The medium intensity was defined as the average of the lowest and highest light intensities.

The study has two parts. 1) In the first part, the participants were asked to stay still while wearing the PPG earring, ring, watch, and a commercial pulse oximeter (BioRadio) as ground truth for two minutes. This part aimed to compare the PPG signal quality from different body locations under ideal, motionless conditions. 2) In the second part, the participants wore the PPG earring, ring, and watch while performing two common daily activities: using a phone and working on a laptop, with each activity lasting two minutes. The second part of the study was designed to assess the PPG signal quality during typical motions encountered in daily life. Both of the two parts of the study were repeated three times with three different light intensity settings.

PPG quality from earring vs. ring vs. watch during still

We compute the SNR results of the PPG signal collected from eight participants while they stayed still and did not move at all.

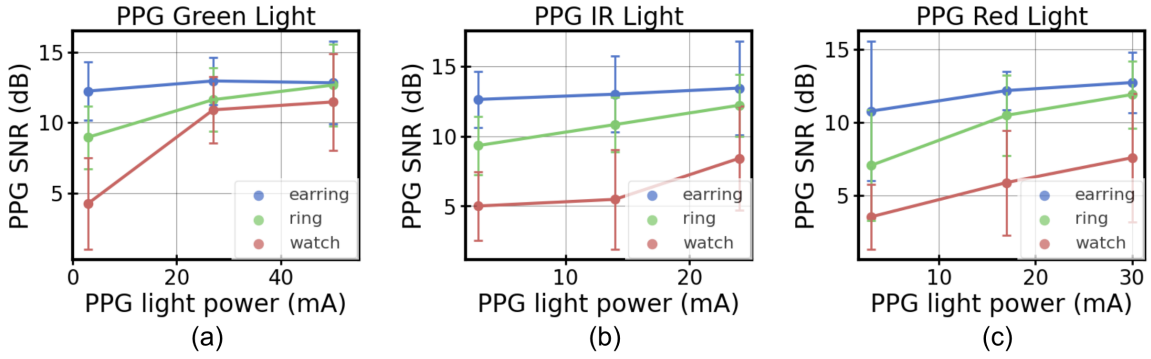

Figure 4.7: The SNR of PPG signal from earring vs. ring vs. watch, (a) using green light, (b) using IR light, and (c) using red light.

Figure 4.7 shows the PPG SNR results of the earring, ring, and watch with green, IR, and red light separately. The results show that the PPG signal obtained from the earring has a much higher SNR than the wrist for all lights and achieves a similar or higher SNR than the finger. It is expected since both the earlobe and finger have rich capillaries close

to the skin surface, while wrist blood vessels are deeper and more sparse. In addition, we noticed that there were three participants who had significantly low-quality PPG signals from the ring. Two of the participants reported cold hands, and another participant had callused skin on the fingers, which likely contributed to the low SNR from the finger. These three participants' data contributed to the ring's overall lower average SNR compared to the earring.

In addition to signal quality differences across measurement sites, Figure 4.7 shows that as PPG light intensity decreases, signal quality diminishes across all locations. However, the earlobe consistently maintains acceptable signal quality even at lower light intensities, whereas the signal from the finger and wrist drops significantly. This is likely due to the thin skin of the earlobe, which allows light to penetrate more easily into the underlying capillaries. These findings highlight the PPG Earring's potential for high-quality, low-power heart rate monitoring, leveraging the natural advantages of the earlobe's thin skin.

Among the three PPG light types, IR and green light deliver similarly high signal quality across all intensities for both the earring and ring, with IR slightly outperforming green for the earring. This is expected since IR penetrates the skin better and is well absorbed by oxyhemoglobin. Green light also performs well, only 0.6 dB lower than IR at the highest intensity for the earring. While green light doesn't penetrate tissue as deeply, its higher power compensates, making it the best choice for the wrist, likely due to the wrist's muscle and tendon composition—explaining why commercial smartwatches use green light for heart rate monitoring. Red light consistently shows the lowest SNR across all locations, especially at lower intensities. In pulse oximeters, red light is used with IR to estimate blood oxygen saturation (SpO2), and is less effective alone for heart rate monitoring.

PPG Earring vs. BioRadio as Ground Truth

We evaluated the PPG Earring's heart rate measurements against the commercial BioRadio pulse oximeter, which served as the ground truth because of its high signal quality and access to raw PPG data. BioRadio is widely used as ground truth in research [54, 58] for its reliability in physiological monitoring. Figure 4.8 (a) presents an example time-series

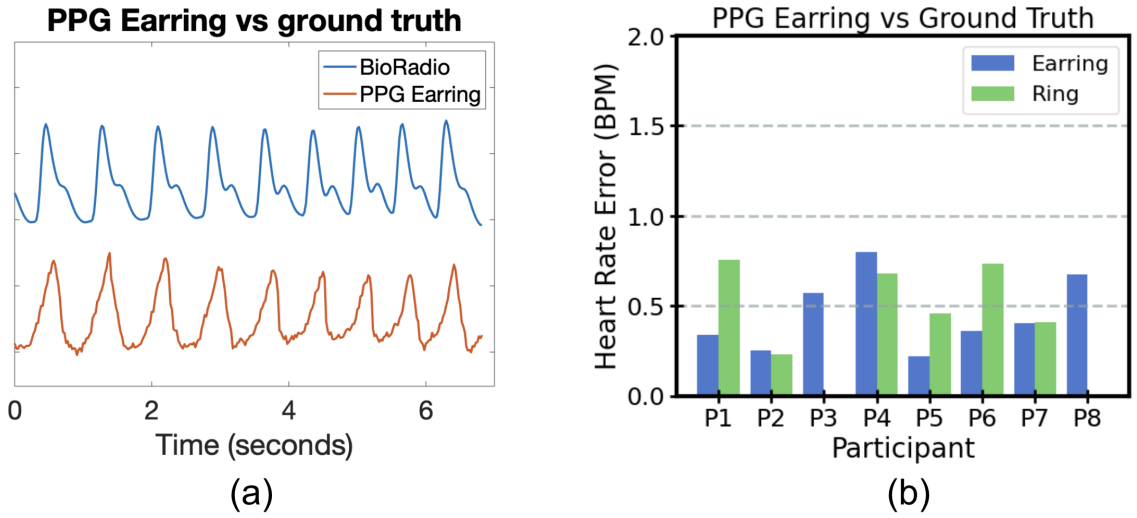

Figure 4.8: (a) Example of the synchronized PPG Earring signal and the BioRadio signal. (b) The average absolute heart rate error of PPG Earring and Ring compared to the BioRadio ground truth signal.

plot comparing the PPG Earring's signal to the BioRadio's PPG signal from the same participant. The signals were synchronized offline using cross-correlation. The heartbeats align well between the two devices, although the PPG waveforms differ slightly. The shape difference arises because 1) the BioRadio employs transmissive PPG while PPG Earring and other wearable devices use reflective PPG [112, 117], and 2) the measurement sites are different (fingertip vs. earlobe).

Figure 4.8 (b) shows the average absolute heart rate differences computed from the PPG Earring device and the ground truth device, as well as the PPG Ring and the ground truth device. Heart rates were computed using a standard peak detection algorithm with a 10-second sliding window and a 5-second overlap. To isolate the system's heart rate monitoring accuracy from signal quality issues on the wrist or fingers, noisy data from the PPG Watch and PPG Ring (P2 and P8) were excluded. On average, the PPG Earring demonstrated a mean absolute difference of 0.45 ± 0.21 BPM compared to the ground truth device, while the PPG Ring showed a mean absolute difference of 0.55 ± 0.22 BPM (excluding P2 and P8). These results demonstrate the high heart rate monitoring accuracy of the PPG Earring.

PPG from earring vs. ring vs. watch during activities

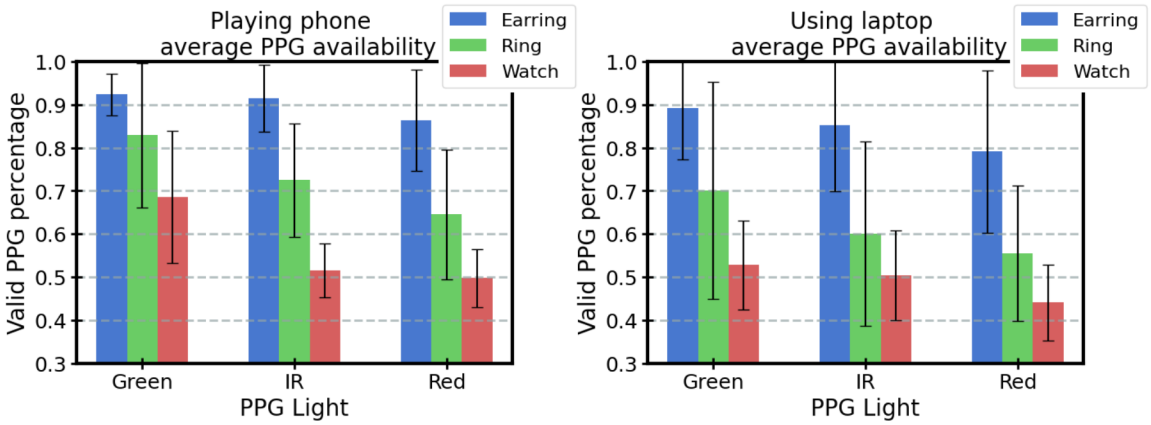

Figure 4.9: (a) The average valid PPG percentage from the earring, ring, and watch while playing on the phone. (b) The average valid PPG percentage from the earring, ring, and watch while using the laptop.

In addition to evaluating the PPG signal when the user is perfectly still, we also explore the PPG performance on the earlobe, finger, and wrist when the user is using a smartphone or laptop. Figure 4.9 (a) and (b) show the valid percentage of PPG while playing on the phone and using laptops, respectively. During playing the phone, earring achieves $92.40 \pm 4.82\%$ with the best light results, while ring and watch only achieves $82.89 \pm 16.769\%$ and $68.61 \pm 15.35\%$ respectively. During using the laptop, the earring achieves $89.25 \pm 12.04\%$, while the ring and watch only achieve $70.12 \pm 25.19\%$ and 52.84 ± 10.31, respectively. The results showed that both ring and watch locations are more significantly affected by subtle motions during these daily activities. Though the earring's valid PPG percentage does not change much between playing on the phone and using the laptop, the ring and watch's valid PPG percentage significantly decreased when using the laptop, likely because of larger and more frequent hand motions when using a laptop, such as scrolling or typing. Besides different PPG sensing locations, different PPG lights also showed different performance during the same activity. Overall, green light always has the highest availability for the earring, ring, and watch, which means green light is less susceptible to motion artifacts. IR light has similar availability for the earring, but significantly lower availability for the

ring and watch. And red light has the lowest availability across all devices. The results are expected as the green light is less susceptible to motion because of its shorter wavelength. IR light can penetrate more, so it is more likely to capture the internal muscle movement on the finger and wrist.

In summary, both green light and IR light can work well for the earring, while only green light might work well for the finger and wrist. The results of the study help guide future PPG sensing setups in different locations.

4.4.2 Exercise Study

Monitoring heart rate during daily activities and exercise is a key feature of modern wearables like smartwatches. However, capturing high-quality PPG signals during exercise is challenging due to strong motion artifacts caused by body movements.

To explore PPG Earring's heart rate monitoring capability during exercise, we recruited eight participants and conducted a semi-controlled exercise study. The participants consist of six females, one male, and one nonbinary gender, with an average age of 27.3 ± 5.4 and skin color range from type I to type V on the Fitzpatrick scale. The participants were asked to wear the PPG Earring at their comfortable tightness, and a commercial Fitbit smartwatch on their wrist at a tightness level that it will not move on the skin. The users were asked to complete three common exercise tasks at their comfortable level of intensity. The study included: 1) walking for five minutes, 2) running for five minutes, 3) performing nine sets of weight lifting using dumbbells. The weight lifting exercise included three sets of bicep curls, three sets of shoulder presses, and three sets of dumbbell rows. Each set includes ten repetitions. The total duration of the weightlifting exercise is around ten minutes, including rest periods. The total duration of the whole exercise study ranges from 20 minutes to 30 minutes for all users. The PPG Earring collected data at 50 Hz, which was later downsampled to 25 Hz to match the Fitbit sampling rate for comparison.

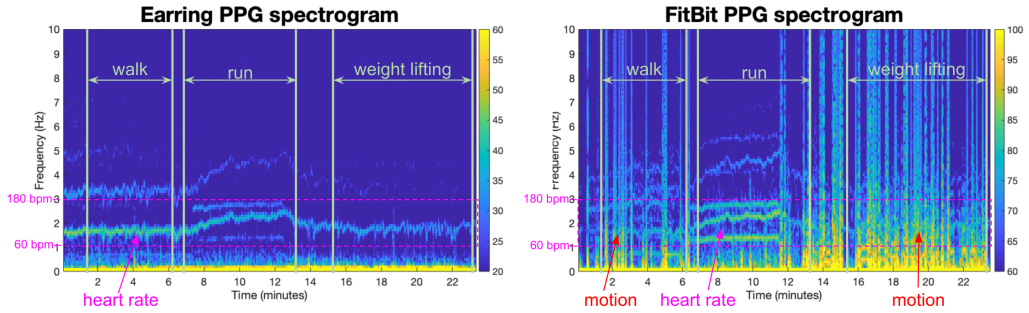

Figure 4.10: (a) The spectrogram of PPG data from the earring during exercise. (b) The spectrogram of PPG data from the Fitbit during exercise.

Example participant's PPG results

Figure 4.10 shows P1's spectrogram of PPG data from the earring versus from the Fitbit. The spectrogram was computed using the Short-Time Fourier Transform (STFT) with a window length of ten seconds and an overlap of five seconds. In Figure 4.10 (a), there is a clear continuous line from the start to the end in the heart rate frequency region (60 bpm to 180 bpm, which equals 1 Hz to 3 Hz). This line stands out distinctly against the background, representing the heart rate signal captured by the PPG Earring. We will validate this signal in a later section by comparing it to the Polar H10 chest strap, which serves as a reference.

In contrast, Figure 4.10 (b) shows the spectrogram from the Fitbit during exercise. As expected, the Fitbit PPG data is significantly affected by motion artifacts. Despite being worn tightly on the wrist, even small movements or muscle contractions in the hand still change the pressure between the wrist and the Fitbit sensor. These variations cause fluctuations or spikes in the reflected PPG light, which can overwhelm the subtle PPG signals, leading to inconsistent heart rate readings.

Valid PPG percentage

As discussed above, the PPG earring appears to be less likely affected by the motion artifacts during exercise and is still able to capture valid PPG data for computing heart rate. Figure 4.11 (a) shows the valid PPG signal percentage from earring versus Fitbit for each participant. The valid percentage of the PPG signal is defined in Section 4.3.

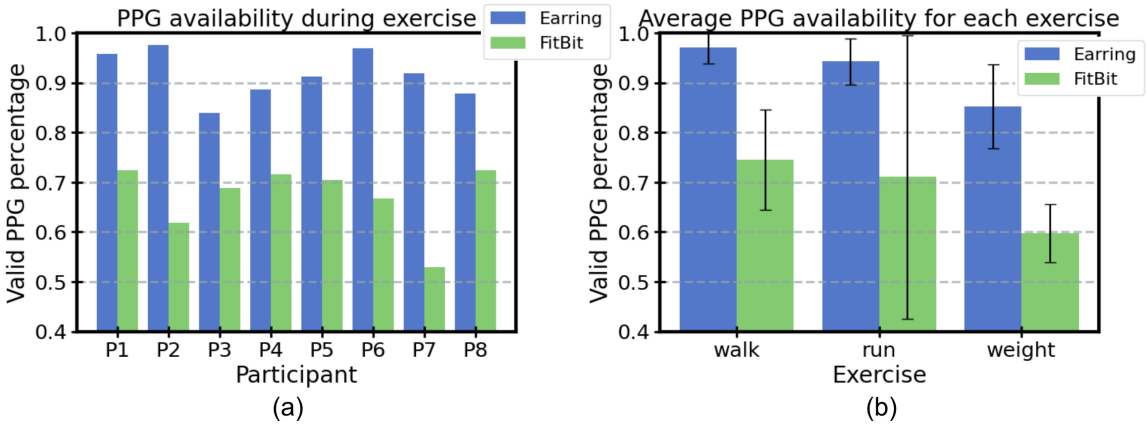

Figure 4.11: (a) The valid percentage of PPG signal from PPG Earring and Fitbit for each participant during exercise. (b) The average valid percentage of PPG signal for each exercise.

Figure 4.11 (a) shows the valid percentage of PPG signals from the Earring and Fitbit for each participant. Overall, PPG Earring captures valid PPG signals for more than 90% for six participants and 80% to 90% for two participants. On average, PPG Earring is able to capture 91.74 ± 4.84 % valid PPG signal during exercise for eight participants. In comparison, Fitbit captures valid PPG signals around 60% to 70% for most participants, except only 53% for P7. On average, Fitbit can only capture 67.16 ± 6.74 % valid PPG signal during exercise for eight participants. Though the Fitbit was worn on all participants not loosely, the natural contacting by the watch band does not guarantee constant pressure between the watch sensor and the skin, which can cause a lot of noise to the PPG signal. In addition, it should be noted that commercial Fitbit smartwatches might use a higher PPG light power than the earring, but we do not have access to the Fitbit PPG light setting.

Figure 4.11 (b) shows the average valid percentage of PPG signals for eight participants across different exercises. On average, PPG Earring achieves a valid PPG percentage of $97.03 \pm 3.13\%$ for walking, $94.25 \pm 4.63\%$ for running, and $85.18 \pm 8.46\%$ for weight lifting. Fitbit achieves $74.55 \pm 10.10\%$ for walking, $71.05 \pm 28.44\%$ for running, and $59.71 \pm 5.84\%$ for weightlifting. It is expected that walking has the highest percentage of valid PPG for both the earring and the Fitbit since walking is the mildest activity here. Running is a more intense activity but PPG Earring still maintained a high quality signal of 94.25% with low variance. Fitbit shows a large variance in the capability of capturing PPG signals

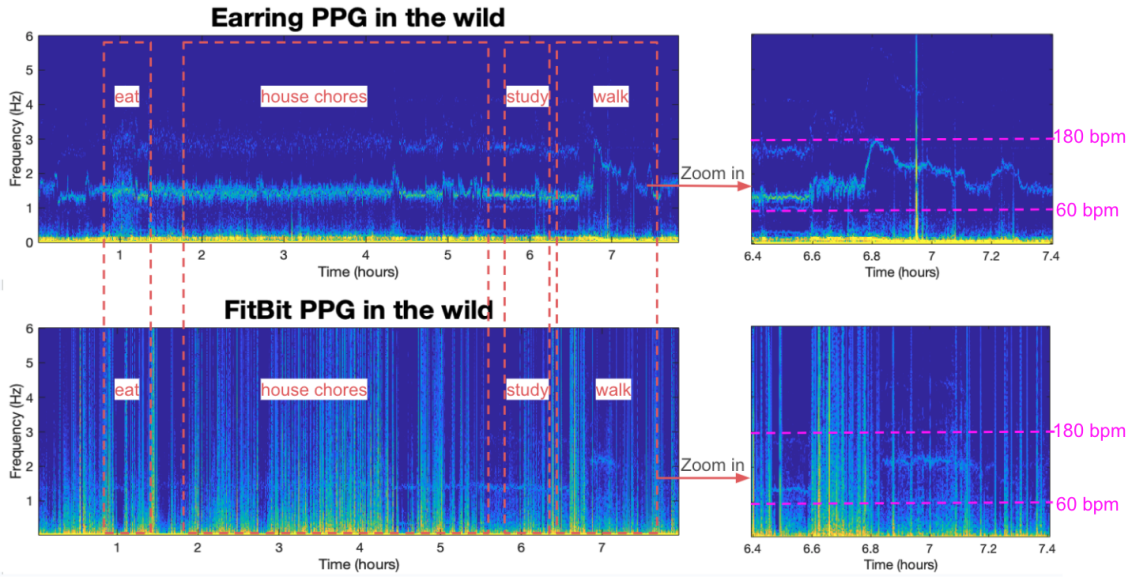

Figure 4.12: The spectrogram of P6's eight hours of PPG data from PPG Earring compared to the Fitbit, along with a zoomed-in spectrogram of one hour of activity.

during running for different participants, likely due to people's different running patterns. In addition, Fitbit shows a low percentage of PPG signals during weightlifting for all users. This is expected since people use arm and hand muscles during weight lifting, which often change the contact pressure between the Fitbit sensor and wrist skin.

In summary, the exercise study results indicate that PPG Earring is more reliable for heart rate monitoring during exercise than the Fitbit and potentially other wrist-worn smartwatches, particularly during intense exercise with frequent movements or hand-involved activities.

4.5 In-the-wild Study

We recruited six participants to wear the PPG Earring and a commercial Fitbit smartwatch for a day (at least eight hours) during their normal daily routines. The participants included four females, one male, and one nonbinary individual, with an average age of 23.67 ± 3.27 years. Their skin tones ranged from Type I to Type IV on the Fitzpatrick scale. Participants were instructed to wear the PPG Earring (without decorative elements) and the Fitbit by

themselves at a comfortable tightness. Some participants may wear the Fitbit more loosely than in the controlled exercise study. Each participant was provided an Android phone with the PPG Earring App to collect data, while the Fitbit data was stored locally on the device. They logged their activities in the Earring App throughout the day. At the end of the study, participants completed an online survey to rate the comfort of both devices and indicate their usual earring- and watch-wearing habits, including how frequently they wear these accessories in daily life.

4.5.1 PPG Earring vs. Fitbit smartwatch

Figure 4.12 presents the spectrograms of P6's eight-hour in-the-wild data collected from both the PPG Earring and the Fitbit. While the entire eight-hour spectrogram is dense and makes it difficult to observe rapid heart rate fluctuations over short time scales, we can still see general heart rate trends over the duration of the PPG Earring spectrogram, especially the increase in heart rate during periods of walking. The figure on the right provides a zoomed-in view of one hour of PPG data to provide details on the time scale, highlighting periods of both sitting and walking. Additionally, we observed that while the PPG Earring is generally less affected by daily motions, it is impacted by eating, specifically during chewing. This is likely due to the proximity of the earlobe to the jaw and facial muscles, where the movements during eating can cause motion artifacts.

When comparing the spectrogram results of the PPG Earring to those of the Fitbit, we noticed frequent vertical lines across all frequency ranges in the Fitbit spectrogram. These vertical lines are likely due to motion artifacts causing sudden changes in the PPG light path. The zoomed-in one-hour spectrogram of the Fitbit on the right shows that there are some short durations where valid heart rate signals are detectable and align well with the PPG Earring results despite the motion interference. Overall, Fitbit's data exhibited significantly more noise and motion artifacts than the PPG Earring data.

Figure 4.13 (a) shows the valid percentage of PPG signal for each participant in the study. One participant (P5) did not collect any data from either the PPG Earring or Fitbit, likely due to mishandling, and therefore, P5 is excluded from Figure 4.13. Across

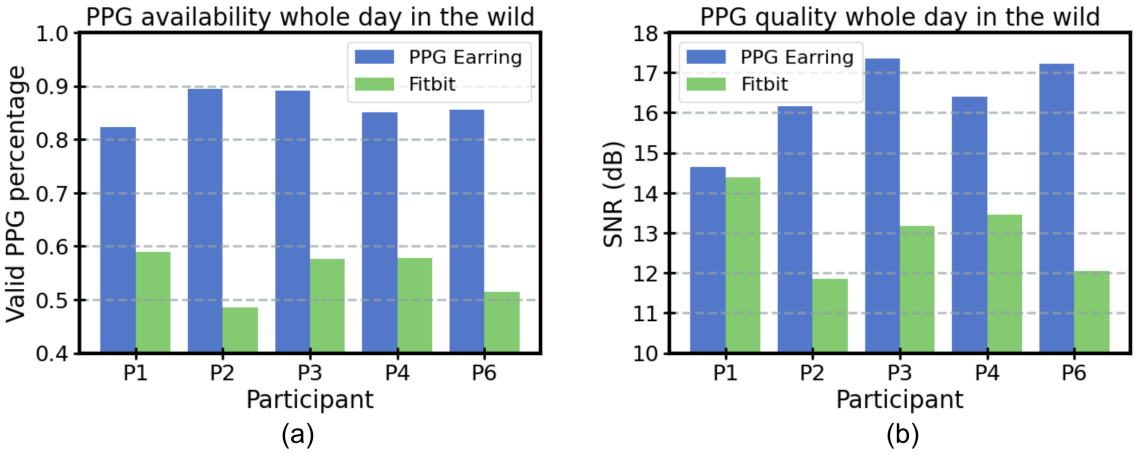

Figure 4.13: (a) The percentage of valid PPG signal during the whole day in the wild study from PPG Earring vs. from Fitbit. (b) The average SNR of PPG during the whole day in the wild study from PPG Earring vs. from Fitbit.

the remaining five participants, PPG Earring achieves an average valid PPG percentage of 86.29±2.96%, while Fitbit achieves 54.88±4.63% valid PPG. We observed that both devices recorded lower valid PPG percentages in the in-the-wild study compared to the exercise study. For PPG Earring, signal disruptions primarily occurred during self-reported eating periods, likely due to chewing or facial muscle movements introducing motion artifacts at the earlobe. This eating activity was present in every participant's data, contributing to the lower overall PPG availability in daily use. For Fitbit, the lower percentage was mainly due to participants wearing the device more loosely for comfort throughout the day, leading to increased motion artifacts.

Figure 4.13 (b) shows the computed average SNR for each participant. The SNR was computed based on the definition in Section 4.3, with an invalid PPG signal window being excluded from the SNR computation. On average, PPG Earring has an average SNR of 16.35±1.09 dB during the in-the-wild study. And Fitbit PPG's average SNR is 12.98±1.05 dB, which is significantly (3.4 dB) lower than PPG Earring.

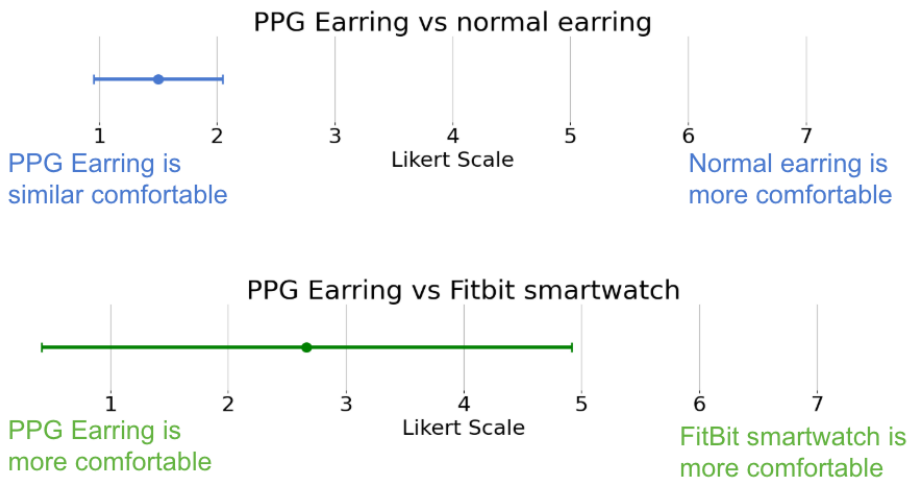

Figure 4.14: The comfort level comparison of PPG Earring vs. normal earring, and PPG Earring vs. Fitbit smartwatch.

4.5.2 PPG Earring Comfort Level Evaluation

After participants finished the in-the-wild study, we further asked them to complete a survey to assess the comfort of the PPG earring prototypes as well as their own earring-wearing habits. The survey evaluated the comfort of the PPG earrings during prolonged wear and compared it with that of the commercial Fitbit smartwatch and their daily earrings. The survey included both Likert scale ratings and open-ended questions to gather information on comfort levels for PPG earrings and Fitbit, participants' willingness to wear the PPG Earring or Fitbit daily, and the wearable comfort assessment for the PPG Earring and Fitbit [75].

PPG Earring's Overall Comfort

All six participants found the PPG Earring highly comfortable, with an average Likert rating of 1.33 $\pm$ 0.52 on a scale from 1 to 7 (where 1 means very comfortable). All participants found the PPG Earring was as comfortable as their normal earring: "***It was just as comfortable - I often forgot I had it on." (P3)***.

Most participants expressed strong willingness to wear the PPG Earring daily, with five

rating their willingness highly (giving a score of 1 or 2) and one participant giving a moderate rating (giving a score of 3). For daily wear duration, five participants were willing to wear the PPG Earring for all day (12+ hours), while one participant preferred 7 hours due to skin sensitivity, as they only wore gold earrings for extended periods. Participants' willingness to wear the PPG earrings for extended hours suggests that it could be an attractive option for people already accustomed to wearing earrings. To further enhance user acceptance, PPG Earring's future designs could incorporate gold or other hypoallergenic materials.

PPG Earring vs. Normal Earring

The Figure 4.14 illustrates the comfort comparison of PPG earring vs. normal earring, and PPG Earring vs. Fitbit. All participants reported PPG earring to be as comfortable as their normal earrings. Three participants rated 1 on the Likert scale, and three participants rated 2 on the Likert scale (where 1 means PPG earring is as comfortable as normal earrings).

Three participants (P3, P4, P6) noted that they were not aware of the earrings' presence: P5 described the PPG earring as *"lighter than my normal ones"*, and P2 mentioned that the PPG earring felt like *"a regular earring with heavier stud or hoop.*"

PPG Earring vs. Fitbit Smartwatch

Figure 4.14 shows the comfort preference of PPG Earring vs. Fitbit. The preference varied significantly across participants, with four participants finding PPG Earring much more comfortable (giving a score of 1 or 2) and two participants preferring Fitbit (giving a score of 5 or 6). While all participants expressed strong to moderate willingness to wear PPG Earring every day, they were less willing to wear the Fitbit daily, with four indicating unwillingness to wear the Fitbit smartwatch.

However, it should be noted that only three participants reported wearing smartwatches regularly (Garmin or Apple Watch), while all participants reported wearing their own earrings regularly, ranging from almost every day to every day. Among these three daily smartwatch users, two rated the Fitbit as more comfortable than the PPG Earring (giving a score of 5 or 6, where 1 indicates a strong preference for the earring and 7 indicates a

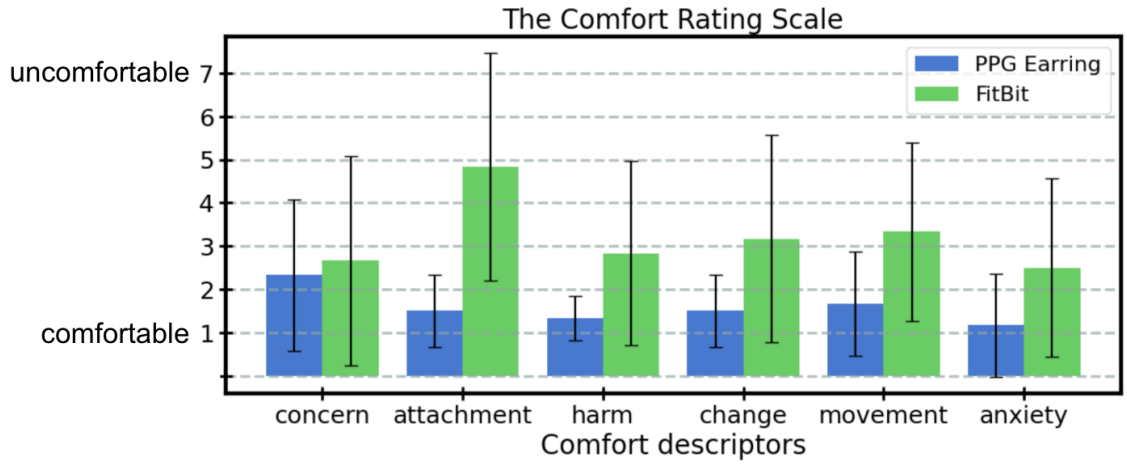

Figure 4.15: The comfort rating scale results of PPG Earring and Fitbit on six comfort aspects of wearables.

strong preference for the smartwatch), even though both rated the PPG Earring as "very comfortable" overall (giving a score of 1). Additionally, one smartwatch user rated the PPG Earring as significantly more comfortable than the Fitbit (giving a score of 1) because they did not like the feeling of the silicone watch band.

Figure 4.15 displays the comfort rating scale results for the PPG earrings and Fitbit across 6 standard comfort descriptors for wearable computers [75]. We explain the six comfort descriptors here:

- **Concern**: Worries about appearance when wearing the device.
- **Attachment:** Awareness of device presence/movement.
- **Harm**: Feeling that the device may cause harm/pain.
- **Change**: Feeling physically different while wearing the device.
- **Movement**: Device restricting movement.
- **Anxiety:** Insecurity while wearing the device.

Overall, PPG Earring consistently scored lower (indicating more comfort) across all descriptors. Notably, it received significantly lower scores in the "attachment" category, with participants reporting they were less aware of the earring compared to the Fitbit, suggesting the PPG Earring may be less intrusive and more comfortable to wear.

Participants' qualitative feedback supported this finding. Half of the participants (P1, P4, P6) mentioned that the smartwatch felt bulky and interfered with daily activities: "*I didn't like how bulky watches are, they inhibit some movement.*" (P1). These findings suggest that the PPG Earring offers a more comfortable, lightweight alternative that minimizes the feeling of wearing a device.

4.6 Discussion

4.6.1 Fashion Design

To enhance the aesthetic appeal of the PPG Earring, we explored the design options for the earring. The primary structure of the PPG Earring features a circular battery at the front of the ear, with the system's PCB positioned at the back, connected by two wires. Since the PCB is discreetly placed behind the earlobe, the design focus is on the battery and the battery wires. Figure **??** (a) (b) shows an example fashion design we had on the battery. We recolored the battery with a layer of copper tape and attached a gold-plated lace pendant to the front of the battery. We also threaded 2mm diameter pearls onto the two wires to decorate the wires, making the PPG Earring look like a hoop earring. While this is just one example, the battery can be decorated with a range of fashionable elements commonly seen in stud earring designs. The wires can also be painted in various colors or wrapped with different materials to create unique textures and shapes, such as a twisted gold wire design. The fashion design of the PPG Earring is highly adaptable, allowing users to customize their look by swapping out decorative battery modules. This modular approach enables users to easily change styles, offering a variety of fashionable options for the PPG Earring system without affecting its functionality.

Universal design

In addition to swapping out the battery module, the PPG Earring could potentially be transformed into a universal earring back, with all components—including the battery—positioned behind the earlobe. This would allow users to wear any normal earrings of their choice and just replace their earring back with a PPG Earring system. This requires a customized battery shape with a central hole to let the earring post go through. This design presents additional challenges, as it limits the battery's thickness, thereby restricting the system's power capacity and requiring more efficient energy consumption.

4.6.2 Smart earring as a sensing platform

While this paper primarily evaluates the PPG Earring for heart rate monitoring, the device is capable of much more. It can measure heart rate variability (HRV), a key well-being indicator affected by stress, exercise, and sleep [123]. Since HRV is even more sensitive to motion artifacts than heart rate, smartwatches and rings typically only assess it opportunistically during stable periods, such as sleep [100]. In contrast, PPG Earring's motion-resilient design shows promise as a continuous HRV tracker, providing timely insights into users' well-being. Besides heart rate and HRV, the PPG Earring also measures SpO2, motion, and earlobe temperature, making it a comprehensive health monitoring platform. SpO2 readings reflect blood oxygen levels, and low levels may indicate respiratory or circulatory issues. The PPG Earring can alert users during these conditions and prompt timely medical attention. The motion sensor tracks steps and estimates calories burned during exercise, while the temperature sensor monitors earlobe temperature, enabling early fever detection and insights into menstrual cycles [150]. Although this paper focuses solely on PPG Earring's heart rate monitoring, we envision it as a general health platform for both users and researchers, providing a foundation for future earlobe-based monitoring of physiological signals, activities, and well-being.

4.6.3 Cardiac diseases detection

Since PPG Earring can sense valid PPG signals most of the time, the PPG signal can potentially be used to detect Atrial fibrillation (AFib) and other cardiac-related diseases such as loss of pulse. While PPG for AFib detection is actively being explored in the research domain, it is largely limited to strict still conditions because motions can cause a lot of false positives on smartwatch PPG [107]. Google recently introduced the loss of pulse detection using the PPG from Pixel watch [55], while the Pixel watch requires a lot of algorithm processing to keep out the false positives of bad PPG signals, PPG earring can potentially achieve this with better accuracy and a simpler algorithm because of the nature of a reliable PPG signal from the earlobe. In addition, most people wear two earrings, which can further reduce the false positive rate of cardiac disease detection.

4.6.4 Limitations and future work

Wearing the PPG Earring requires a pierced earlobe, which limits the target user group, as approximately 80% of women in the U.S. have pierced earlobes [127], while the percentage is significantly lower among men. While we have explored a magnet-based earring that does not require piercing, its performance was suboptimal due to increased susceptibility to motion artifacts and a higher likelihood of detachment during high-intensity movements. For the final design, we selected the pierced earring attachment due to its secure and consistent mechanical stability, which significantly improves signal quality. However, this choice also restricts the potential user base. In the future, a piercing-free, magnet-based earring could be an alternative if the overall weight of the PPG Earring system can be significantly reduced, allowing the magnets to hold the earring securely in place.

In this paper, we did not compare the PPG Earring's signal quality to a medical-grade heart rate monitor, such as an electrocardiogram (ECG), as PPG is a well-established and extensively studied technology. However, a clinical-grade study remains a crucial future step, particularly for cardiac disease detection applications.

PPG signal quality varies significantly based on skin color, with a well-known reduction in signal strength for darker skin tones [3]. We observed that IR light on the earlobe

performs better for darker skin, while green light generally offers superior signal quality for lighter skin tones. This is likely due to IR light's ability to penetrate deeper into the skin and reach the blood vessels, whereas green light is more likely to be absorbed by darker skin. In future iterations, the PPG Earring could incorporate automatic adjustments to both light color and power settings, optimizing performance for different skin tones and environmental conditions.

In this paper, we only explored PPG Earring's usage during the daytime, instructing participants to remove it during sleep to avoid accidental damage. However, heart rate monitoring during sleep provides valuable insights into the user's sleep quality. In the future, with more careful mechanical design and rigorous testing, the PPG earring could be adapted for use during sleep, enabling the collection of sleep quality data from the earlobe.

We observed that eating or chewing can cause significant noise on the PPG data on the earring, likely due to the jaw and facial muscle movement causing motion artifacts. While this movement interferes with PPG signal clarity, it could also be leveraged as a detection signal for eating behavior, allowing for monitoring of eating time and duration, which are important factors in overall health and wellness tracking.

While none of our participants reported issues with the PPG Earring's fit, individuals with significantly smaller than average earlobes ($19.6mm \times 18.8mm$) might find its $14mm$ diameter challenging to wear [24]. Future earring designs could be half the size through a double-layer PCB integration, accommodating potential users with very small earlobes.

4.7 Summary

We present PPG Earring, a smart earring for heart rate monitoring using PPG. PPG Earring measures 14 mm in diameter, weighs 2.0 g, and offers 21 hours of continuous PPG and motion sensing wirelessly. In experiments comparing PPG signal quality across earrings, rings, and watches under identical light settings, the earlobe provided 1.2 to 8.0 dB better signal quality than the wrist, and 0.2 to 3.3 dB better than the finger. We compared the PPG Earring's performance to a commercial Fitbit smartwatch in an exercise study and a whole-day in-the-wild study. The exercise study shows that PPG Earring captures valid heart rate data for 91.74 ± 4.84 % of the time during exercise, which is 24.5% higher than

Fitbit. In our whole-day study, PPG Earring captured valid PPG for $86.29 \pm 2.96\%$ of time, which is 32% higher than Fitbit and has a 3.4 dB higher SNR. In addition, all participants in the in-the-wild study found the PPG Earring as comfortable as their regular earrings, and five out of six participants expressed a strong willingness to wear the PPG Earring all the time every day. Our study results not only validate PPG Earring's signal quality but also prove its comfort, highlighting its potential as a reliable daily health monitoring device.

Chapter 5

ECG NECKLACE

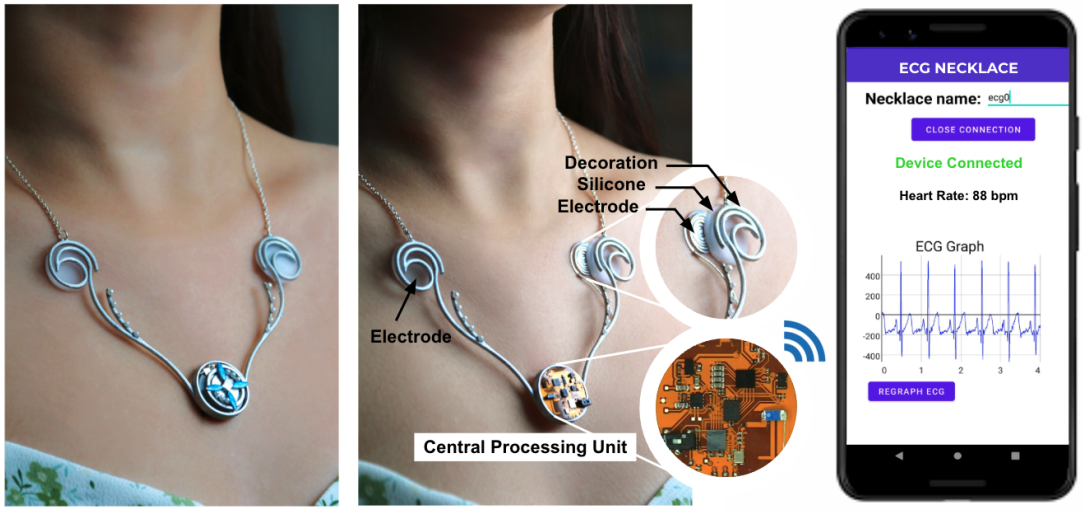

(a) ECG Necklace final form factor (b) ECG Necklace exploded view (c) ECG Necklace App

Figure 5.1: (a) The ECG Necklace with fashion design. (b) An exploded view of the ECG Necklace, showing the PCB beneath the central pendant and the novel skin moisture-enhanced electrodes. c) The smartphone app visualizing ECG data wirelessly transmitted from the necklace.

5.1 Introduction

Cardiovascular diseases are the leading cause of death globally, accounting for an estimated 17.9 million lives or 32% of global deaths [147]. Electrocardiogram (ECG) is a key diagnostic tool in medicine to diagnose heart conditions. They record the electrical activity of the heart over a period of time using two or more electrodes placed on the skin. While widely used in clinics, ECG is difficult to schedule, and many heart conditions, such as arrhythmias, are transient, with symptoms that may disappear before diagnosis. In addition, 20% to 50% of heart attacks are "silent", meaning patients experience no symptoms or

unrelated symptoms, such as flu-like symptoms, instead of traditional symptoms like chest pain [30, 121, 35]. Without continuous ECG monitoring, these silent critical warning signs are unnoticed, and up to 50% of cases are diagnosed only after heart disease has progressed to a later stage [45].

Continuous, everyday ECG monitoring is critical for detecting the onset of heart diseases and enabling early intervention. However, achieving this in a daily wearable format remains challenging due to the trade-off between accurate electrode placement and wearability. Standard electrode placement, with electrodes far apart on different sides of the heart, is critical for accurate diagnosis but limits wearability. ECG Holter monitors use cumbersome cables to achieve standard placement but sacrifice comfort, making them suitable only for ambulatory monitoring. ECG patches improve wearability but rely on non-standard placements, limiting their clinical utility to arrhythmia detection only. Consumer wearables like smartwatches, which use the left and right hand for electrode placement, cannot provide continuous monitoring. They require users to touch the watch crown to complete the circuit, allowing only brief 30-second recordings, which limits their suitability for continuous ECG tracking.

We address this challenge and provide continuous, clinically valuable ECG monitoring in a wearable format by leveraging the necklace's natural shape around the chest. As shown in Figure 5.1, the necklace's positioning allows two electrodes to be placed on the left and right sides of the heart, enabling similar to standard Lead I placement to capture horizontal heart activity for diagnosing a broad range of conditions. The ECG Necklace comprises a compact processing unit as the central pendant and two non-adhesive electrodes as adjacent pendants. In a study with 12 participants, we demonstrated that the necklace's ECG signal is comparable to a Holter monitor with standard Lead I placement, providing a reliable signal for heart diagnostics. As necklaces are widely accepted as everyday accessories worn by millions, this form factor has the potential to become a consumer-friendly wearable for daily use.

Achieving continuous ECG sensing while ensuring long-term comfort presents significant challenges. Standard adhesive gel electrodes, while effective, are uncomfortable for extended wear due to skin irritation and are single-use only because of gel evaporation. To address

this, we design a novel skin moisture-enhanced electrode that uses natural skin moisture as the electrode "gel" to improve the electrode performance. Since skin moisture (i.e., sweat) is deformable and conductive due to electrolytes, it improves the skin contact with the metal electrode and improves the signal quality [8, 70], like traditional ECG gels. As human skin continuously produces moisture that evaporates into the air [4], we leveraged a thin layer of skin-friendly silicone that acts as a barrier against water evaporation from the skin, creating a moisturizing micro-environment as "gel" for the electrode. Unlike adhesive electrodes, the skin-friendly necklace electrodes avoid skin irritation and do not suffer from gel evaporation by leveraging the continuous production of moisture by the body.

In addition to electrode comfort, developing a wireless smart necklace requires addressing several technical challenges related to size, weight, and battery life to ensure long-term wearability. Size constraints directly affect power consumption due to the limited energy density of batteries. To design a wireless system within these limitations, we utilized a highly integrated ECG analog front-end chip and an ultra-compact nRF52 microcontroller. By carefully optimizing both size and power consumption, we achieved a compact design with a 22 mm, 4-gram pendant—over four times smaller than the smallest continuous ECG patches [14, 160, 140]. The ECG necklace offers a 4-day battery life with continuous 250 Hz sampling and wireless streaming, which can be further extended by reducing the sampling rate.

We investigated various aspects of the ECG necklace design, including electrode placement, electrode design, and the necklace's overall performance in natural daily scenarios. We evaluate the novel electrode design by a benchmark test and a twelve users experiment, showing that our electrode with diameters between 15-25 mm achieve impedance and Signal-to-Noise Ratio (SNR) comparable to those of the standard adhesive gel electrodes. We compare the ECG Necklace's performance versus an FDA-approved Holter monitor in real-world testing, with twelve participants performing common activities (talking, using laptops and smartphones). We validated the difference between the key features from the ECG necklace and Holter monitor is only 3.2 ms for the R peak, 8.5 ms for the P peak, and 15.7 ms for the T peak, all of which are well within the generally acceptable error range of 20 ms [34]. In addition, we conducted a whole-day in-the-wild study with ten users wearing

the necklace and a consumer heart rate chest strap with ECG sensing. The ECG Necklace demonstrates comparable ECG signal availability to the tightly worn chest strap and 1.5 dB higher signal quality than the chest strap. In addition, nine out of ten users strongly prefer the necklace over the commercial chest strap in terms of comfort, indicating its potential as a daily ECG and health monitoring system.

We summarize this paper's **contributions** below:

- We developed a wireless necklace for continuous ECG monitoring by utilizing the necklace's unique shape for accurate electrode placement while maintaining wearability. The ECG necklace features a compact design with a 22-millimeter diameter pendant with an 88-hour-long battery life.

- We designed a novel skin-moisture-based electrode using silver PCB and silicone. We conducted a benchmark test and an on-user experiment to characterize the electrode's size, frequency response, impedance at different moisture levels, and actual on-user performance.

- We conducted real-world studies to assess the ECG Necklace's signal quality compared to an FDA-approved ECG monitor. We further conducted a whole-day in-the-wild study to evaluate the ECG Necklace's signal availability, quality, and comfort level in natural daily settings compared to a commercial chest strap.

5.2 Background on ECG

ECG operates by detecting small electrical voltages generated by the depolarization and repolarization of the heart muscles during each cardiac cycle. ECG can be measured by placing a pair of ECG electrodes at two locations on the body and recording the voltage difference between them. Each pair of electrodes forms a lead and represents the axis along which the cardiac vector is visualized.

The typical ECG waveform, as shown in Figure 5.2, consists of three primary elements: the P wave, the QRS complex, and the T wave, each corresponding to a different part of the heart. Medical professionals analyze the ECG by examining the waveform's overall shape,

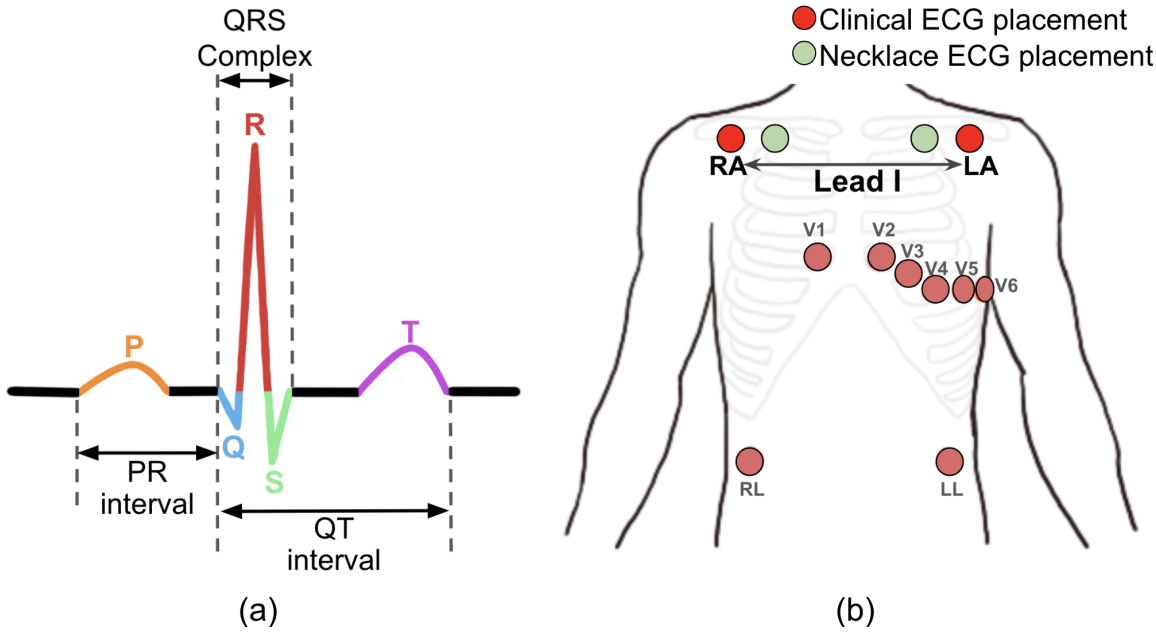

Figure 5.2: (a) Example of an ECG waveform from a heart in normal sinus rhythm. (b) The electrode placement in clinical standard 12-Lead ECG and the necklace's electrode placement.

timing and magnitude of the P, QRS, and T wave. Variations in these parameters can reveal a wide array of cardiac conditions. For example, atrial fibrillations (AFib) is diagnosed by looking for the absence of regular P waves and the presence of irregular R-R intervals.

5.2.1 Electrode Placement Requirement

Electrode placements have to follow standard guidelines, which clinicians heavily rely on for accurate diagnosis [116, 72]. Figure 5.2 (b) shows the standard 12-lead ECG setup utilizing 10 electrodes. They can be simplified by choosing just the RA, LA, and LL electrodes to form a 3-lead or 1-lead ECG. Lead I setup is one of the most common setups, with the negative electrode (RA) positioned on the right shoulder below the right clavicle and the positive electrode (LA) positioned on the left shoulder. Lead I captures the heart's electrical activity along the horizontal axis and provides insight into a wide range of heart conditions, making it suitable for the ECG necklace setup. We will discuss and evaluate electrode placement in the ECG necklace in Section 5.3.3.

5.2.2 Electrode Design

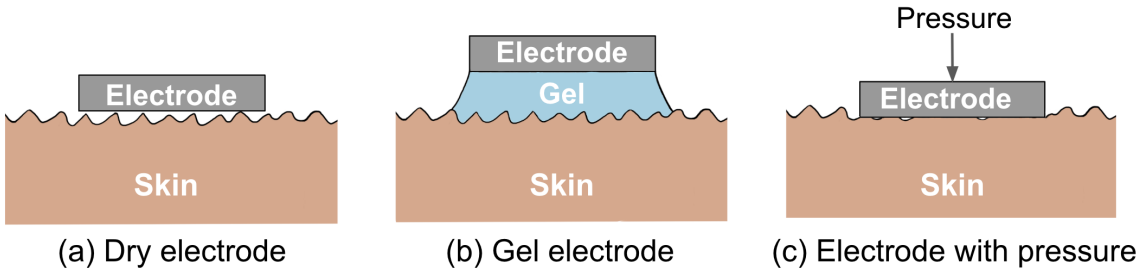

Figure 5.3: Demonstration of skin contact with (a) a simple dry electrode, (b) a gel electrode, (c) a dry electrode when pressed to the skin

ECG electrodes are essential parts for obtaining accurate ECG signals. These electrodes, typically made from conductive metals, are attached to the skin to transmit voltage signals from the body to the ECG device. The most common electrodes are adhesive gel electrodes that adhere tightly to the skin, with a layer of conductive gel between the skin and the electrode to enhance ECG voltage signal transmission. The necessity for conductive gel arises from the skin's uneven textures on a micro-level, which limits the amount of contact surface between the skin and the electrode.

As shown in Figure 5.3 (a), without conductive gel, the contact surface area between skin and electrode is minimal. The resulting air gap between the skin and electrode acts as an insulator to voltage, ultimately reducing the quality of the obtained signal. In comparison, conductive gel bridges the skin-electrode gap as shown in Figure 5.3 (b), which not only significantly increases skin-electrode surface contact but also improves the impedance mismatch between the human body and the electrode. Although adhesive gel electrodes ensure a high-quality ECG signal, they are uncomfortable to wear for extended periods, and the residue from the adhesive layer can remain on the skin for multiple days. Additionally, the electrodes stop working once the gel evaporates, typically within two hours of air exposure.

Besides adhesive gel electrodes, applying increased pressure on the electrode towards the skin can also enhance skin-electrode contact, as demonstrated in Figure 5.3 (c). Devices such as chest strap-based ECG and smartwatches use elastic bands to apply this pressure

and improve signal quality. However, excessive pressure can be uncomfortable for users and unsuitable for devices like necklaces.

5.3 System Design

Designing a smart necklace wearable device requires a careful balance between functionality, user comfort, and aesthetic appeal. In this section, we will introduce the key components of the ECG necklace system. As shown in Figure 5.4 These include the ECG sensing front-end chip, the innovative design and strategic placement of ECG electrodes, an accelerometer for motion tracking, wireless communication technology for seamless data syncing, and the battery that powers the entire system. We will discuss how each element has been thoughtfully selected and integrated to optimize both performance and design aesthetics.

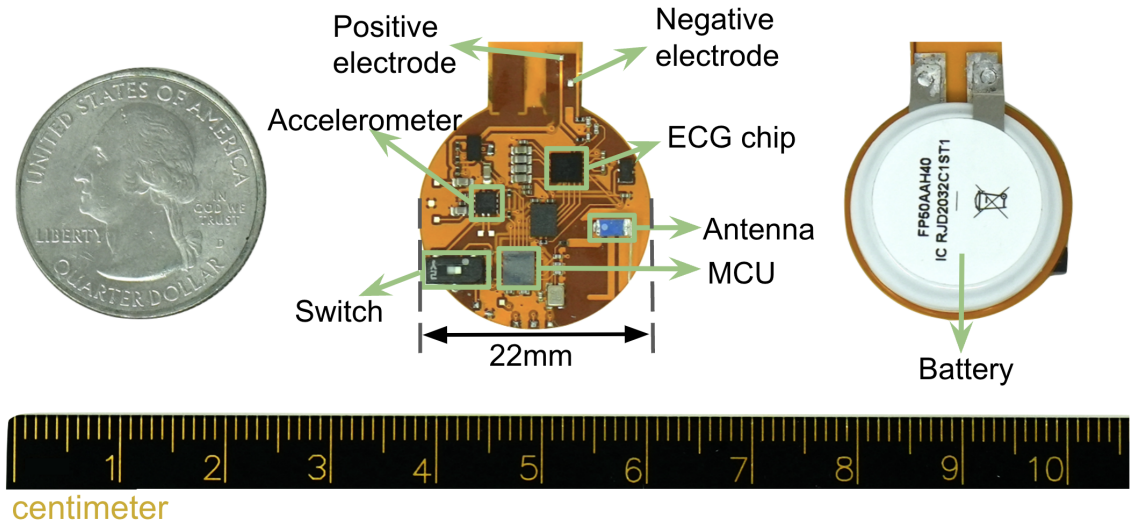

Figure 5.4: The front and back sides of the ECG necklace system, with a US coin as reference for size.

5.3.1 ECG Analog Front End

We implemented the ECG sensing analog front end using the MAX30003 chip, which features a compact size of 2.3 mm by 2.8 mm and ultra-low-power consumption of 100 µA. To maximize the quality of ECG readings, the MAX30003 was set to operate at its highest

amplification gain setting of 160 V/V and a sampling frequency of 250 Hz. The communication between the chip and the system's microcontroller is established through an SPI communication interface. ECG data captured by the MAX30003 is temporarily stored in a FIFO buffer, capable of holding up to 32 samples. This configuration allows the microcontroller to retrieve data from the buffer every 64 milliseconds, ensuring timely processing of ECG samples while reducing the frequency of microcontroller wake-ups to conserve power.

5.3.2 Dry Electrode

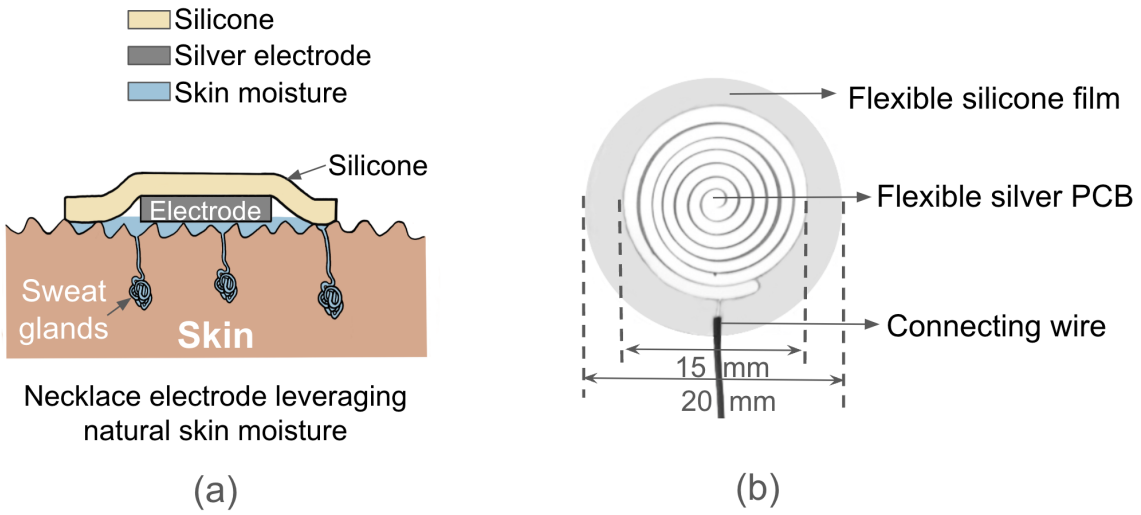

Figure 5.5: (a) The demonstration of the necklace electrode that leverages natural human skin moisture as the ECG "gel". (b) The components of the necklace electrode.

As discussed in Section 5.2.2, acquiring a high-quality ECG signal typically requires the use of either conductive gel, sufficient pressure, or adhesion to ensure the electrode's contact with the skin without any air gaps. However, excessive pressure and strong adhesion are not suitable for long-term comfort.

To address these challenges, we have developed an innovative solution: a flexible silver-based electrode with a flexible silicone film layer as its substrate. This design leverages the flexibility of the silicone layer to not only secure the electrode against the skin but also to create a moisturizing micro-environment between the skin and the electrode. Given that

human skin naturally loses moisture through transepidermal water loss (TEWL), where the silicone layer acts as a barrier against water evaporation, ensuring a moist interface. Additionally, the natural conductivity of human sweat, because of electrolytes such as sodium, chloride, potassium, and magnesium, facilitates its role as a conductive gel in this setup. Silicone was chosen because of its skin-friendliness. It is biocompatible, hypoallergenic, and does not promote bacterial growth, making it widely used in a range of skincare and medical applications, including being a gold standard for non-invasive scar treatment [143]. Silicone patches occlude and hydrate the stratum corneum of the treated skin area. After applying the silicone patch, the rate of water loss via evaporation of the treated skin area is much less than the untreated area, making the skin adequate but not over-hydrated [129]. Furthermore, the design is enhanced by the electrode pendant's weight, which applies a gentle and comfortable pressure to augment skin contact without compromising comfort.

Figure 5.5 shows the structure of our designed electrode. The conductive layer is a silver-coated flexible PCB, which can be fabricated through the standard process. This PCB, with a diameter of 15 mm and a thickness of 0.1 mm, is coated with silver to ensure optimal conductivity [73]. Its flexibility is further augmented by a laser-cut swirl pattern, enabling it to conform to the skin's texture. A thin wire is soldered to the silver-coated flexible PCB to connect the electrode with the necklace's central system. As any wire on the skin side of the flexible PCB could significantly increase the air gap between the skin and the electrode, we utilized vias on the PCB to connect the front side and the back side of the PCB, and the wire is soldered on the back side of the PCB to avoid causing air gap. The silicone layer is produced using Smooth-On EcoFlex 00-10, a user-friendly pourable silicone. Inspired by silicone scar patch and silicone wrinkle patch, we mixed the silicone base liquid, its curing agent, and simple body lotion in a 1:1:1 ratio. By curing it at room temperature, a highly flexible and stretchable silicone rubber is formed. The addition of lotion makes the silicone patch slightly adhesive without the need for glue, enhancing its ability to adhere to the skin without causing irritation. Our innovative necklace electrode is easy to manufacture yet effective. We will evaluate the performance of the electrode in Section 5.5.2.

5.3.3 *Electrode Placement Design Space*

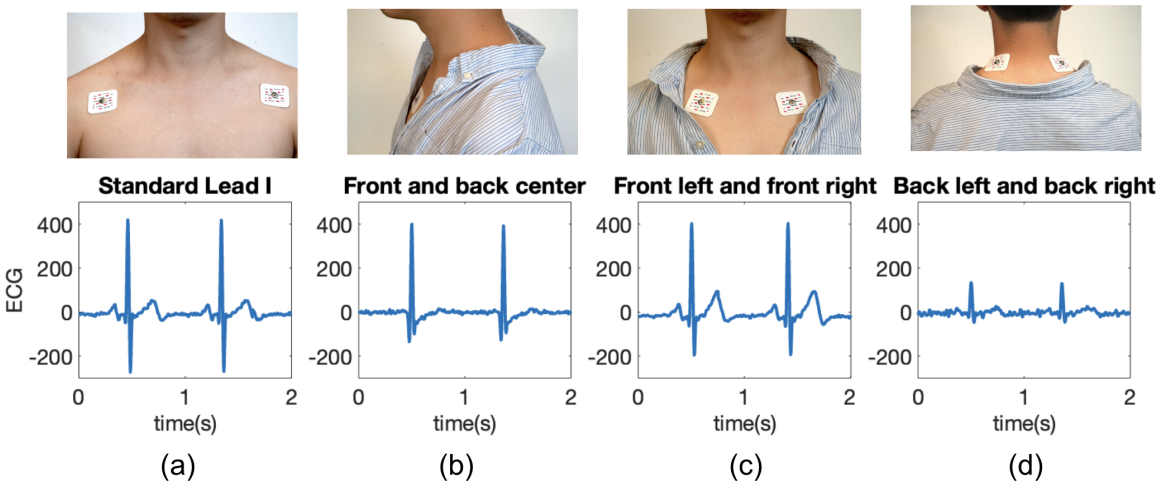

Figure 5.6: ECG signals from different electrodes placement: (a) standard clinical lead I placement, (b) front center and back center, (c) front left and front right under the collarbones, (d) back left and back right.

We explore the necklace's unique design space by testing five different electrode placements to achieve a balance between clinical value and aesthetic appeal. Figure 5.6 illustrates the electrode placements we tested and the corresponding example ECG signals obtained from each configuration.

Standard Lead I configuration: Figure 5.6 (a) shows the electrode placement and its corresponding signal from Lead I configuration. It clearly contains the P wave, QRS complex, and T wave, and we will use it as the reference for the electrode placement experiment.

Front center and back center: Figure 5.6 (b) shows the placement and data from the front center and back center. This placement is particularly convenient for concealing the technology within the necklace, with the electrodes hidden behind the central pendant. As shown in Figure 5.6 (b), ECG signals obtained from this placement showed clear QRS complex but almost no P wave, which is important for many heart conditions diagnosis such as AFib and heart attack. Despite its limited clinical value, this setup can still provide valid

heart rate and arrhythmia monitoring and detect Ventricular Hypertrophy from a widened QRS complex, which is worth exploring in the future.

Front left and front right: Figure 5.6 (c) shows the placement and data from front left and front right. The electrodes were placed at the extended line of the neck and below the clavicle. Given that the width of an adult's heart is approximately 8 cm (3.5 inches)—about the size of a person's fist [37]—and typically narrower than the neck width. This placement strategy allows for capturing the heart's ECG signal on the horizontal axis, and its signal shows valid P wave, QRS complex, and T wave, with almost the same shape as the standard lead I placement, with the potential to provide highly valuable clinical data.

Back left and back right: Figure 5.6 (d) shows the back left and back right electrode placement and corresponding signal. This electrode setup captures the heart's activity from a similar horizontal angle as those on the front, yet they have a much higher noise level, likely due to more attenuation.

In addition to the electrode placements shown in Figure 5.6, we have also tested the electrode placements combining the front center with either the back left or back right. However, this electrode placement does not show consistent ECG waveforms across different users, which is likely due to these configurations capturing only half of the heart's electrical activity, leading to distorted and variable ECG waveforms. So we do not recommend these electrode placements, and they are not included in Figure 5.6.

Design choice: We chose the electrode placement on the front left and right for our final design, considering its high SNR and similarity to standard Lead I configuration. However, there is a trade-off between aesthetic appeal and clinical value. While some electrode configurations may capture only partial ECG data, they are still valuable to explore in the future.

5.3.4 Other Sensing Capabilities

Though this paper mainly focuses on the ECG sensing part, we envision the necklace has the potential to become a daily health and fitness tracker. Thus, we have integrated motion sensing capability to it. We selected the LIS2DW12 accelerometer to sense the user's

movements. It features a low active current consumption of 1 uA and a sensitivity of 0.244 mg/digit, which offers configurable settings for both the sensing scale and sampling rate. The accelerometer is set to sample at 50 Hz, which is high enough to track human motions. This addition can potentially turn the necklace into a comprehensive health monitoring platform capable of tracking physical activity, breathing patterns, and subtle seismocardiography (SCG) signals. However, since the accelerometer signal analysis on the chest is well studied [28, 103], this work does not focus on analyzing the accelerometer data.

5.3.5 Bluetooth Communication and MCU

The ECG necklace is designed to be fully wireless, prioritizing comfort and ease of use. Bluetooth Low Energy (BLE) was chosen for its low power consumption, sufficient range, and reliable data transfer rates, making it ideal for this application. The nRF52832 microcontroller was chosen to implement BLE data streaming and interfacing with the sensors. It features a compact size (3.0 x 3.2 mm) and energy efficiency, which are essential for the compact design of the ECG necklace. To conserve energy, the microcontroller operates primarily in deep sleep mode, waking briefly for data exchanges and BLE transmission.

Every 120 milliseconds, the nRF microcontroller retrieves data from the FIFO buffers of the MAX30003 ECG chip and the LIS2DW12 accelerometer chip. This interval matches the ECG chip's capacity to store up to 32 samples, preventing data loss. During each wake cycle, the microcontroller reads 30 ECG samples and 18 accelerometer samples (6 from each axis), packages them into a single transmission packet, and sends it via Bluetooth before returning to deep sleep. This efficient process minimizes active time, maximizing battery life while enabling continuous, real-time monitoring.

5.3.6 Battery

We selected the RJD2032C1ST1 rechargeable battery to power the entire ECG necklace system. This battery offers an 87 mAh capacity and features a compact, round form factor with a diameter of 20 mm and a thickness of 3.5 mm. While certain hearing aid batteries of a similar size offer higher capacities, they cannot be recharged due to their chemical

compositions.

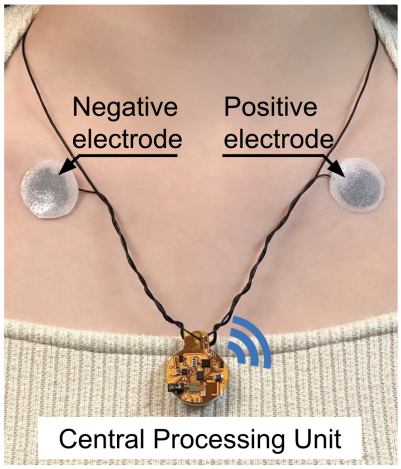

Figure 5.7: Demonstration of wearing the ECG Necklace (without any fashion decorations).

5.3.7 The Final Necklace Design

Figure 5.7 shows the final necklace design and how a user would wear it. The pendant contains the main necklace system and is made on a round, flexible Printed Circuit Board (PCB). The front side of the PCB houses all the electronics, including the ECG front-end chip, Bluetooth microcontroller, and an accelerometer for potential motion sensing. The positive and negative electrodes for ECG sensing are wired to this side of the PCB. Meanwhile, the back side of the PCB is dedicated exclusively to the battery. This double-sided PCB design maximizes the use of the limited area while maintaining a slim and wearable profile. The battery life is 88 hours, supporting continuous ECG signal streaming at 250 Hz and accelerometer signal streaming via Bluetooth. Besides the pendant, the two electrodes are placed under the collarbone, with a thin piece of silicone to hold it onto the skin. The entire necklace system weighs approximately 5 grams, with the central pendant (including the battery) weighing 4 grams and the two silicone-covered electrodes weighing 1 gram. Additionally, fashion components can be added to the necklace to enhance its aesthetic appeal and social acceptance. With the 3D-printed fashion design cover shown in

Figure 5.1, the necklace has a total weight of 7 grams. We further discuss adding fashion components to the necklace in Section. 5.8.1.

5.4 Signal Processing Pipeline

In this section, we present the signal processing pipeline for the ECG data and define the evaluation metrics for later sections.

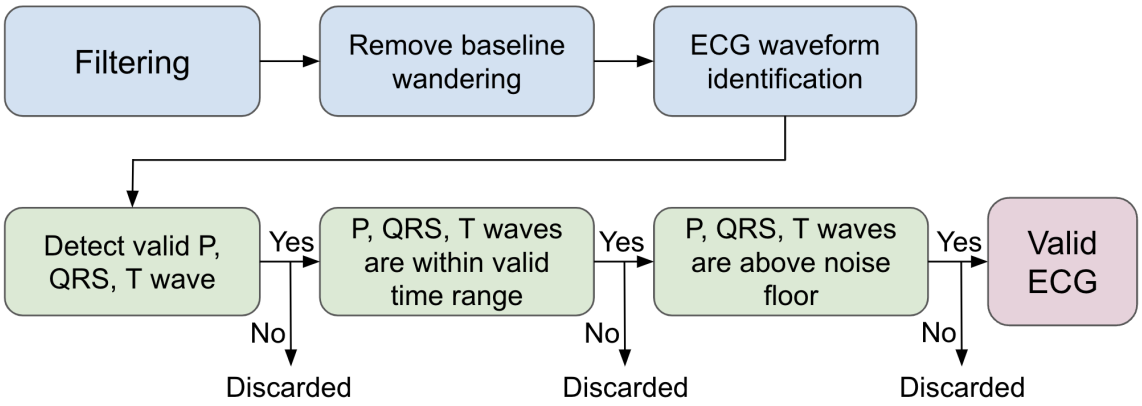

Figure 5.8: The processing pipeline for ECG data.

Filtering: Indoor environments contain significant electrical interference, primarily from 60 Hz or 50 Hz powerline signals coupled to the human body. To address this issue, we designed a band-stop filter targeted specifically at 60 Hz or 50 Hz—depending on the country's powerline standard—as well as at its harmonics at 120 Hz or 100 Hz. The filter has a narrow 2 Hz stopping bandwidth to minimize impact on other frequencies.

Remove baseline wandering: Baseline wander is a common low-frequency artifact in ECG recordings caused by movements and breathing. To address this, we used a wavelet decomposition-based method proposed by Sargolzaei et al. [120], now widely used in ECG processing. This method analyzes the power of the baseline relative to the ECG signal through continuous signal decomposition. Unlike high-pass filters that require fine-tuned parameters and risk introducing artifacts, the wavelet-based approach is automatic and parameter-free, ensuring effective artifact removal.

ECG waveform identification: After removing noise and motion artifacts from the ECG signal, we identify the P, R, and T waves in the ECG signals using a popular open-source Python library NeuroKit2 [88]. These identified peak results are later used to assess the validity of the ECG waveform and its signal-to-noise ratio (SNR). It should be noted that ECG is a complex signal containing three main peaks but with various shapes. Even the highest accuracy processing method can still generate errors. NeuroKit2 yields the best detecting accuracy among the other toolkits we tested, thus it is chosen for our final signal processing pipeline.

Valid ECG identification: We used the detected P, R, T wave from NeuoroKit2 to classify whether the signal is a valid ECG. We define a valid ECG as:

1) the NeuroKit2 tool can successfully detect valid P waves, R waves, and T waves instead of returning NaN.

2) The identified P wave, R wave, and T wave are within a reasonable time interval range. Specifically, the interval between P peak and R peak should be in 50 to 200 milliseconds range [79], and the interval between the R peak and T peak should be in 200 to 400 milliseconds range [79].

3) The identified P wave, R wave, and T wave's amplitude is higher than the noise floor in the heartbeat cycle. The noise signal is defined as the signals between two adjacent heartbeat cycles.

Signal to Noise Ratio (SNR): We use the detected P, R, and T wave's amplitude and timing information to compute the SNR of the ECG signal. There have been different definitions of SNR for ECG signals, in this work, we use the traditional SNR definition that has also been used by many previous works: $SNR = \frac{P(signal)}{P(noise)} = \frac{A^2(signal)}{A^2(noise)}$. In the evaluation section, we reported the SNR in decibels, which is $SNR_{db} = 10log_{10}SNR$. The signal amplitude $A(signal)$ is the peak value of the P, R, or T wave, while the noise amplitude $A(noise)$ is derived from signals between two heartbeats. The noise segment starts 350 ms after the R peak (end of the T wave for most healthy adults [79]) and ends 200 ms before the next R peak (before the P wave [79]). Although the noise segment ideally spans from the end of the T wave to the start of the next P wave, detecting these boundaries robustly is challenging. Tools like NeuroKit2 can introduce errors, even with ground-truth data. Thus,

we use this timing-based segmentation as a practical proxy for assessing ECG signal quality.

5.5 Electrode Evaluation

We conducted a benchmark test and an on-user experiment to evaluate our novel electrode, with a diameter ranging from 25 mm to 5 mm, as shown in Figure 5.9. Larger electrodes, providing greater skin contact area, typically result in better signal quality. This variation in size helps us explore the limitations of dry electrodes and identify the optimal balance between signal quality and electrode size. All the studies in this paper have received Institutional Review Board (IRB) approval, and participants were compensated based on their involvement in the different studies.

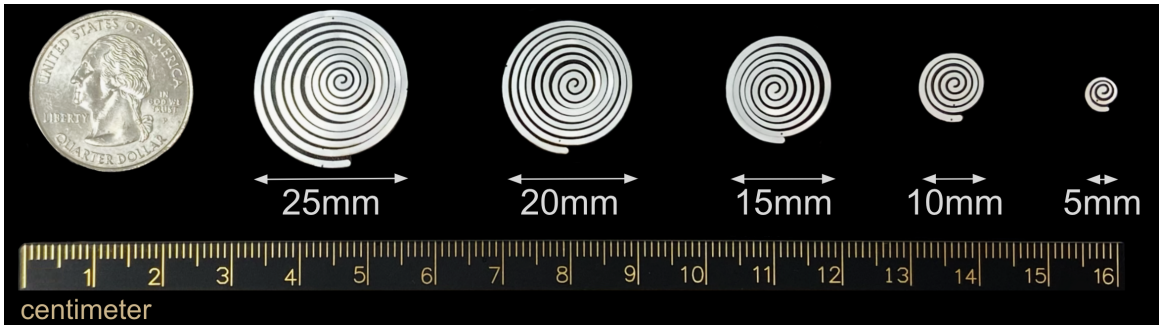

Figure 5.9: Tested necklace electrodes with diameters ranging from 25 mm to 5 mm.

5.5.1 Electrode Benchmark Test

We conducted benchmark tests to evaluate our electrode's frequency response in comparison to standard adhesive electrodes, as well as to assess how its impedance varies with different moisture levels.

Electrode Frequency Response

Skin-electrode impedance is a key metric for evaluating an electrode's performance, as it reflects how effectively the ECG signal is transmitted from the body to the electrode.

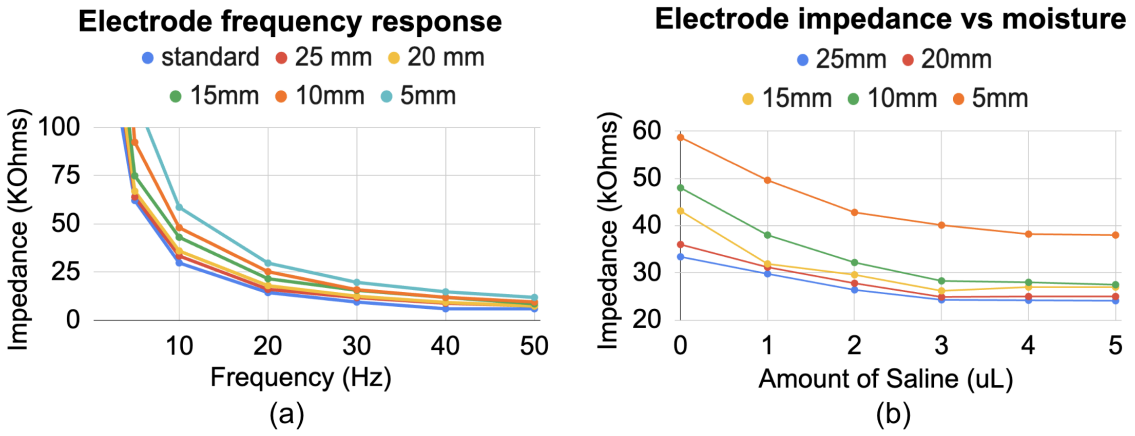

Figure 5.10: (a) The impedance of our electrodes (without moisture) and the standard adhesive electrode at different frequencies. (b) The impedance of our electrode at 10 Hz with different amounts of moisture level.

Lower impedance indicates better signal quality, with reliable ECG measurements typically requiring impedance below $50k\Omega$ at 10 Hz, and values under $10k\Omega$ being optimal [98].

We measured the skin-electrode impedance with diameters ranging from 5 mm to 25 mm, as well as a standard adhesive electrode, across different frequencies. The impedance was determined using a standard measurement circuit that computes voltage drop and current through the skin-electrode interface [125, 136, 13]. Since ECG signals predominantly span 1–100 Hz, with most power concentrated in the 1–50 Hz range [149], we focused on this frequency range. Figure 5.10 (a) shows that skin-electrode impedance decreases with increasing frequency, consistent with existing studies [136, 13, 153]. The standard gel electrode (3M Red Dot electrode) was measured as $169k\Omega$ at 1 Hz, $29k\Omega$ at 10 Hz, and $6k\Omega$ at 50 Hz. Among our designs, the 25 mm electrode had the lowest impedance, measuring $203k\Omega$ at 1 Hz, $33.4k\Omega$ at 10 Hz, and $7.5k\Omega$ at 50 Hz. In contrast, the 5 mm diameter electrode, due to its smaller contact area, exhibited the highest impedance: $502k\Omega$ at 1 Hz, $58.7k\Omega$ at 10 Hz, and $12k\Omega$ at 50 Hz. While the 25mm, 20mm, and 15mm all demonstrated impedance below $50k\Omega$ at 10 Hz, their values are higher than the standard adhesive electrode. However, this can be compensated by the body moisture, as demonstrated in the later experiment. In addition, it should be noted that these tests were conducted without skin preparation

to simulate everyday usage scenarios. While this results in higher impedance compared to ideal conditions, the findings align well with previous studies [137, 136, 21].

Electrode Impedance Versus Moisture Amount

We further investigated the effect of moisture on skin-electrode impedance by applying different amounts of saline to the skin using a pipette to simulate body moisture. Figure 5.10 (b) demonstrates how skin-electrode impedance at 10 Hz changes with the amount of saline added. All electrodes demonstrated a clear reduction in impedance with increased moisture. Specifically, the 15 mm, 20 mm, and 25 mm electrodes achieved impedance values comparable to standard adhesive electrodes with just $2uL$ of saline, while the 10 mm electrodes required $3uL$ to reach similar values. The impedance of the 5 mm electrode also decreased but did not match the performance of the larger electrodes, likely due to its limited contact area. The impedance of all electrodes converged with saline amounts exceeding $4uL$. On average, adults sweat approximately $105g/m^2/h$ at the front chest during rest and $248g/m^2/h$ during exercise [39]. For a 20 mm diameter electrode, this corresponds to a sweat production of $105g/m^2/h \times (\pi \times (0.01m)^2) = 0.033g/h = 0.55mg/min$ during rest. Assuming a saline/sweat density of $1mg/uL$, it would take about 6 minutes to generate $3uL$ of moisture under ideal conditions. However, in real-world scenarios, this process may take longer since the silicone cover can reduce moisture evaporation but does not completely stop it [129].

5.5.2 Electrode Performance Evaluation

We evaluated our necklace electrode's performance over time with varying electrode sizes. For this evaluation, twelve participants were recruited (eight females, four males, average age 28.2 ± 4.8, average BMI 21.9 ± 2.2), each of whom wore five necklaces with different electrode sizes. The sequence in which the necklaces were worn was determined using a modified balanced Latin square order to eliminate any effects from the order of testing. Participants were instructed to wear each necklace for 20 minutes while engaging in their typical daily activities, such as working on a computer while seated. In addition, participants were asked to remain relatively still for at least 30 seconds every three minutes, allowing us

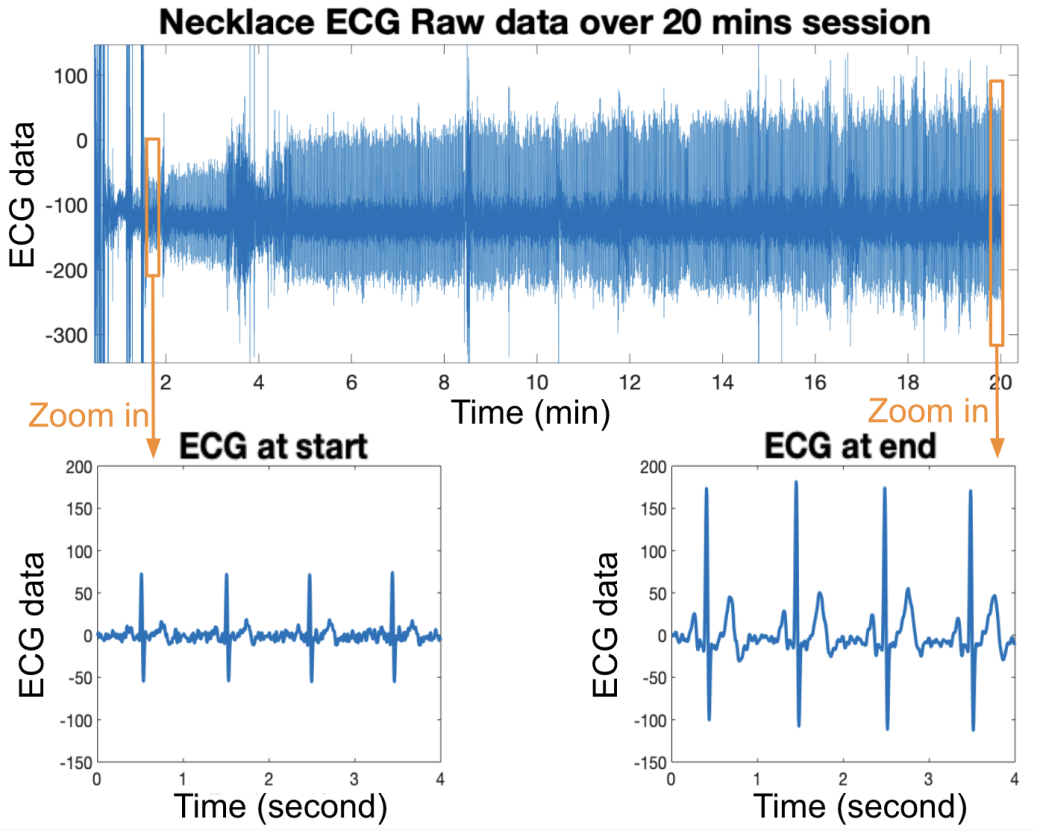

Figure 5.11: Example of an ECG signal obtained from the necklace electrode over a 20-minute period, with the zoomed-in plots on the signal at the start and at the end.

to obtain reliable spot-check ECG readings free from motion artifacts. Besides testing the necklace electrode with various diameters, we also collected ECG signals using a standard adhesive gel electrode for one minute, which serves as a reference.

As discussed in Section 5.3.2, our necklace electrode uses a silicone layer to retain natural skin moisture, acting as a conductive gel to enhance signal quality. Since human skin continuously produces moisture, the ECG signal improves over time. Figure 5.11 shows an example from a 20-minute session. Initially noisy, with an SNR of 23 dB, the signal improved to 32 dB by the end. The SNR increased rapidly in the first few minutes as moisture filled the gap between the electrode and skin, then stabilized or improved gradually upon reaching an optimal moisture level. Similar patterns were observed in all participants, though the

time to reach saturation varied between individuals.

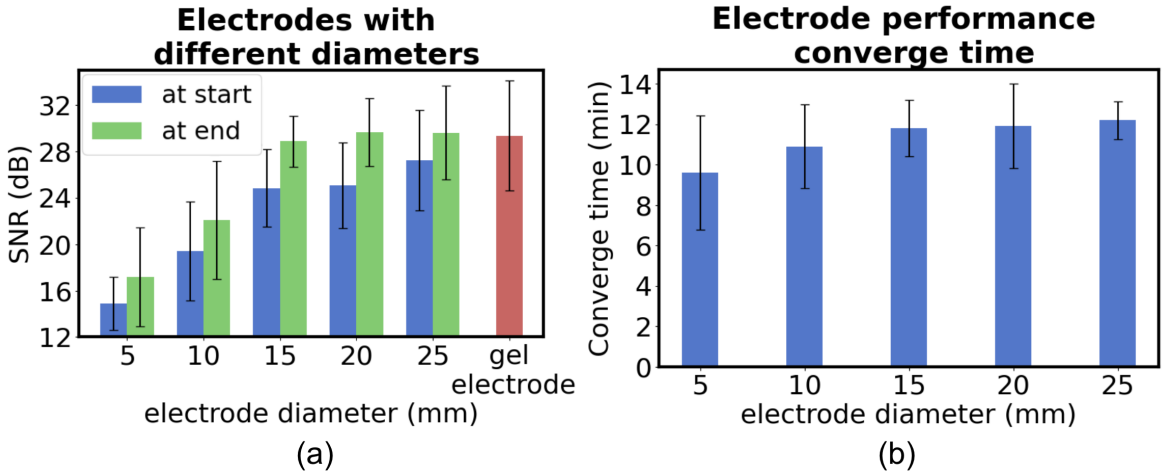

Figure 5.12: (a) The average ECG SNR obtained from electrodes with different diameters. (b) The average ECG signal quality converging time.

Figure 5.12 (a) shows the aggregated users' QRS peak SNR results over 20 minutes with five electrode sizes. It was noted that the electrode performance improvements over time occurred across all electrode sizes and participants. Electrodes with diameters of 15 mm, 20 mm, and 25 mm get an averaged converged SNR of 28.88 ± 2.21 dB, 29.67 ± 2.93 dB, and 29.63 ± 4.03 dB, respectively, which is equal or close to the performance of the standard adhesive gel electrode at 29.47 ± 4.77 dB. Electrodes with diameters of 10 mm and 5 mm showed significantly lower SNR of 22.10 ± 5.11 dB and 17.10 ± 4.29 dB. It should be noted that these SNR results are all based on the QRS complex, the highest wave in the ECG signals. For the 5 mm and 10 mm electrodes, while some participants exhibited clear ECG signals, others did not present an identifiable P or T wave, making the ECG signals unsuitable for diagnostic purposes, although still capable of heart rate monitoring. Considering the performance and the size of the electrode, we chose the electrode with a 15 mm diameter for our later experiments. Figure 5.12 (b) displays the average signal SNR convergence time, defined as the duration until the SNR stabilizes within a 10% range of the final optimal SNR for the 20-minute session. ECG signal quality may fluctuate or degrade during the experiment, likely caused by electrode movement on the skin due to user

motions. The signal typically reconverges; however, signals that did not stabilize during the experiment were excluded from the convergence time analysis. No distinct pattern emerges regarding convergence time relative to electrode size, as most values fall within an eight to twelve-minute range. Additionally, convergence time may vary depending on individual factors such as hydration, skin moisture level, and rate of insensible water loss.

These results from the dry electrode experiments demonstrate the effectiveness of the skin's natural sweating process in enhancing dry electrode performance. Moreover, the findings provide guidance on selecting electrode sizes for balancing signal quality and aesthetic preference. Participants reported no discomfort from wearing the silicone electrodes, and none of them experienced any skin irritation following the experiments, which further demonstrated the skin-friendliness of the necklace electrode.

5.6 Necklace vs. Ground Truth Evaluation

We evaluate the performance of the ECG Necklace compared to an FDA-approved Holter monitor during controlled activities. The study is designed to evaluate the necklace's performance in real-world conditions with activity labels.

5.6.1 Study Protocol

Given ECG Necklace is aimed to monitor ECG signals during everyday context, we designed a real-world experiment to evaluate the ECG signal's quality and availability during common daily activities, such as using a laptop, chatting, playing phones, and walking. We recruited twelve participants (eight females, four males, average age 24.1 ± 2.5, average BMI 21.3 ± 1.5) for this study. Each participant was asked to wear an ECG necklace with electrodes 15 mm in diameter, as well as an FDA-approved Lepu PC-80B EasyECG holter monitor. Participants were asked to perform various common activities in a large office environment. The environment contains typical electronic interference from over twenty computers, monitors, and the presence of other individuals.

The **study protocol** was structured as follows:

1) Preparation: Participants wear the ECG necklace for twenty minutes to prepare the electrodes (as discussed in Section 5.5.2). During this period, they are free to engage in

any activities.

2) Laptop round 1: Participants use their own laptops in a natural manner for five minutes.

3) Chatting round 1: Participants chat naturally for five minutes, either with the researchers or anyone.

4) Smartphone round 1: Participants naturally use their smartphone for five minutes.

5) Walking: Participants walk indoors at their normal pace for ten minutes, including walking up and down stairs. This task is guided by researchers, and participants are allowed to rest whenever needed.

6) Round 2: Repeat 2), 3), 4) again.

The structure of the study is designed to collect data in real-world conditions with activity labels. In addition, the 10-minute walking session is a common, mild task that promotes the user's natural sweating. We will further compare the ECG signal quality and valid percentage before and after walking.

5.6.2 Valid ECG Percentage

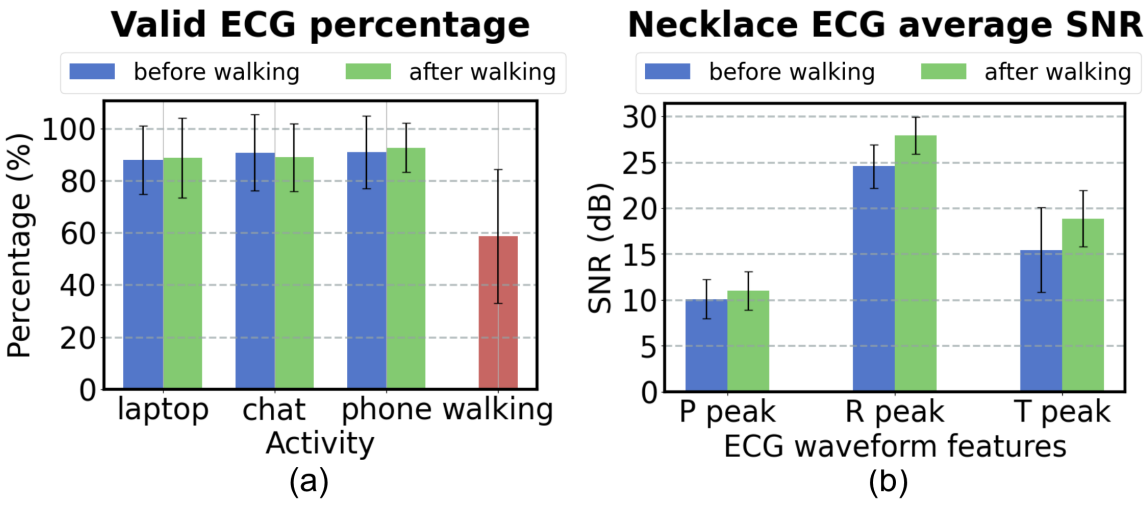

Figure 5.13: (a) The percentage of available valid ECG signal from the necklace during different activities. (b) The average SNR of the P, R, and T peaks in the ECG signals captured by the necklace.

Figure 5.13 (a) shows the percentage of valid ECG waveforms during each activity. The

valid ECG waveform was defined in Section 5.4. As expected, using laptops, chatting, and using smartphones all yield a high percentage of valid ECG signals.

For using laptops, the average available percentage of valid ECG across the twelve users is $87.96 \pm 13.21\%$ during the laptop round 1 session, and $88.80 \pm 15.31\%$ during the laptop round 2 session. The highest valid ECG rate was 98.94% (P4), while the lowest was 55.64% (P2). Differences are likely from user activity; stationary tasks like reading or watching videos produced more stable ECG signals than typing, which involves shoulder muscles that can affect the ECG signal from the necklace. For natural chatting, the average available percentage is $90.76 \pm 14.63\%$ during chatting round 1, and $88.89 \pm 13.05\%$ during chatting round 2. During using smartphones, the average valid ECG percentage is $90.92 \pm 13.9\%$ during smartphone round 1, and $92.65 \pm 9.48\%$ during smartphone round 2, with a maximum percentage up to 100% from P4 and P7.

During walking, even when there were large motions, the average valid ECG percentage during walking was $58.7 \pm 25.73\%$, with a high of 95.05% (P8) and a low of 18.36% (P5). Variability likely arose from walking patterns; stable leg-only movements had less impact on the signal, while significant shoulder movement or jumping can disrupt the ECG. This is likely because the shoulder movement can alter skin-electrode contact and introduce additional muscle-generated voltage signals that interfere with the ECG.

Overall, the results show that it is possible to capture valid ECG signals during these common daily activities, but people's behavior can vary. In addition, we do not observe a significant change in valid ECG percentage for sessions before and after walking.

5.6.3 SNR Results

Figure 5.13 (b) shows the average SNR results of the P peak, R peak, and T peak of the valid ECG identified in Section 5.6.2 before and after walking. Since the P wave is the smallest wave in ECG, it has the lowest SNR compared to the R peak and T peak but still offers 10.08 ± 2.13 dB from the sessions before walking and 10.99 ± 2.26 dB from the sessions after walking. R peak corresponds to the depolarization of the main mass of the ventricles; hence, it is the largest wave. The average R peak SNR is 24.5 ± 2.35 dB from sessions

before walking, and 27.92 ± 2.01 dB from sessions after walking. The T peak corresponds to ventricular repolarization and is an asymmetrical wave with round peak that is usually below R wave but higher than P wave. The average T wave SNR is 15.48 ± 4.63 dB from sessions before walking, and 18.85 ± 3.09 dB after walking.

The ECG signal obtained from the necklace did show a significant SNR improvement after 10 minutes of walking, even though most participants reported they did not feel sweating. This is likely because of an increased metabolic rate during walking, which triggers the body's thermal regulation even during mild activities. As a result, even without noticeable sweating, the necklace electrode performance was enhanced by the generated skin moisture. This finding indicates that everyday activities like walking could further enhance the performance of the ECG necklace.

5.6.4 ECG timing accuracy

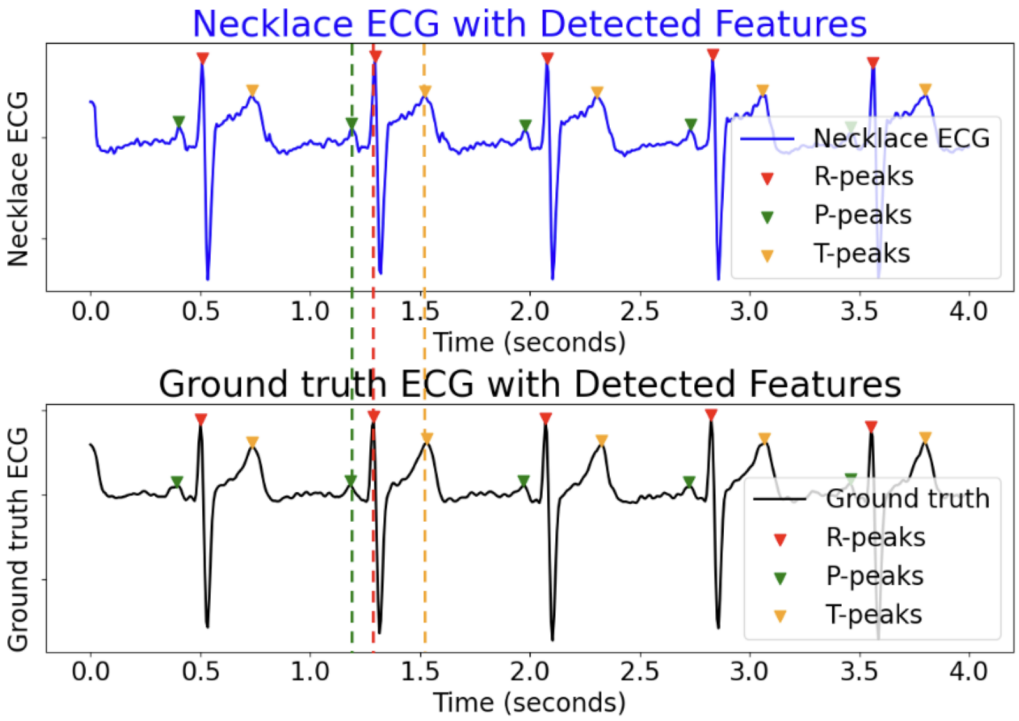

Figure 5.14: An example of synchronized ECG signals obtained from the ECG necklace and the ground truth device, with the P, R, and T waves identified by the NeuroKit2 Python tool.

We compared the ECG Necklace to an FDA-approved Holter monitor by analyzing the timing of detected P, R, and T waves, a key metric for diagnosing cardiac conditions. The necklace ECG signal was resampled from 250 Hz to 150 Hz to match the Holter monitor's sampling rate and then synchronized using cross-correlation. Both signals were processed using the pipeline described in Section 5.4, and timing errors were calculated by comparing the indices of detected peaks. It is important to note that while the electrodes were placed as closely as possible for simultaneous recording, slight differences in placement introduced minor variations in the ECG signals.

Figure 5.14 shows an example of the synchronized ECG signals from the necklace and the ground truth device, highlighting the P, R, and T peaks identified by the NeuroKit2 functions. We compared the timing difference of these detected P, R, and T peaks from our necklace ECG and the ground truth ECG. This analysis was restricted to ECG signals that are considered valid only, as discussed in Section 5.6.2. The average absolute timing error for the P, R, T peak across participants is shown in Figure 5.15.

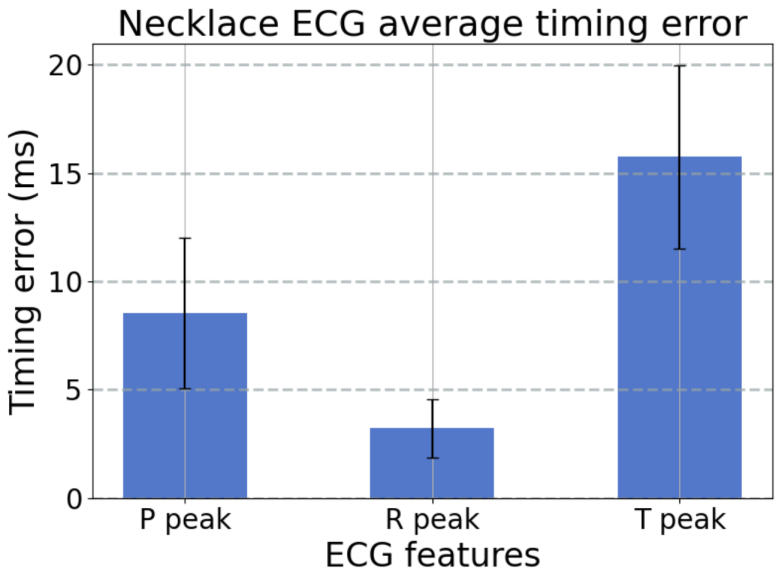

Figure 5.15: The average timing error of P, R, T peaks identified from the necklace ECG versus from the ground truth.

The average absolute timing difference of P peak from necklace versus from the ground

truth device is only 8.53 ± 3.46 milliseconds, which correspond to 1.3 samples of the ECG data with 150 Hz sampling rate. The average timing difference of R peak is 3.22 ± 1.34 milliseconds, which corresponds to 0.5 samples. The R peak is the sharpest wave in the ECG signals, which makes it easy to identify and less likely to be affected by noise, thus it has the highest alignment accuracy with the ground truth ECG. The average timing difference of T peak is 15.74 ± 4.22 milliseconds, which corresponds to 2.4 samples in the ECG signal. The T wave is usually a more round shape peak instead of a sharp peak compared to R wave and P wave, so the T peak is more likely to be identified as an ambiguous peak by the NeoroKit2 tool. In addition, the T wave duration is typically around 160 to 240 milliseconds, much longer than the P wave and QRS complex. Given that the generally acceptable timing error range for ECG peaks is 20 milliseconds [34], our system demonstrates high accuracy with a well-acceptable error range. In addition, it should also be noted that some of the timing errors may be caused by the detection capabilities of the NeuroKit2 tool, which can introduce errors in identifying the P, R, and T peaks in both the necklace and ground truth ECGs.

5.7 In-the-wild study

We recruited ten participants to wear the ECG Necklace for approximately eight daytime hours during their normal daily routines. The participants included six female, three male, and one non-binary individuals, with an average age of 24.8 ± 3.1 years and an average BMI of 22.3 ± 2.1. The participants were instructed to wear the ECG Necklace (without the fashion design components) and a Polar H10 chest strap for comparison while continuing their normal daily activities. Although the Polar H10 chest strap is primarily designed for heart rate monitoring with non-standard electrode placement, it was selected for its wearability, continuous ECG sensing, and raw ECG data access. ECG patch monitors are not available for comparison since they require prescriptions and only report analyzed results instead of raw ECG data. Each participant was provided an Android phone with the ECG Necklace app to collect data and an iPhone to record Polar chest strap data. They were told that they could take off any device early if they felt discomfort. At the end of the study, participants were also asked to complete an online survey to rate the comfort of

ECG Necklace.

5.7.1 ECG Signal Availability and SNR

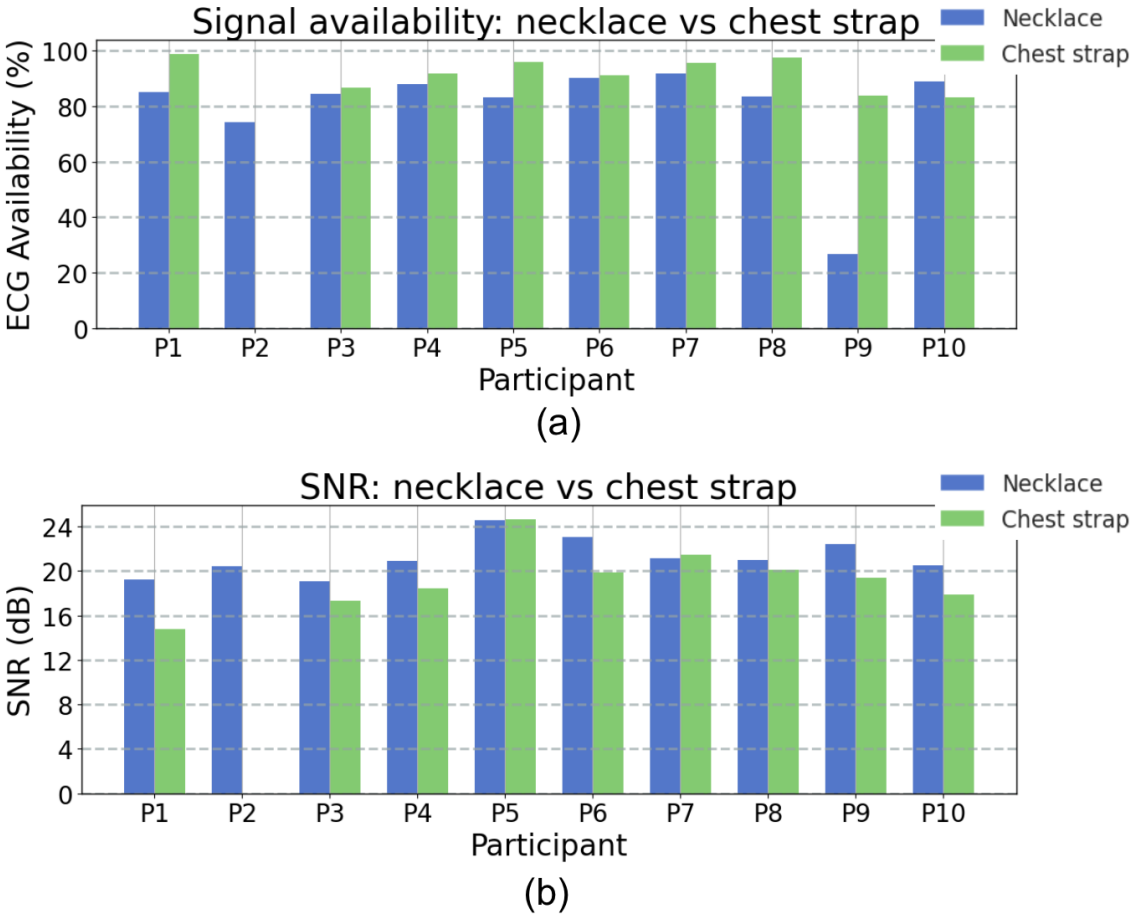

Figure 5.16: (a) The percentage of valid ECG signals by necklace versus by chest strap for each participant. (b) The average SNR results by necklace versus by chest strap for each participant.

Figure 5.16 (a) shows the percentage of valid ECG signals captured for each participant using the ECG necklace and the Polar chest strap. For P2, the chest strap failed to record any data due to a dead battery, so only the necklace results are presented for this participant. The ECG necklace demonstrated slightly lower but comparable signal availability to the tightly worn chest strap. On average, the necklace captured valid ECG signals 79.65 ± 18.3

% of the time, while the chest strap achieved 91.69 ± 5.6 %. The larger variance in necklace performance stems primarily from P9, which only had 26% valid ECG signals recorded. This discrepancy is likely caused by motion or pose changes, leading to deterioration in the electrode's contact with the skin. Additionally, we noticed that P2's signals exhibited a sudden drop in ECG availability from the necklace during the last two hours of the study, likely due to similar motion-induced detachment. Future improvements could involve adding a weighted pendant to the electrodes to enhance resilience to motion. While the chest strap performed well in terms of ECG signal availability, its tightly worn design caused discomfort for several participants, which we will discuss in the later section.

Figure 5.16 (b) shows the R-peak SNR of the ECG signals recorded by the necklace and chest strap. These SNR values are computed using only the valid ECG signals. The necklace demonstrated higher SNR values for most participants except P5 and P7. On average, the necklace achieved a higher SNR of 21.23 ± 1.6 dB, compared to the chest strap's 19.33 ± 2.6 dB. This result suggests that, despite slightly lower signal availability, the necklace provides better signal quality for the majority of participants. Indeed, we expected these results, as the Polar chest strap is primarily designed for heart rate monitoring during physical activity rather than diagnostic-grade ECG signal acquisition. However, the chest strap remains the closest ECG wearable monitor available on the market for comparison. These results further demonstrate the potential of the ECG Necklace to bridge the gap for daily wearable ECG monitors. These results highlight the ECG Necklace as a promising solution for continuous and accurate use in everyday life.

5.7.2 ECG Necklace Comfort Level

We collected the participant's comfort level with the necklace and the chest strap after wearing each for a whole day. Figure 5.17 (a) shows the user preference for the necklace versus the chest strap. Most users strongly preferred the necklace over the chest strap for daily wear, with eight users giving a score of 1 or 2, with 1 meaning that they strongly preferred the necklace; one user giving a score of 3, which means that they slightly preferred the necklace; and one user giving a score of 5, indicating that they preferred the chest

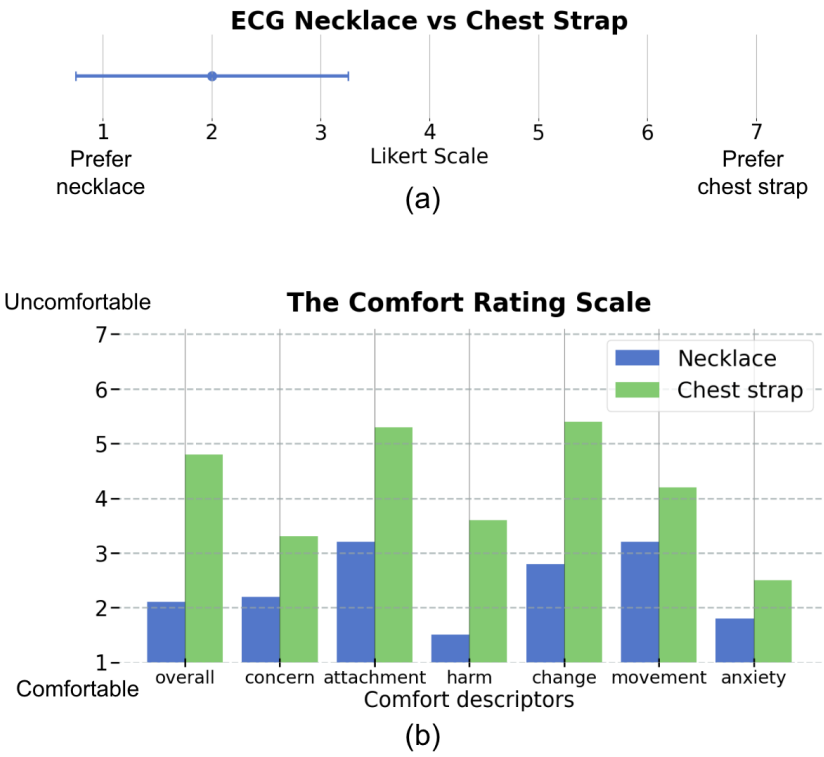

Figure 5.17: (a) The overall comfort level of ECG Necklace and the Polar chest strap. (b) The comfort rating scale results of ECG Necklace and Polar chest strap.

strap. The user who gave a score of 5 indicated that they "felt very aware of the necklace with the fear that it could get disconnected (to the phone)", and the user was "anxious about potentially disturbing the signal." However, this user also indicated that "but when everything was working as it should, I thought it was less noticeable", and "Actually, the silicone stick-on tabs were very comfortable, it felt like a second skin."

We further analyzed the participant's comfort level by asking them to rate their comfort levels with each device based on Knight et al.'s comfort rating scales, designed to measure the comfort of wearable devices across 6 dimensions [75]:

- **Concern**: Worries about appearance when wearing the device.
- **Attachment:** Awareness of device presence/movement.
- **Harm**: Feeling that the device may cause harm/pain.

- **Change**: Feeling physically different while wearing the device.
- **Movement**: Device restricting movement.
- **Anxiety:** Insecurity while wearing the device.

The ECG Necklace consistently received lower (indicating more comfortable) scores for overall comfort and across all comfort descriptors, as shown in Figure 5.17 (b). Specifically, eight out of ten users rated the necklace as overall very comfortable (giving a score of 1 or 2), while only 3 users rated the chest strap as comfortable (one score of 2, and two score of 3). Four participants found the chest strap highly uncomfortable (giving a score of 7 or 6), with some reporting uncomfortable breathing after wearing it for more than an hour. One female participant also mentioned that the chest strap's placement felt "strange" and "awkward". In addition, the Necklace was rated significantly more comfortable than the chest strap in the "attachment" and "change" category.

In conclusion, our findings show that ECG Necklace is considerably more comfortable than the chest strap, the most commonly used device for continuous ECG monitoring. The fact that all participants rated ECG Necklace as comfortable and most participants are willing to wear it every day shows that it is a promising platform for longitudinal health monitoring.

5.8 Discussion

5.8.1 Fashion Design

Fashion considerations are essential when integrating technology into necklaces, as they are primarily designed as fashion accessories. Since the ECG necklace consists of a central processing unit and two electrodes connected by wires, our fashion design focused on decorating these components while maintaining the system's functionality. Figure 5.1 shows our example fashion design for the ECG necklace. Inspired by the silver spiral patterns on the electrodes, the design incorporates similar shapes to connect the central pendant with the electrodes seamlessly. The design was 3D-printed, featuring a decorative pendant that

conceals the central processing unit and two subtly spiral-shaped covers for the electrodes. To enhance its aesthetic, small pearls were added as decorative elements.

While the showcased design is 3D-printed, alternative designs could incorporate gemstone, pearl, or metal-based pendants paired with chains made from various materials such as metal, leather, or string to achieve a distinct aesthetic. Necklace structural variations, such as positioning the electrodes at the front and back center, are also worth exploring, though they may come with trade-offs in signal quality. Additionally, the electrodes could be redesigned as thin, chain-like elements that seamlessly integrate with the necklace chain, enhancing both functionality and visual appeal.

5.8.2 Necklace as a health monitoring platform

In this work, we primarily explored the ECG sensing capability of the necklace. However, we envision that a smart necklace could serve as a versatile health monitoring platform beyond ECG. Our necklace prototype integrates an accelerometer and a temperature sensor, offering additional functionalities. Positioned directly on the chest, the accelerometer can capture subtle chest movements to detect breathing and heartbeat. Furthermore, measuring skin temperature at the chest can provide a more accurate approximation of core body temperature compared to other wearables, such as smartwatches.

Our initial exploration demonstrated that the accelerometer from the necklace can detect breathing signals and seismocardiography (SCG). However, these capabilities were not extensively evaluated or included in this paper, as they fall outside the primary scope. Future work could explore sensor fusion between ECG and SCG signals, leveraging their timing differences to derive valuable physiological insights. Additionally, the accelerometer could detect moments of user stability to opportunistically trigger ECG sensing, enhancing both energy efficiency and data quality.

5.8.3 Limitation and future work

It is well-known that body hair can significantly degrade the quality of ECG signals, even with standard adhesive electrodes. Our study did not include participants with noticeable

body hair around the neck area. Typically, individuals are required to shave and prepare the skin before a standard ECG test to eliminate air gaps caused by body hair, which can interfere with electrode contact [94].

For future research directions, we aim to assess the clinical utility of the ECG necklace by involving patients with heart conditions. Additionally, we plan to enhance the necklace by integrating advanced algorithms or machine learning models to facilitate computational diagnosis, such as detecting atrial fibrillation (Afib).

5.9 Summary

We developed a compact wireless necklace for longitudinal ECG monitoring. Leveraging the unique position and shape of the necklace, the ECG necklace can accommodate two electrodes that are positioned on different sides of the heart, enabling continuous ECG monitoring that other wearables located on the limbs cannot achieve. In addition to the necklace system, we introduced an innovative skin moisture-enhanced electrode that maintains high signal quality without causing skin irritation or suffering performance degradation due to gel evaporation. This electrode utilizes skin-friendly silicone to create a moisturizing microenvironment, leveraging the natural moisture produced by the human body as a conductive "gel". We explored several design aspects of the necklace, including the electrode placement and its size. The results showed that our necklace can provide ECG signals similar to those of a clinical standard Lead I ECG, and our electrode performance is comparable to that of standard adhesive gel electrodes as well. We further performed real-world experiments to evaluate the percentage of valid ECG signals during common daily activities and compared their signal quality to that of an FDA-approved ECG device. The high percentage of valid ECG data and high accuracy compared to an FDA-approved device during these natural activities demonstrates the practicality and effectiveness of our ECG necklace in typical daily settings.

Chapter 6

LESSONS LEARNED & GENERAL DESIGN PRINCIPLES

This section summarizes the lessons learned during the projects in this dissertation and examines the key considerations for designing smart jewelry and other tiny wearable devices. We will outline general methodologies for developing smart jewelry and a broader range of low-power wearables while preserving their small form factors.

6.1 Wearable Form Factor Design

Choosing the appropriate wearable form factor is a foundational step. The choice of sensing site significantly impacts measurement accuracy; the form factor determines user acceptance and long-term wearability; and the attachment method influences both comfort and signal reliability. All three aspects must be carefully integrated to ensure a wearable system is both functional and practical for daily use.

6.1.1 Choosing the Right Sensing Site

The location of the sensor on the body plays a critical role in determining signal quality, especially for physiological monitoring. Placing sensors close to the physiological source of interest, such as the heart or brain, typically yields significantly better signals than relying on downstream signal enhancement through algorithms. A high-quality raw signal often outperforms what even the most advanced processing can extract from suboptimal placements.

Sensing site selection should be application-driven. For health-related applications, clinical literature can provide useful guidance on optimal sensor locations. For example, cardiac monitoring using ECG, SCG, or BCG benefits from placements near the chest, while stress or cognitive-state monitoring may favor regions near the head. Prioritizing signal fidelity at the source is essential for achieving accurate and robust measurements.

However, theoretical recommendations must be complemented with empirical validation. Signal quality can vary significantly across individuals and real-world conditions. For example, although the finger is clinically considered an ideal site for PPG-based heart rate monitoring, we observed that it does not work reliably for all users. Individuals with cold hands often experience reduced blood circulation, leading to significantly degraded PPG signal quality at the finger.

Therefore, it is crucial to test candidate sensing sites in practice before proceeding to system integration and deployment. Empirical validation helps uncover real-world limitations and ensures the chosen site is suitable for long-term use in diverse, uncontrolled environments, such as during in-the-wild studies.

6.1.2 User Acceptance

While certain sensing sites may offer superior signal quality, they are not always practical or socially acceptable for everyday wear. The wearable design must carefully balance between technical performance and user acceptance. Devices that draw unwanted attention, disrupt daily routines, or appear out of place in social or professional settings are unlikely to be adopted or worn consistently.

The user acceptance of the wearable form factor directly affects how often and how long the users will wear it, which impacts the monitoring duration and the amount of longitudinal data we can get for understanding the user behaviors. Designing around culturally familiar and socially accepted form factors, such as earrings, necklaces, watches, or rings, can significantly improve user acceptance. These familiar forms help the device blend into daily life, making users more willing to wear them consistently.

Form factor selection should also be tailored to the specific application and target user group. For example, wearables designed for athletes or race car drivers may naturally integrate into helmets or performance gear. Different applications attract different demographics, each with their own habits, preferences, and accessory norms. Conducting user interviews can reveal key insights into what users are willing to wear, what feels comfortable, and what fits their lifestyle and aesthetics. Understanding these needs early in the

design process helps ensure the final product aligns with both functional goals and user expectations.

6.1.3 Attachment Method

Beyond placement and form factor, a wearable's attachment method plays a critical role in both signal quality and comfort. Attachment methods influence how well a device couples with the body, directly affecting the stability and quality of physiological measurements. Key factors such as applied pressure, contact surface area, material softness, and adjustability all contribute to comfort and signal quality. Careful consideration of these physical design elements is essential for creating wearables that are not only accurate but also comfortable and unobtrusive for everyday use.

The same type of wearable or accessory can have different attachment methods. For example, earrings can be attached via traditional piercing posts or through magnetic clips. Magnetic attachments offer broader accessibility, accommodating users without pierced ears. However, pierced attachments typically provide more secure and consistent pressure against the skin, which improves sensor contact and reduces motion artifacts. As a result, they often yield higher signal fidelity during movement. In many cases, such insights can only be uncovered through real-world experiments and testing.

6.2 Size Minimization

The smart wearable should match the form factor of the original accessory, requiring it to be compact and lightweight to ensure comfort and long-term wearability. Designing such devices requires careful selection and integration of minimal, lightweight components to preserve both functionality and user comfort.

6.2.1 Hardware Selection

It is important to choose sensors, microcontrollers, and ICs available in compact wafer-level packages, some of which include built-in wireless features such as Bluetooth and WiFi.

However, smaller chips often come with limitations in performance. Careful consider-

ation is needed to balance these trade-offs while maintaining the device's compact size. For example, microcontrollers like the nRF52832 offer a small physical footprint but have limited memory and processing capabilities, which may restrict the complexity of onboard tasks. Similarly, small passive components such as capacitors may have higher leakage currents, which can reduce voltage stability and power efficiency. Compact inductors may have higher DC resistance, which can cause inefficiencies or even failures in power regulation circuits.

Therefore, component selection must be guided by a clear understanding of the system's performance requirements. The goal is to choose the smallest components that still meet the necessary electrical and thermal constraints, ensuring reliable operation without compromising functionality or efficiency.

6.2.2 Hardware Integration

Integrating multiple hardware components into a compact device requires a carefully optimized Printed Circuit Board (PCB) layout to make efficient use of limited space while maintaining performance and reliability.

Following the layout guidelines in component datasheets is essential for understanding requirements such as minimum spacing, trace widths, and grounding practices. Unless specified in the datasheets, components can often be placed very close to each other, and PCB traces can be as narrow as the minimum allowed by the manufacturing process. Special attention should be given to reducing crosstalk, electromagnetic noise, and radio frequency interference to ensure reliable operation.

In addition, it is useful to consider how different parts or modules of the wearable system can be distributed by leveraging the accessory's original form factor. For example, Thermal Earring locates most electronics in the dangling portion, with only the sensing element on the earlobe for skin contact. In tight designs, essential sensing parts can be placed at the contact point, with other modules moved to less constrained areas.

6.2.3 Battery Choice

The battery is typically the largest and heaviest component in a wearable system. Reducing its size while maintaining reasonable operating life is challenging due to the limited energy density of batteries. Broadly, there are two types of batteries: rechargeable batteries, which are common in commercial wearables, and non-rechargeable batteries, often used in products with replaceable cells such as hearing aids. Non-rechargeable batteries can offer higher energy density and capacity, but their single-use nature makes them less suitable for many wearable applications.

Battery selection should be guided by both the application requirements and the constraints of the wearable's form factor. For example, a smart ring might use a curved lithium polymer (LiPo) battery to match its circular form factor, while a smart bandage might use an ultra-thin film battery to maintain flexibility and comfort.

Smaller or ultra-thin batteries often have limitations, such as being unable to provide sustained high current. In such cases, adding a capacitor in parallel with the battery can buffer energy and supply short bursts of higher current, which is an effective solution for applications like periodic high-power BLE packet transmissions.

6.3 Power Optimization

The wearable device must have a reasonable battery life, allowing users to wear it continuously without needing to take it off after a few hours. We summarize three effective methods to optimize power consumption below.

6.3.1 Wireless Communication Strategies

Wireless communication is often the most power-intensive part of a small wearable system since it operates at radio frequencies. Therefore, selecting an appropriate wireless protocol is essential for maintaining energy efficiency. Bluetooth Low Energy (BLE) is a popular choice due to its balance of wireless range, throughput, and compatibility with smartphones. BLE supports both connection mode for continuous data streaming and advertising mode for low-duty periodic updates. Other common options include WiFi, LoRa, and backscatter. WiFi

offers higher throughput, but at the cost of higher power consumption. LoRa can achieve long-range communication but typically requires larger hardware. Backscatter offers ultra-low power and smaller size compared to BLE, but often lacks direct compatibility with smartphones. Ultimately, the optimal choice depends on the system's requirements for data rate, transmission range, device size, power budget, and application case.

In addition, the wireless communication power consumption is directly related to the length of transmitted data, so optimizing the transmitted data format can help optimize the power consumption significantly. For example, transmitting a Bluetooth packet at 2.4 GHz typically draws around 5 mA (at 3 V) during transmission. At a data rate of 1 Mbps, sending 125 bytes (1000 bits) takes about 1 ms, resulting in a total energy cost of approximately 5 mA $\times$ 3 V $\times$ 1 ms. By reducing data length through simple on-device processing, such as computing heart rate on the microcontroller instead of transmitting the entire PPG waveform, transmission time can be shortened, leading to a significant reduction in average energy consumption.

6.3.2 Power Management Techniques

An effective way to reduce power consumption is to place the system in deep sleep mode during periods of inactivity. This approach can save hundreds of times more power since wearable devices can be idle for most of their operating time. For example, the nRF52832 microcontroller draws more than 3 mA in its default idle state but consumes less than 5 uA in deep sleep mode. Thermal Earring system was configured to wake for only about 400 microseconds each second for sensor interfacing and Bluetooth transmission, drawing 5 mA during this active period, while remaining in an ultra-low power state at 2.4 uA for the rest of the time. This strategy reduced Thermal Earring's power consumption by roughly a factor of 1000.

6.3.3 Energy Harvesting

Energy harvesting can be another way to extend the battery life. While the wearable's primary power can come from batteries for reliable performance, the complementary energy

harvesting can extend run time. There are several ways to harvest energy for wearables, such as using solar cells to capture ambient light, motion harvesters to generate power from user activity, thermoelectric generators to convert body heat into electricity, and RF harvesters to capture energy from environmental signals. A hybrid system that combines batteries with energy harvesters can maintain reliable operation while reducing the frequency of recharging or battery replacement.

Chapter 7

CONCLUSION AND FUTURE DIRECTIONS

7.1 Conclusion

This dissertation presented the following thesis statement:

New wearable form factors can unlock new opportunities, advancing the wearable space in sensing accuracy, continuity, and capability. This dissertation demonstrates this by transforming conventional jewelry into smart wearable devices without changing their typical form factors, enabling novel health monitoring applications that are traditionally challenging or impossible to achieve.

To achieve this vision of next-generation wearables for unobtrusive health monitoring, we took a bottom-up, end-to-end approach. First, by creating new low-power wearables, we enabled more accurate and continuous sensing. Then, by deploying these practical devices in real-world settings, we ensured they were comfortable, effective for long-term use, and capable of collecting longitudinal physiological data from users. Finally, by analyzing this real-world data, we unlocked new insights from these unique data streams, enabling applications that were previously difficult or impossible to achieve.

This dissertation introduced three novel wearable devices that unlock new applications by transforming everyday accessories into intelligent systems:

- Thermal Earring demonstrates how selecting a new sensing site can significantly improve the accuracy of physiological monitoring, enabling new applications in daily wellness.

- PPG Earring shows how system-level optimization can improve temporal coverage, enabling more continuous sensing despite the interruptions that often occur in daily use.

- ECG Necklace demonstrates how rethinking form factor design can make clinical-grade sensing feasible in contexts where traditional wearables fall short.

Together, this dissertation demonstrates that creating new kinds of wearables while maintaining their original form factor can advance the wearable space in accuracy, continuity, and capability. This opens the door to better long-term monitoring, capturing signals that were previously inaccessible. Ultimately, it can enable unobtrusive health intelligence embedded in daily life, empowering people to live healthier and happier.

7.2 Future Directions

This dissertation has shown that the wearable space can expand beyond smartwatches to include new form factors such as smart jewelry. The following outlines key future directions.

7.2.1 Bridge the gap between everyday health and clinic

While this dissertation shows a promising start, there are still a lot of things that current wearables cannot yet achieve. Beyond temperature, heart rate, and ECG that we have explored, clinical metrics such as blood pressure, glucose levels, and blood biomarkers are still largely restricted to clinical environments. A key future direction is to push wearable capabilities closer to those of medical-grade devices, enabling more comprehensive health assessments outside the clinic.

Wearables also have the potential to transform clinical workflows by supporting continuous, passive monitoring outside traditional healthcare environments. With rich, continuous data from next-generation wearables, future directions should explore how to integrate computing and AI into the wearable ecosystem, automating parts of the diagnostic process and delivering real-time health feedback directly to users.

7.2.2 Expanding the wearable space for enhanced capabilities

Future directions include continuing to push the boundaries of what wearables can do by exploring the different sites and form factors. For example, Smart nail accessories can track finger motions. When people's hands shake uncontrollably, it can be an indicator of stress.

Additionally, it can help monitor Parkinson's disease over time or detect stroke. Finger nail can also be a good location for tracking the hemoglobin level. A Flexible Smart band-aid can be placed anywhere on the body to analyze sweat and electrolyte levels, providing insights into stress and hydration levels. Smart teeth retainer has great potential for sensing nutrition intake, such as tracking how much sugar or salt you consume.

Beyond individual wearables, future systems can consist of multiple interconnected wearables working together. Since smart jewelry is unobtrusive and people already wear multiple accessories, users could comfortably wear several devices at once. Specifically, these devices can unlock new sensing capabilities if they connect and synchronize with each other. For example, by capturing synchronized PPG signals from both an earring and a ring, we can measure the pulse transit time between the earlobe and the finger. This metric reflects how quickly blood travels through the body and is correlated with blood pressure. Tracking it continuously and unobtrusively could enable early detection of serious conditions such as stroke or cardiovascular events.

7.2.3 Unique dataset to enable advanced AI models

Next-generation wearables offer improved sensing accuracy and enable rich, large-scale datasets, which can enable advanced AI models.

These novel wearables can transform research that currently relies on smartwatch data. For example, wearable sensor foundation models are typically trained on watch data. However, the limited quality and signal fidelity of smartwatches make it difficult to detect subtle but important states such as stress, emotion, or early signs of illness. The new devices introduced in this dissertation provide access to higher-quality physiological signals, unlocking opportunities to build richer datasets and more capable AI models for understanding and tracking health and behavior.

These easy-to-deploy wearables are well suited for large-scale community sensing and longitudinal studies, enabling the development of personalized models that adapt to each individual's lifestyle. They can provide real-time guidance on sleep, stress, nutrition, and recovery, supporting healthier daily choices. Beyond long-term wellness, their continuous,

high-fidelity monitoring may also help detect or even predict acute medical events, such as heart attacks and strokes, before symptoms appear, offering the potential for earlier intervention.

7.2.4 Broadening the scope

While this dissertation focuses on novel wearables for health applications, the underlying technology can extend to other research domains. These wearables can serve as platforms for exploring new forms of on-body interaction, rethinking input, feedback, and user experience in ways that are more intuitive and seamlessly integrated into daily life.

Beyond human use, the devices can be adapted for animals to support biological research. For example, in collaboration with researchers studying hummingbird heart function, we modified the PPG earring into a lightweight backpack that the birds could wear in flight, enabling real-time heart rate monitoring. This approach can support wildlife monitoring, animal health research, and disease tracking, such as bird flu.

The same low-power, compact sensing systems can also be extended to broader wireless sensing applications in the environment. These technologies could be adapted to environmental sensing, smart homes, and smart cities.

BIBLIOGRAPHY

[1] Ray-ban meta smart glasses. https://www.meta.com/smart-glasses/. Accessed: 2024-4-29.

[2] Fitbit health monitoring, 2021.

[3] Ajmal, Tananant Boonya-Ananta, Andres J Rodriguez, VN Du Le, and Jessica C Ramella-Roman. Monte carlo analysis of optical heart rate sensors in commercial wearables: the effect of skin tone and obesity on the photoplethysmography (ppg) signal. *Biomedical optics express*, 12(12):7445–7457, 2021.

[4] M Akdeniz, S Gabriel, A Lichterfeld-Kottner, U Blume-Peytavi, and J Kottner. Transepidermal water loss in healthy adults: a systematic review and meta-analysis update. *British Journal of Dermatology*, 179(5):1049–1055, 2018.

[5] Carla Alfonso, Miguel A Garcia-Gonzalez, Eva Parrado, Jessyca Gil-Rojas, Juan Ramos-Castro, and Lluis Capdevila. Agreement between two photoplethysmography-based wearable devices for monitoring heart rate during different physical activity situations: a new analysis methodology. *Scientific reports*, 12(1):15448, 2022.

[6] Tiance An, David Vera Anaya, Shu Gong, Lim Wei Yap, Fenge Lin, Ren Wang, Mehmet R Yuce, and Wenlong Cheng. Self-powered gold nanowire tattoo triboelectric sensors for soft wearable human-machine interface. *Nano Energy*, 77:105295, 2020.

[7] Leonardo Angelini, Maurizio Caon, Stefano Carrino, Luc Bergeron, Nathalie Nyffeler, Mélanie Jean-Mairet, and Elena Mugellini. Designing a desirable smart bracelet for older adults. In *Proceedings of the 2013 ACM conference on Pervasive and ubiquitous computing adjunct publication*, pages 425–434, 2013.

[8] Apple. Apple wacth healthcare. https://www.apple.com/healthcare/apple-watch/, 2023. Accessed: 2024-04-20.

[9] Apple. Apple watch. https://www.apple.com/watch/, 2023. Accessed: 2023-04-12.

[10] Apple. Track your nightly wrist temperature changes with apple watch. https://support.apple.com/en-us/HT213275, 2023. Accessed: 2023-05-10.

[11] KR Arunkumar and M Bhaskar. Heart rate estimation from wrist-type photoplethysmography signals during physical exercise. *Biomedical Signal Processing and Control*, 57:101790, 2020.

[12] Daniel Ashbrook, Patrick Baudisch, and Sean White. Nenya: subtle and eyes-free mobile input with a magnetically-tracked finger ring. In *Proceedings of the SIGCHI Conference on Human Factors in Computing Systems*, pages 2043–2046, 2011.

[13] C Assambo, A Baba, R Dozio, and MJ Burke. Determination of the parameters of the skin-electrode impedance model for ecg measurement. In *Proceedings of the 6th WSEAS international conference on electronics, hardware, wireless and optical communications*, pages 90–95, 2007.

[14] BardyDx. Bardydx carnation ambulatory monitor specifications. https://www.bardydx.com/wp-content/uploads/2023/07/DN000697B-BDx_CAM_SpecSheet.pdf, 2024. Accessed: 2024-11-19.

[15] Carolyn Beans. Wearable tech meets tattoo art in a bid to revolutionize both. *Proceedings of the National Academy of Sciences*, 115(14):3504–3506, 2018.

[16] Sarnab Bhattacharya, Mohammad Nikbakht, Alec Alden, Philip Tan, Jieting Wang, Taha A Alhalimi, Sangjun Kim, Pulin Wang, Hirofumi Tanaka, Animesh Tandon, et al. A chest-conformable, wireless electro-mechanical e-tattoo for measuring multiple cardiac time intervals. *Advanced Electronic Materials*, page 2201284, 2023.

[17] Dwaipayan Biswas, Luke Everson, Muqing Liu, Madhuri Panwar, Bram-Ernst Verhoef, Shrishail Patki, Chris H Kim, Amit Acharyya, Chris Van Hoof, Mario Konijnenburg, et al. Cornet: Deep learning framework for ppg-based heart rate estimation and biometric identification in ambulant environment. *IEEE transactions on biomedical circuits and systems*, 13(2):282–291, 2019.

[18] Dwaipayan Biswas, Neide Simões-Capela, Chris Van Hoof, and Nick Van Helleputte. Heart rate estimation from wrist-worn photoplethysmography: A review. *IEEE Sensors Journal*, 19(16):6560–6570, 2019.

[19] Carlo Alberto Boano, Matteo Lasagni, and Kay Römer. Non-invasive measurement of core body temperature in marathon runners. In *2013 IEEE International conference on body sensor networks*, pages 1–6. IEEE, 2013.

[20] Guy Boivin, Isabelle Hardy, Guy Tellier, and Jean Maziade. Predicting influenza infections during epidemics with use of a clinical case definition. *Clinical infectious diseases*, 31(5):1166–1169, 2000.

[21] Antonio Bosnjak, Alan Kennedy, Pedro Linares, Maira Borges, James McLaughlin, and Omar J Escalona. Performance assessment of dry electrodes for wearable long term cardiac rhythm monitoring: Skin-electrode impedance spectroscopy. In *2017 39th Annual International Conference of the IEEE Engineering in Medicine and Biology Society (EMBC)*, pages 1861–1864. IEEE, 2017.

[22] Joseph Breda, Mastafa Springston, Alex Mariakakis, and Shwetak Patel. Feverphone: Accessible core-body temperature sensing for fever monitoring using commodity smartphones. *Proceedings of the ACM on Interactive, Mobile, Wearable and Ubiquitous Technologies*, 7(1):1–23, 2023.

[23] Jas Brooks, Shan-Yuan Teng, Jingxuan Wen, Romain Nith, Jun Nishida, and Pedro Lopes. Stereo-smell via electrical trigeminal stimulation. In *Proceedings of the 2021 CHI Conference on Human Factors in Computing Systems*, pages 1–13, 2021.

[24] Michael J Brucker, Jagruti Patel, and Patrick K Sullivan. A morphometric study of the external ear: age-and sex-related differences. *Plastic and reconstructive surgery*, 112(2):647–652, 2003.

[25] Thisum Buddhika, Haimo Zhang, Samantha WT Chan, Vipula Dissanayake, Suranga Nanayakkara, and Roger Zimmermann. Fsense: Unlocking the dimension of force for gestural interactions using smartwatch ppg sensor. In *Proceedings of the 10th Augmented Human International Conference 2019*, pages 1–5, 2019.

[26] Alessio Burrello, Daniele Jahier Pagliari, Pierangelo Maria Rapa, Matilde Semilia, Matteo Risso, Tommaso Polonelli, Massimo Poncino, Luca Benini, and Simone Benatti. Embedding temporal convolutional networks for energy-efficient ppg-based heart rate monitoring. *ACM Transactions on Computing for Healthcare (HEALTH)*, 3(2):1–25, 2022.

[27] Alessio Burrello, Daniele Jahier Pagliari, Matteo Risso, Simone Benatti, Enrico Macii, Luca Benini, and Massimo Poncino. Q-ppg: Energy-efficient ppg-based heart rate monitoring on wearable devices. *IEEE Transactions on Biomedical Circuits and Systems*, 15(6):1196–1209, 2021.

[28] Yetong Cao, Fan Li, Huijie Chen, Xiaochen Liu, Li Zhang, and Yu Wang. Guard your heart silently: Continuous electrocardiogram waveform monitoring with wrist-worn motion sensor. *Proceedings of the ACM on Interactive, Mobile, Wearable and Ubiquitous Technologies*, 6(3):1–29, 2022.

[29] Alexander J Casson, Arturo Vazquez Galvez, and Delaram Jarchi. Gyroscope vs. accelerometer measurements of motion from wrist ppg during physical exercise. *Ict Express*, 2(4):175–179, 2016.

[30] CDC. Heart disease facts. `https://www.cdc.gov/heart-disease/data-research/facts-stats/index.html`, 2024. Accessed: 2024-11-15.

[31] Sungwoo Chun, Da Wan Kim, Sangyul Baik, Heon Joon Lee, Jung Heon Lee, Suk Ho Bhang, and Changhyun Pang. Conductive and stretchable adhesive electronics with miniaturized octopus-like suckers against dry/wet skin for biosignal monitoring. *Advanced Functional Materials*, 28(52):1805224, 2018.

[32] Sungwoo Chun, Wonkyeong Son, Da Wan Kim, Jihyun Lee, Hyeongho Min, Hachul Jung, Dahye Kwon, A-Hee Kim, Young-Jin Kim, Sang Kyoo Lim, et al. Water-resistant and skin-adhesive wearable electronics using graphene fabric sensor with octopus-inspired microsuckers. *ACS applied materials & interfaces*, 11(18):16951–16957, 2019.

[33] Hung-Yuan Chung, Yao-Liang Chung, and Chih-Yen Liang. Design and implementation of a novel system for correcting posture through the use of a wearable necklace sensor. *JMIR mHealth and uHealth*, 7(5):e12293, 2019.

[34] Gari D Clifford, Francisco Azuaje, Patrick Mcsharry, et al. Ecg statistics, noise, artifacts, and missing data. *Advanced methods and tools for ECG data analysis*, 6(1):18, 2006.

[35] Cleveland Clinic. Silent heart attack. https://my.clevelandclinic.org/health/diseases/21630-silent-heart-attack, 2021. Accessed: 2024-04-20.

[36] Cleveland Clinic. Blood oxygen level. https://my.clevelandclinic.org/health/diagnostics/22447-blood-oxygen-level, 2024. Accessed: 2024-11-13.

[37] Cleveland Clinic. Heart. https://my.clevelandclinic.org/health/body/21704-heart, 2024. Accessed: 2024-04-20.

[38] Nicholas Constant, Orrett Douglas-Prawl, Samuel Johnson, and Kunal Mankodiya. Pulse-glasses: An unobtrusive, wearable hr monitor with internet-of-things functionality. In *2015 IEEE 12th international conference on wearable and implantable body sensor networks (BSN)*, pages 1–5. IEEE, 2015.

[39] Nicole A Coull, Anna M West, Simon G Hodder, Patrick Wheeler, and George Havenith. Body mapping of regional sweat distribution in young and older males. *European journal of applied physiology*, 121:109–125, 2021.

[40] Madeleine IG Daepp, Alex Cabral, Vaishnavi Ranganathan, Vikram Iyer, Scott Counts, Paul Johns, Asta Roseway, Charlie Catlett, Gavin Jancke, Darren Gehring, et al. Eclipse: an end-to-end platform for low-cost, hyperlocal environmental sensing in cities. In *2022 21st ACM/IEEE International Conference on Information Processing in Sensor Networks (IPSN)*, pages 28–40. IEEE, 2022.

[41] Oscar Danielsson, Magnus Holm, and Anna Syberfeldt. Augmented reality smart glasses in industrial assembly: Current status and future challenges. *Journal of Industrial Information Integration*, 20:100175, 2020.

[42] Isabel del Agua, Daniele Mantione, Usein Ismailov, Ana Sanchez-Sanchez, Nora Aramburu, George G Malliaras, David Mecerreyes, and Esma Ismailova. Dvs-crosslinked

pedot: Pss free-standing and textile electrodes toward wearable health monitoring. *Advanced Materials Technologies*, 3(10):1700322, 2018.

[43] Artem Dementyev, Tomás Vega Gálvez, and Alex Olwal. Sensorsnaps: Integrating wireless sensor nodes into fabric snap fasteners for textile interfaces. In *Proceedings of the 32nd Annual ACM Symposium on User Interface Software and Technology*, pages 17–28, 2019.

[44] Statista Research Department. United states: Pierced body parts in 2017, by gender. https://www.statista.com/statistics/722656/pierced-body-parts-of-americans-by-gender/, 2023. Accessed: 2023-05-01.

[45] Luke Eckersley, Lynn Sadler, Emma Parry, Kirsten Finucane, and Thomas L Gentles. Timing of diagnosis affects mortality in critical congenital heart disease. *Archives of disease in childhood*, 101(6):516–520, 2016.

[46] Empatica. Embraceplus, the world's most advanced smartwatch for continuous health monitoring. https://www.empatica.com/en-int/embraceplus/, 2023. Accessed: 2023-05-08.

[47] Andrea Ferlini, Alessandro Montanari, Chulhong Min, Hongwei Li, Ugo Sassi, and Fahim Kawsar. In-ear ppg for vital signs. *IEEE Pervasive Computing*, 21(1):65–74, 2021.

[48] Laura M Ferrari, Sudha Sudha, Sergio Tarantino, Roberto Esposti, Francesco Bolzoni, Paolo Cavallari, Christian Cipriani, Virgilio Mattoli, and Francesco Greco. Ultraconformable temporary tattoo electrodes for electrophysiology. *Advanced Science*, 5(3):1700771, 2018.

[49] Fitbit. How can fitbit help me track my temperature? https://help.fitbit.com/articles/en_US/Help_article/2458.htm, 2023. Accessed: 2023-05-10.

[50] Jutta Fortmann, Vanessa Cobus, Wilko Heuten, and Susanne Boll. Waterjewel: design and evaluation of a bracelet to promote a better drinking behaviour. In *Proceedings of the 13th international conference on mobile and ubiquitous multimedia*, pages 58–67, 2014.

[51] Jutta Fortmann, Erika Root, Susanne Boll, and Wilko Heuten. Tangible apps bracelet: Designing modular wrist-worn digital jewellery for multiple purposes. In *Proceedings of the 2016 ACM Conference on Designing Interactive Systems*, pages 841–852, 2016.

[52] Frontier. Frongier x2 heart monitor. https://fourthfrontier.com/products/frontier-x, 2024. Accessed: 2024-01-29.

[53] CHEN Ge, XIE Jiarong, DAI Guangli, Peijun Zheng, HU Xiaqing, LU Hongpeng, XU Lei, CHEN Xueqin, and CHEN Xiaomin. Validity of the use of wrist and forehead temperatures in screening the general population for covid-19: A prospective real-world study. *Iranian journal of public health*, 49(Suppl 1):57, 2020.

[54] Shrimanti Ghosh, Ankur Banerjee, Nilanjan Ray, Peter W Wood, Pierre Boulanger, and Raj Padwal. Continuous blood pressure prediction from pulse transit time using ecg and ppg signals. In *2016 IEEE Healthcare Innovation Point-Of-Care Technologies Conference (HI-POCT)*, pages 188–191. IEEE, 2016.

[55] Google. Loss of pulse detection: A first-of-its-kind feature on pixel watch 3. https://blog.google/products/pixel/pixel-watch-3-loss-of-pulse-detection/, 2024. Accessed: 2024-11-13.

[56] ThM Govaert, GJ Dinant, K Aretz, and JA Knottnerus. The predictive value of influenza symptomatology in elderly people. *Family practice*, 15(1):16–22, 1998.

[57] Amos Grünebaum, Frank A Chervenak, Laurence B McCullough, Joachim W Dudenhausen, Eran Bornstein, and Philip A Mackowiak. How fever is defined in covid-19 publications: a disturbing lack of precision. *Journal of Perinatal Medicine*, 49(3):255–261, 2021.

[58] Tian Hao, Chongguang Bi, Guoliang Xing, Roxane Chan, and Linlin Tu. Mindfulwatch: A smartwatch-based system for real-time respiration monitoring during meditation. *Proceedings of the ACM on Interactive, Mobile, Wearable and Ubiquitous Technologies*, 1(3):1–19, 2017.

[59] Yun Jung Heo and Shoji Takeuchi. Towards smart tattoos: implantable biosensors for continuous glucose monitoring. *Advanced healthcare materials*, 2(1):43–56, 2013.

[60] Minh Long Hoang, Marco Carratù, Vincenzo Paciello, and Antonio Pietrosanto. Body temperature—indoor condition monitor and activity recognition by mems accelerometer based on iot-alert system for people in quarantine due to covid-19. *Sensors*, 21(7):2313, 2021.

[61] Christian Holz and Edward J Wang. Glabella: Continuously sensing blood pressure behavior using an unobtrusive wearable device. *Proceedings of the ACM on Interactive, Mobile, Wearable and Ubiquitous Technologies*, 1(3):1–23, 2017.

[62] Min-Chieh Hsiu, Chiuan Wang, Da-Yuan Huang, Jhe-Wei Lin, Yu-Chih Lin, De-Nian Yang, Yi-ping Hung, and Mike Chen. Nail+ sensing fingernail deformation to detect finger force touch interactions on rigid surfaces. In *Proceedings of the 18th International Conference on Human-Computer Interaction with Mobile Devices and Services*, pages 1–6, 2016.

[63] Hubert Hymczak, Aleksandra Gołab, Konrad Mendrala, Dariusz Plicner, Tomasz Darocha, Paweł Podsiadło, Damian Hudziak, Radosław Gocoł, and Sylweriusz Kosiński. Core temperature measurement—principles of correct measurement, problems, and complications. *International Journal of Environmental Research and Public Health*, 18(20):10606, 2021.

[64] Grogran Jewelers. How much does a pair of earrings weigh? https://blog.groganjewelers.com/how-much-does-a-pair-of-earrings-weigh, 2023. Accessed: 2023-04-20.

[65] Joule. Joule earring backings. https://shopjoule.com, 2022. Accessed: 2023-04-20.

[66] Shideh Kabiri Ameri, Rebecca Ho, Hongwoo Jang, Li Tao, Youhua Wang, Liu Wang, David M Schnyer, Deji Akinwande, and Nanshu Lu. Graphene electronic tattoo sensors. *ACS nano*, 11(8):7634–7641, 2017.

[67] Haik Kalantarian, Nabil Alshurafa, Tuan Le, and Majid Sarrafzadeh. Non-invasive detection of medication adherence using a digital smart necklace. In *2015 IEEE International Conference on Pervasive Computing and Communication Workshops (PerCom Workshops)*, pages 348–353. IEEE, 2015.

[68] Hsin-Liu Kao, Artem Dementyev, Joseph A Paradiso, and Chris Schmandt. Nailo: fingernails as an input surface. In *Proceedings of the 33rd Annual ACM Conference on Human Factors in Computing Systems*, pages 3015–3018, 2015.

[69] Hsin-Liu Kao, Christian Holz, Asta Roseway, Andres Calvo, and Chris Schmandt. Duoskin: rapidly prototyping on-skin user interfaces using skin-friendly materials. In *Proceedings of the 2016 ACM International Symposium on Wearable Computers*, pages 16–23, 2016.

[70] Kardia. Apple wacth healthcare. https://store.kardia.com/products/kardiamobile, 2023. Accessed: 2024-04-29.

[71] Justin Kavanagh, Rod Barrett, and Steven Morrison. The role of the neck and trunk in facilitating head stability during walking. *Experimental brain research*, 172:454–463, 2006.

[72] Kirti Khunti. Accurate interpretation of the 12-lead ecg electrode placement: A systematic review. *Health Education Journal*, 73(5):610–623, 2014.

[73] Hyeonseok Kim, Eugene Kim, Chanyeong Choi, and Woon-Hong Yeo. Advances in soft and dry electrodes for wearable health monitoring devices. *Micromachines*, 13(4):629, 2022.

[74] Taehoon Kim, Junyong Park, Jongmoo Sohn, Donghwi Cho, and Seokwoo Jeon. Bioinspired, highly stretchable, and conductive dry adhesives based on 1d–2d hybrid carbon nanocomposites for all-in-one ecg electrodes. *ACS nano*, 10(4):4770–4778, 2016.

[75] James Knight, Chris Baber, Anthony Schwirtz, and Huw Bristow. The comfort assessment of wearable computers. *Proceedings. Sixth International Symposium on Wearable Computers*, pages 65–72, 2002.

[76] OC Koumar, R Beaufils, C Chesneau, H Normand, and N Bessot. Validation of e-celsius gastrointestinal telemetry system as measure of core temperature. *Journal of Thermal Biology*, page 103471, 2023.

[77] Pin-Sung Ku, Kunpeng Huang, Nancy Wang, Boaz Ng, Alicia Chu, and Hsin-Liu Cindy Kao. Skinlink: On-body construction and prototyping of reconfigurable epidermal interfaces. *Proceedings of the ACM on Interactive, Mobile, Wearable and Ubiquitous Technologies*, 7(2):1–27, 2023.

[78] Young-Tae Kwon, Yun-Soung Kim, Shinjae Kwon, Musa Mahmood, Hyo-Ryoung Lim, Si-Woo Park, Sung-Oong Kang, Jeongmoon J Choi, Robert Herbert, Young C Jang, et al. All-printed nanomembrane wireless bioelectronics using a biocompatible solderable graphene for multimodal human-machine interfaces. *Nature communications*, 11(1):3450, 2020.

[79] PhD FACC Lawrence Rosenthal, MD. Normal electrocardiography (ecg) intervals. https://emedicine.medscape.com/article/2172196-overview, 2024. Accessed: 2024-04-29.

[80] Jongshill Lee, Minseong Kim, Hoon-Ki Park, and In Young Kim. Motion artifact reduction in wearable photoplethysmography based on multi-channel sensors with multiple wavelengths. *Sensors*, 20(5):1493, 2020.

[81] Lik-Hang Lee and Pan Hui. Interaction methods for smart glasses: A survey. *IEEE access*, 6:28712–28732, 2018.

[82] Qingsong Li, Geng Chen, Yajing Cui, Shaobo Ji, Zhiyuan Liu, Changjin Wan, Yuping Liu, Yehu Lu, Changxian Wang, Nan Zhang, et al. Highly thermal-wet comfortable and conformal silk-based electrodes for on-skin sensors with sweat tolerance. *ACS nano*, 15(6):9955–9966, 2021.

[83] Xiaoping Liang, Haifang Li, Jinxin Dou, Qi Wang, Wenya He, Chunya Wang, Donghang Li, Jin-Ming Lin, and Yingying Zhang. Stable and biocompatible carbon nanotube ink mediated by silk protein for printed electronics. *Advanced Materials*, 32(31):2000165, 2020.

[84] Li-Wei Lo, Junyi Zhao, Haochuan Wan, Yong Wang, Shantanu Chakrabartty, and Chuan Wang. An inkjet-printed pedot: Pss-based stretchable conductor for wearable health monitoring device applications. *ACS Applied Materials & Interfaces*, 13(18):21693–21702, 2021.

[85] Fei Lu, Chenshuo Wang, Rongjian Zhao, Lidong Du, Zhen Fang, Xiuhua Guo, and Zhan Zhao. Review of stratum corneum impedance measurement in non-invasive penetration application. *Biosensors*, 8(2):31, 2018.

[86] Elle Luo, Ruixuan Fu, Alicia Chu, Katia Vega, and Hsin-Liu Kao. Eslucent: an eyelid interface for detecting eye blinking. In *Proceedings of the 2020 ACM International Symposium on Wearable Computers*, pages 58–62, 2020.

[87] Michele Magno, Giovanni A Salvatore, Petar Jokic, and Luca Benini. Self-sustainable smart ring for long-term monitoring of blood oxygenation. *IEEE access*, 7:115400–115408, 2019.

[88] Dominique Makowski, Tam Pham, Zen J. Lau, Jan C. Brammer, François Lespinasse, Hung Pham, Christopher Schölzel, and S. H. Annabel Chen. NeuroKit2: A python toolbox for neurophysiological signal processing. *Behavior Research Methods*, 53(4):1689–1696, feb 2021.

[89] Fahad L Malallah, Baraa T Shareef, Mustafah Ghanem Saeed, and Khaled N Yasen. Contactless core-temperature monitoring by infrared thermal sensor using mean absolute error analysis. *Recent Patents on Engineering*, 15(4):100–111, 2021.

[90] Pilar Martín-Escudero, Ana María Cabanas, María Luisa Dotor-Castilla, Mercedes Galindo-Canales, Francisco Miguel-Tobal, Cristina Fernández-Pérez, Manuel Fuentes-Ferrer, and Romano Giannetti. Are activity wrist-worn devices accurate for determining heart rate during intense exercise? *Bioengineering*, 10(2):254, 2023.

[91] Mahdi Boloursaz Mashhadi, Ehsan Asadi, Mohsen Eskandari, Shahrzad Kiani, and Farokh Marvasti. Heart rate tracking using wrist-type photoplethysmographic (ppg) signals during physical exercise with simultaneous accelerometry. *IEEE Signal Processing Letters*, 23(2):227–231, 2015.

[92] Jane McCann and David Bryson. *Smart clothes and wearable technology*. Woodhead Publishing, 2022.

[93] McFarlane. The simple guide to earring length. https://mcfarlanefinejewellery.com/blogs/the-lovelist/earring-length-guide, 2023. Accessed: 2023-05-14.

[94] John Hopkins Medicine. Electrocardiogram. https://www.hopkinsmedicine.org/health/treatment-tests-and-therapies/electrocardiogram#, 2024. Accessed: 2024-04-25.

[95] Stefan Mitrasinovic, Elvis Camacho, Nirali Trivedi, Julia Logan, Colson Campbell, Robert Zilinyi, Bryan Lieber, Eliza Bruce, Blake Taylor, David Martineau, et al. Clinical and surgical applications of smart glasses. *Technology and health care*, 23(4):381–401, 2015.

[96] Marie Muehlhaus, Jürgen Steimle, and Marion Koelle. Feather hair: Interacting with sensorized hair in public settings. In *Proceedings of the 2022 ACM Designing Interactive Systems Conference*, pages 1228–1242, 2022.

[97] Robert A Nawrocki, Hanbit Jin, Sunghoon Lee, Tomoyuki Yokota, Masaki Sekino, and Takao Someya. Self-adhesive and ultra-conformable, sub-300 nm dry thin-film electrodes for surface monitoring of biopotentials. *Advanced Functional Materials*, 28(36):1803279, 2018.

[98] National Institute of Health. Subject preparation: Ecg/ekg. `https://megcore.nih.gov/index.php/Subject_Preparation:_ECG/EKG`, 2024. Accessed: 2024-12-09.

[99] Ali Emre Ok, Nuri A Basoglu, and Tugrul Daim. Exploring the design factors of smart glasses. In *2015 Portland international conference on management of engineering and technology (PICMET)*, pages 1657–1664. IEEE, 2015.

[100] Oura. Heart rate variability. `https://support.ouraring.com/hc/en-us/articles/360025441974-Heart-Rate-Variability`, 2024. Accessed: 2024-11-13.

[101] OuraRing. Oura ring: An introduction to body temperature. `https://support.ouraring.com/hc/en-us/articles/360025587493-An-Introduction-to-Body-Temperature`. Accessed: 2023-3-22.

[102] Alba Páez-Montoro, José Ángel Miranda-Calero, Juan Marcos-Torero, and Celia López-Ongil. Towards a smart earring for continuous heart rate and audio monitoring. In *2022 37th Conference on Design of Circuits and Integrated Circuits (DCIS)*, pages 01–06. IEEE, 2022.

[103] Jaeyeon Park, Hyeon Cho, Rajesh Krishna Balan, and JeongGil Ko. Heartquake: Accurate low-cost non-invasive ecg monitoring using bed-mounted geophones. *Proceedings of the ACM on Interactive, Mobile, Wearable and Ubiquitous Technologies*, 4(3):1–28, 2020.

[104] RC Parmar, DR Sahu, SB Bavdekar, et al. Knowledge, attitude and practices of parents of children with febrile convulsion. *Journal of postgraduate medicine*, 47(1):19, 2001.

[105] Stefanie Passler, Niklas Müller, and Veit Senner. In-ear pulse rate measurement: a valid alternative to heart rate derived from electrocardiography? *Sensors*, 19(17):3641, 2019.

[106] Jayun Patel and Ragib Hasan. Smart bracelets: Towards automating personal safety using wearable smart jewelry. In *2018 15th IEEE Annual Consumer Communications & Networking Conference (CCNC)*, pages 1–2. IEEE, 2018.

[107] Marco V Perez, Kenneth W Mahaffey, Haley Hedlin, John S Rumsfeld, Ariadna Garcia, Todd Ferris, Vidhya Balasubramanian, Andrea M Russo, Amol Rajmane, Lauren Cheung, et al. Large-scale assessment of a smartwatch to identify atrial fibrillation. *New England Journal of Medicine*, 381(20):1909–1917, 2019.

[108] Peripherii. Peripherii smartearrings. https://peripherii.com/, 2023. Accessed: 2023-04-12.

[109] Ming-Zher Poh, Daniel J McDuff, and Rosalind W Picard. Advancements in noncontact, multiparameter physiological measurements using a webcam. *IEEE transactions on biomedical engineering*, 58(1):7–11, 2010.

[110] Ming-Zher Poh, Daniel J McDuff, and Rosalind W Picard. Non-contact, automated cardiac pulse measurements using video imaging and blind source separation. *Optics express*, 18(10):10762–10774, 2010.

[111] Ming-Zher Poh, Nicholas C Swenson, and Rosalind W Picard. Motion-tolerant magnetic earring sensor and wireless earpiece for wearable photoplethysmography. *IEEE Transactions on Information Technology in Biomedicine*, 14(3):786–794, 2010.

[112] Jiří Přibil, Anna Přibilová, and Ivan Frollo. Comparative measurement of the ppg signal on different human body positions by sensors working in reflection and transmission modes. *Engineering proceedings*, 2(1):69, 2020.

[113] Harvard Health Publishing. What is a normal heart rate? https://www.health.harvard.edu/heart-health/what-your-heart-rate-is-telling-you, 2024. Accessed: 2024-11-15.

[114] Ryan Quinn, Nathan Leader, Gerald Lebovic, Chi-Ming Chow, and Paul Dorian. Accuracy of wearable heart rate monitors during exercise in sinus rhythm and atrial fibrillation. *Journal of the American College of Cardiology*, 83(12):1177–1179, 2024.

[115] Ho-Kyeong Ra, Jungmo Ahn, Hee Jung Yoon, Dukyong Yoon, Sang Hyuk Son, and JeongGil Ko. I am a" smart" watch, smart enough to know the accuracy of my own heart rate sensor. In *Proceedings of the 18th International Workshop on Mobile Computing Systems and Applications*, pages 49–54, 2017.

[116] R Rajaganeshan, CL Ludlam, DP Francis, SV Parasramka, and R Sutton. Accuracy in ecg lead placement among technicians, nurses, general physicians and cardiologists. *International journal of clinical practice*, 62(1):65–70, 2008.

[117] Sukesh Rao, Roopa B Hegde, and Sanith C Bangera. A comparative analysis of reflective and transmissive ppg sensor in pulse acquisition system. In *2023 International Conference on Computer, Electronics & Electrical Engineering & their Applications (IC2E3)*, pages 1–4. IEEE, 2023.

[118] Mohammad Rezaei, Avik S Basu, and Amar S Basu. Trace: an earlobe mounted sensor for continuous measurement of heart rate dynamics. In *2019 IEEE SENSORS*, pages 1–4. IEEE, 2019.

[119] Seyed MA Salehizadeh, Duy Dao, Jeffrey Bolkhovsky, Chae Cho, Yitzhak Mendelson, and Ki H Chon. A novel time-varying spectral filtering algorithm for reconstruction of motion artifact corrupted heart rate signals during intense physical activities using a wearable photoplethysmogram sensor. *Sensors*, 16(1):10, 2015.

[120] Arman Sargolzaei, Karim Faez, and Saman Sargolzaei. A new robust wavelet based algorithm for baseline wandering cancellation in ecg signals. In *2009 IEEE International Conference on Signal and Image Processing Applications*, pages 33–38. IEEE, 2009.

[121] Harvard Medical School. The danger of "silent" heart attack. https://www.health.harvard.edu/heart-health/the-danger-of-silent-heart-attacks, 2020. Accessed: 2024-04-20.

[122] Sougata Sen and David Kotz. Vibering: Using vibrations from a smart ring as an out-of-band channel for sharing secret keys. In *Proceedings of the 10th International Conference on the Internet of Things*, pages 1–8, 2020.

[123] Fred Shaffer and Jay P Ginsberg. An overview of heart rate variability metrics and norms. *Frontiers in public health*, 5:258, 2017.

[124] Katherine Wei Song, Christine Dierk, Szu Ting Tung, and Eric Paulos. Lotio: Lotion-mediated interaction with an electronic skin-worn display. In *Proceedings of the 2023 CHI Conference on Human Factors in Computing Systems*, pages 1–15, 2023.

[125] Madison S Spach, Roger C Barr, James W Havstad, and E Croft Long. Skin-electrode impedance and its effect on recording cardiac potentials. *Circulation*, 34(4):649–656, 1966.

[126] Statista. Wearable devices ownership in selected countries 2022. https://www.statista.com/forecasts/1101101/wearable-devices-ownership-in-selected-countries, 2023. Accessed: 2023-05-08.

[127] Statista. United states: Pierced body parts in 2017, by gender. https://www.statista.com/statistics/722656/pierced-body-parts-of-americans-by-gender/, 2024. Accessed: 2025-02-10.

[128] Hsiu-Wei Su, Yu-Chiao Yi, Ting-Yen Wei, Ting-Chang Chang, and Chao-Min Cheng. Detection of ovulation, a review of currently available methods. *Bioengineering & translational medicine*, 2(3):238–246, 2017.

[129] Takaki Suetake, Shu Sasai, Ya-Xian Zhen, and Hachiro Tagami. Effects of silicone gel sheet on the stratum corneum hydration. *British journal of plastic surgery*, 53(6):503–507, 2000.

[130] Minyoung Suh, Katherine E Carroll, and Nancy L Cassill. Critical review on smart clothing product development. *Journal of textile and apparel, technology and management*, 6(4), 2010.

[131] Bohan Sun, Richard N McCay, Shivam Goswami, Yadong Xu, Cheng Zhang, Yun Ling, Jian Lin, and Zheng Yan. Gas-permeable, multifunctional on-skin electronics based on laser-induced porous graphene and sugar-templated elastomer sponges. *Advanced Materials*, 30(50):1804327, 2018.

[132] Ruojia Sun, Ryosuke Onose, Margaret Dunne, Andrea Ling, Amanda Denham, and Hsin-Liu Kao. Weaving a second skin: exploring opportunities for crafting on-skin interfaces through weaving. In *Proceedings of the 2020 ACM Designing Interactive Systems Conference*, pages 365–377, 2020.

[133] SS Sundaram, N Hari Basker, and L Natrayan. Smart clothes with bio-sensors for ecg monitoring. *International Journal of Innovative Technology and Exploring Engineering*, 8(4):298–301, 2019.

[134] Kenji Suzuki, Taku Hachisu, and Kazuki Iida. Enhancedtouch: A smart bracelet for enhancing human-human physical touch. In *Proceedings of the 2016 CHI Conference on Human Factors in Computing Systems*, pages 1282–1293, 2016.

[135] Anna Syberfeldt, Oscar Danielsson, and Patrik Gustavsson. Augmented reality smart glasses in the smart factory: Product evaluation guidelines and review of available products. *Ieee Access*, 5:9118–9130, 2017.

[136] Bahareh Taji, Adrian DC Chan, and Shervin Shirmohammadi. Effect of pressure on skin-electrode impedance in wearable biomedical measurement devices. *IEEE Transactions on Instrumentation and Measurement*, 67(8):1900–1912, 2018.

[137] Bahareh Taji, Shervin Shirmohammadi, and Voicu Groza. Measuring skin-electrode impedance variation of conductive textile electrodes under pressure. In *2014 IEEE International Instrumentation and Measurement Technology Conference (I2MTC) Proceedings*, pages 1083–1088. IEEE, 2014.

[138] Lieva Van Langenhove and Carla Hertleer. Smart clothing: a new life. *International journal of clothing science and technology*, 16(1/2):63–72, 2004.

[139] Katia Vega and Hugo Fuks. Beauty technology: body surface computing. *Computer*, 47(4):71–75, 2014.

[140] Vivalink. Vivalink wearable ecg monitor. https://www.vivalink.com/wearable-ecg-monitor, 2024. Accessed: 2024-11-19.

[141] Vuzix. Vuzix smart glasses. https://www.vuzix.com/, 2023. Accessed: 2023-05-13.

[142] Edward Jay Wang, Junyi Zhu, Mohit Jain, Tien-Jui Lee, Elliot Saba, Lama Nachman, and Shwetak N Patel. Seismo: Blood pressure monitoring using built-in smartphone accelerometer and camera. In *Proceedings of the 2018 CHI conference on human factors in computing Systems*, pages 1–9, 2018.

[143] Fan Wang, Xiaoxue Li, Xiuyun Wang, and Xian Jiang. Efficacy of topical silicone gel in scar management: a systematic review and meta-analysis of randomised controlled trials. *International wound journal*, 17(3):765–773, 2020.

[144] Wenjin Wang, Albertus C Den Brinker, Sander Stuijk, and Gerard De Haan. Algorithmic principles of remote ppg. *IEEE Transactions on Biomedical Engineering*, 64(7):1479–1491, 2016.

[145] Zhi Wang, Beihong Jin, Siheng Li, Fusang Zhang, and Wenbo Zhang. Ecg-grained cardiac monitoring using uwb signals. *Proceedings of the ACM on Interactive, Mobile, Wearable and Ubiquitous Technologies*, 6(4):1–25, 2023.

[146] Peter Wei, Chenye Yang, and Xiaofan Jiang. Low-cost multi-person continuous skin temperature sensing system for fever detection. In *Proceedings of the 18th Conference on Embedded Networked Sensor Systems*, pages 705–706, 2020.

[147] WHO. Cardiovascular diseases. https://www.who.int/health-topics/cardiovascular-diseases, 2024. Accessed: 2024-04-25.

[148] Wikipedia contributors. Peukert's law — Wikipedia, the free encyclopedia, 2023. [Online; accessed 18-July-2023].

[149] Liping Xie, Zilong Li, Yihan Zhou, Yiliu He, and Jiaxin Zhu. Computational diagnostic techniques for electrocardiogram signal analysis. *Sensors*, 20(21):6318, 2020.

[150] Qiuyue Shirley Xue, Yujia Liu, Joseph Breda, Mastafa Springston, Vikram Iyer, and Shwetak Patel. Thermal earring: Low-power wireless earring for longitudinal earlobe temperature sensing. *Proceedings of the ACM on Interactive, Mobile, Wearable and Ubiquitous Technologies*, 7(4):1–28, 2024.

[151] Hui-Shyong Yeo, Wenxin Feng, and Michael Xuelin Huang. Watouch: Enabling direct input on non-touchscreen using smartwatch's photoplethysmogram and imu sensor fusion. In *Proceedings of the 2020 CHI Conference on Human Factors in Computing Systems*, pages 1–10, 2020.

[152] Tianhong Catherine Yu, Nancy Wang, Sarah Ellenbogen, and Cindy Hsin-Liu Kao. Skinergy: Machine-embroidered silicone-textile composites as on-skin self-powered input sensors. In *Proceedings of the 36th Annual ACM Symposium on User Interface Software and Technology*, pages 1–15, 2023.

[153] Israel Zepeda-Carapia, Agustin Marquez-Espinoza, and Carlos Alvarado-Serrano. Measurement of skin-electrode impedance for a 12-lead electrocardiogram. In *2005 2nd International Conference on Electrical and Electronics Engineering*, pages 193–195. IEEE, 2005.

[154] Kang Zhang, Naiwen Kang, Bo Zhang, Ruijie Xie, Jingyu Zhu, Binghua Zou, Yihan Liu, Yuanyuan Chen, Wei Shi, Weina Zhang, et al. Skin conformal and antibacterial ppy-leather electrode for ecg monitoring. *Advanced Electronic Materials*, 6(8):2000259, 2020.

[155] Lei Zhang, Kirthika Senthil Kumar, Hao He, Catherine Jiayi Cai, Xu He, Huxin Gao, Shizhong Yue, Changsheng Li, Raymond Chee-Seong Seet, Hongliang Ren, et al. Fully organic compliant dry electrodes self-adhesive to skin for long-term motion-robust epidermal biopotential monitoring. *Nature communications*, 11(1):4683, 2020.

[156] Ruidong Zhang, Mingyang Chen, Benjamin Steeper, Yaxuan Li, Zihan Yan, Yizhuo Chen, Songyun Tao, Tuochao Chen, Hyunchul Lim, and Cheng Zhang. Speechin: A smart necklace for silent speech recognition. *Proceedings of the ACM on Interactive, Mobile, Wearable and Ubiquitous Technologies*, 5(4):1–23, 2021.

[157] Shibo Zhang, Yuqi Zhao, Dzung Tri Nguyen, Runsheng Xu, Sougata Sen, Josiah Hester, and Nabil Alshurafa. Necksense: A multi-sensor necklace for detecting eating activities in free-living conditions. *Proceedings of the ACM on interactive, mobile, wearable and ubiquitous technologies*, 4(2):1–26, 2020.

[158] Tengxiang Zhang, Xin Zeng, Yinshuai Zhang, Ke Sun, Yuntao Wang, and Yiqiang Chen. Thermalring: Gesture and tag inputs enabled by a thermal imaging smart ring. In *Proceedings of the 2020 CHI Conference on Human Factors in Computing Systems*, pages 1–13, 2020.

[159] Xin Zhang, Karteek Kadimisetty, Kun Yin, Carlos Ruiz, Michael G Mauk, and Changchun Liu. Smart ring: a wearable device for hand hygiene compliance monitoring at the point-of-need. *Microsystem Technologies*, 25:3105–3110, 2019.

[160] Zio. Zio at information. https://fcc.report/FCC-ID/2AFBP-AT18G/3875382.pdf, 2024. Accessed: 2024-11-19.